COPPE
Instituto Alberto Luiz Coimbra de Pós-Graduação e Pesquisa de Engenharia UFRJ

ANALYSIS OF CARDIAC RHYTHMS USING A DYNAMICS PERSPECTIVE: NONLINEARITIES, RANDOMNESSES AND CHAOS

Augusto Luiz Cheffer de Melo

Tese de Doutorado apresentada ao Programa de Pós-graduação em Engenharia Mecânica, COPPE, da Universidade Federal do Rio de Janeiro, como parte dos requisitos necessários à obtenção do título de Doutor em Engenharia Mecânica.

Orientador: Marcelo Amorim Savi

Rio de Janeiro
Outubro de 2021

ANALYSIS OF CARDIAC RHYTHMS USING A DYNAMICS PERSPECTIVE: NONLINEARITIES, RANDOMNESSES AND CHAOS

Augusto Luiz Cheffer de Melo

TESE SUBMETIDA AO CORPO DOCENTE DO INSTITUTO ALBERTO LUIZ COIMBRA DE PÓS-GRADUAÇÃO E PESQUISA DE ENGENHARIA DA UNIVERSIDADE FEDERAL DO RIO DE JANEIRO COMO PARTE DOS REQUISITOS NECESSÁRIOS PARA A OBTENÇÃO DO GRAU DE DOUTOR EM CIÊNCIAS EM ENGENHARIA MECÂNICA.

Orientador: Marcelo Amorim Savi

Aprovada por: Prof. Marcelo Amorim Savi
Profª. Aline Souza de Paula
Prof. José da Rocha Miranda Pontes
Prof. Thiago Gamboa Ritto
Prof. Wallace Moreira Bessa

RIO DE JANEIRO, RJ - BRASIL
OUTUBRO DE 2021

Cheffer de Melo, Augusto Luiz

Analysis of cardiac rhythms using a dynamics perspective: Nonlinearities, randomnesses and chaos. / Augusto Luiz Cheffer de Melo. – Rio de Janeiro: UFRJ/ COPPE, 2021.

VIII, 74 p.: il.; 29,7 cm.

Orientador: Marcelo Amorim Savi

Tese (Doutorado) – UFRJ/ COPPE/ Programa de Engenharia Mecânica, 2021.

Referências Bibliográficas: p. 67-74.

1. Dinâmica Não Linear. 2. Ritmos Cardíacos. I. Savi, Marcelo Amorim. II. Universidade Federal do Rio de Janeiro COPPE, Programa de Engenharia Mecânica. III. Título.

***Para Luciana e Ana Lúcia*.**

AGRADECIMENTOS

Agradeço à minha família, principalmente à minha mãe Luciana e minha tia Ana Lúcia, por todo amor e cuidado que sempre recebi e pelas oportunidades imprecindíveis a toda minha trajetória. À Nathalya, por todo carinho e incentivo ao longo do tempo que estamos juntos e por ter escolhido dividir os desafios e conquistas (espero que incontáveis) daqui em diante.

Agradeço a todos os professores com os quais pude e posso contar no interminável processo de aprendizado. Em especial, ao professor Marcelo Savi, pela orientação na realização desta pesquisa; e a longa e contínua transmissão de ensinamentos e conselhos sobre atividades acadêmicas, docência e produção científica.

Aos grandes amigos Alberto, Gabriel, Philippe, Raphael, Ribas e Ricardo, por permanecerem presentes e pela manutenção das discussões filosóficas etílicas. A Jean Frazzoli, cujo brilhantismo continua influenciando os que tiveram a experiência singular de seu convívio. Aos colegas de trabalho no Mecanon pelos auxílios, críticas e principalmente pela manutenção de um ambiente harmonico, sem deixar de mencionar que, seja nas conversas no café ou no boteco, é sempre um prazer inenarrável.

Por fim, agradeço à Coordenação de Aperfeiçoamento de Pessoal de Nível Superior (CAPES) e à Fundação Carlos Chagas Filho de Amparo à Pesquisa do Estado do RJ (FAPERJ), pelo apoio financeiro, fundamental para a realização deste trabalho.

Resumo da Tese apresentada à COPPE/ UFRJ como parte dos requisitos necessários para a obtenção do grau de Doutor em Ciências (D.Sc).

ANÁLISE DOS RITMOS CARDÍACOS USANDO UMA PERSPECTIVA DINÂMICA: NÃO-LINEARIDADES, ALEATORIEDADES E CAOS

Augusto Luiz Cheffer de Melo

Outubro/2021

Orientador: Marcelo Amorim Savi

Programa: Engenharia Mecânica

Os ritmos biológicos são fundamentais para a compreensão do funcionamento fisiológico dos organismos, sendo úteis na prevenção e tratamento de doenças. O ritmo cardíaco é um exemplo notável de biorritmos, sendo tratado neste trabalho pela avaliação da atividade elétrica do coração, registrada pelo eletrocardiograma (ECG). Um modelo matemático composto por três osciladores não lineares acoplados com defasagem temporal é empregado para a descrição do sistema cardíaco. Simulações numéricas fornecem ECGs sintéticos, que reproduzem uma grande variedade de respostas cardíacas, incluindo comportamentos normais e patológicos. Nesse sentido, a modelagem matemática pode ser útil para destacar tipos distintos de comportamentos, o que pode ser interessante para aplicações clínicas. Ainda, as simulações numéricas são comparadas com ECGs experimentais. Além disso, situações determinísticas e não determinísticas são tratadas mostrando a possibilidade da combinação de aspectos não lineares e aleatórios para definir a complexidade dos ritmos cardíacos. Aspectos não determinísticos são incorporados considerando conexões aleatórias entre osciladores. Duas abordagens estocásticas são aplicadas: paramétrica, considerando acoplamentos descritos por variáveis aleatórias; e não paramétrica, por meio da teoria da matrizes aleatórias. Diferentes ferramentas, incluindo mapas de Poincaré, diagramas de bifurcação, histogramas RR e expoentes de Lyapunov são empregados para mostrar possibilidades úteis em eventuais aplicações na identificação, monitoramento e controle de ritmos cardíacos.

Abstract of Thesis presented to COPPE/UFRJ as a partial fulfillment of the requirements for the degree of Doctor of Science (D.Sc).

ANALYSIS OF CARDIAC RHYTHMS USING A DYNAMICS PERSPEVTIVE: NONLINEARITIES, RANDOMNESSES AND CHAOS

Augusto Luiz Cheffer de Melo

October/2021

Advisor: Marcelo Amorim Savi

Department: Mechanical Engineering

Biological rhythms are fundamental for the comprehension of the physiological functioning of organisms, being useful in disease prevention and treatments. Cardiac rhythm is a remarkable example of bio-rhythms and is treated in this work by evaluating the electrical activity of the heart based on ECG observations. A mathematical model composed by three nonlinear oscillators coupled by time-delayed connections is employed for cardiac system description. Numerical simulations provide synthetic ECGs and a great variety of cardiac responses, including normal and pathological behaviors, is reproduced. In this regard, mathematical modeling can be useful to highlight distinct kinds of behavior, being interesting for clinical purposes. Also, numerical simulations are compared with experimental ECGs. Besides, deterministic and non-deterministic situations are treated showing the possibility of the combination of nonlinear and random aspects to define the rhythmic complexity. Nondeterministic aspects are incorporated by considering random connections between oscillators. Two stochastic approaches are investigated: parametric, considering couplings described by random variables; and non-parametric, by means of random matrix theory. Different tools including Poincaré maps, bifurcation diagrams, RR histograms and Lyapunov exponents are employed in order to show interesting possibilities that can help in identification, monitoring and controlling cardiac rhythms.

Table of Contents

1 INTRODUCTION

Natural phenomena have essential nonlinear characteristics responsible for the variety and richness of behaviors. Rhythms constitute one of the most relevant manifestations of natural systems being possible to be regular or irregular in time and space. In this regard, periodic and non-periodic dynamics can be related to either normal or pathological physiological functioning. This idea motivates the natural system analysis through a dynamical perspective that usually can be performed based on either mathematical models or time series analysis (Savi, 2005).

Chaotic dynamics is pointed out by several works as advantageous for biological systems in order to increase their adaptability. (Pool, 1989; Goldberger *et al.*, 1990; Skinner *et al.*, 1990). According to Pool (1989), "chaos may provide a healthy flexibility to the heart, brain, and other parts of the body". Classical dynamical invariants are widely employed to characterize biochaos, including power spectrum, fractal dimension and short-term predictability, having the Lyapunov exponents as the most widespread method. Chaos identification in cardiac and neural systems, which can be performed by time series analysis, has been treated in several research efforts (Herbschleb *et al.*, 1980; Chen *et al.*, 1998; Skanes *et al.*,1998; Glass & Mackey, 1988; Rapp, 1993).

The cardiac system is one of the possibilities where dynamical perspective has showing to be useful, being applicable either for clinical or control purposes. In brief, heart is a muscular organ activated by electrical stimuli with the function of pumping blood through all the organs and tissues of the body. In mammals, the heart is divided into 4 cavities: 2 atria and 2 ventricles, as shown in Figure 1-a. The conduction of the electrical impulse in the cardiac system can be understood as a network of self-excitatory elements formed by sinoatrial node (SA), atrioventricular node (AV) and His-Purkinje complex (HP) (Gois & Savi, 2009; Glass, 2009). The initial excitation occurs in the SA node, natural pacemaker, and propagates as a wave, stimulating atria. Upon reaching the AV node, it initiates a pulse that excites the bundle of His and, afterward, the Purkinje fibers. The fibers distribute the stimulus to the myocardial cells, causing the ventricles contraction (Dubbin, 1996).

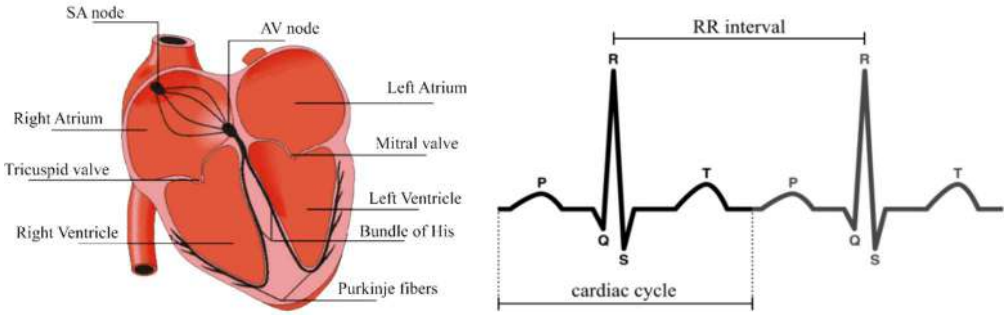

(a) (b)

Figure 1 – Schemes of: (a) human heart and (b) normal cardiac cycle.

A representative and widespread register of cardiac rhythm is the electrocardiogram (ECG) that records the heart electrical activity in the form of waves. In brief, it is possible to represent the electrical current in different areas of the heart allowing a comprehension about heart rhythms, elucidating the difference between healthy or pathological signals. Figure 1-b shows a schematic picture of an ECG normal cardiac cycle. Three important components should be pointed out: P wave, QRS complex and T wave. P wave represents the impulse generated by the SA node. The QRS complex is formed by ventricular contraction. T wave reflects ventricular repolarization.

A relevant analysis from ECGs is based on instantaneous heart rate variations using RR interval time series to define the so-called Heart Rate Variability (HRV) (Malik & Camm, 1995), which can be considered one of the best predictors of arrhythmic events (Mansier *et al.*, 1996). Unavoidable noise contamination demands reliable signal processing techniques (Goldberger & Goldberger, 1977) and, among them, it is important to cite the detection of R-peaks (Pan & Tompkins, 1985; Kaplan, 1990) and calculation of heart rate variability and breathing (Mood *et al.*, 1985; Malik & Camm, 1995).

Determinism and predictability in heart time series is explored by Gomes *et al.* (2000) and Lefebvre *et al.* (1993). Some works point that a chaotic response can be predicted for a short period (Abarbanel *et al.*, 1990; Farmer & Sidorowich, 1987; Sugihara & May, 1990), being explored by several papers treating cardiac dynamics. Govindan *et al.* (1998) investigated the existence of deterministic chaos in human ECGs by using surrogate data analysis, short term prediction, correlation dimension and Lyapunov exponents. Regression methods for prediction of short time series are treated by (Barahona & Poon, 1996; Poon & Barahona, 2001; Wu *et al.*, 2009).

HRV can be considerably different even in the absence of physical or mental stress and this information has been applied for clinical and research purposes. The existence of HRV points that, besides nonlinear characteristics, heart system can present some random behavior. Influences of external factors on the HRV as the increase of physical effort or breathing are treated by several researches. Glass (2009) discussed three main points: stochastic stimulus influences, respiratory influences and multiple feedback circuits. In a theoretical investigation of a modulation model of normal SA rhythm, Zhang *et al*. (2009) showed that the stochastic release of the acetylcholine regulator in the vicinity of the SA node leads to an irregular, chaotic-like rhythm. It is known that breathing influences heart rate in such a way that the heartbeat rate increases during inspiration and decreases on exhalation. Wessel *et al*. (2009) employed regression methods to investigate such coupling and concluded that the heart rate variability is directly caused by fluctuations on respiratory rate. Buchner *et al*. (2009) investigated the bidirectional coupling between respiration and cardiac rates using stochastic methods. Tobón *et al*. (2017) proposed a new method to HRV analysis for highly noised ECG signals, called MD-HRV (modulation domain HRV). This method is based on a spectro-temporal ECG representation, separating cardiac components from artifacts. Shiraishi *et al*. (2018) realized a HVR analysis that provides a real time visualization of power spectra during physical exercise. A group composed of healthy individuals and people who suffered heart attack provided the data. Wang *et al*. (2018) investigated differences between normal sinus rhythm (NSR) and congestive heart failure (CHF) by applying three approaches: time-domain, frequency-domain and non-linear indexes. Hu *et al*. (2019) developed a method based on seven time-scales to identify NSR and CHF using HRV measures of Physio Bank data. Recently, Iconaru *et al.* (2021) introduce a study to evaluate the efficiency of Poincaré maps in measuring reaction time variability in serial tests, whose results indicate satisfactory performance of the mentioned method.

Deterministic chaos and random noise of the heart rhythm analysis are compared by Kantz & Schreiber (2002). Bozoki (1997) developed a data acquisition method for fetal heart rate suitable to be used by both power spectral analysis (statistical) and chaos theory (deterministic). An analysis of canine ECGs made by Kaplan & Cohen (1990) suggested that fibrillation is similar to a random signal. It is also shown that a deterministic dynamical system can generate random-looking, non-chaotic behavior. The challenges to take decision between determinist or statistical analysis to treat human cardiovascular behavior are presented by Yates & Benton (1994). Deng et al. (2018)

presented an ECG identification framework via deterministic dynamical neural learning mechanism for human cardiac pattern classification. According to a symbolic analysis in atrial fibrillation surrogate data made by Aronis *et al*. (2018), pathological response is not driven by a rescaled linear stochastic process or a fractional noise. They supported the development of deterministic or nonlinear stochastic modeling. Son *et al*. (2019) developed a stochastic cardiovascular-pump model representing the effects of left ventricular assist devices on heart hemodynamics. Based on these references, it is possible to conclude that deterministic and random aspects are important for the comprehension of heart system dynamics.

The presence of different time scales in heartbeat time series is indicated by Peng et al. (1995). These results are extended by Alvarez-Ramirez et al. (2009) with the introduction of time lags into detrended fluctuation analysis. Biological time delays were identified in various cardiac feedback control loops. Multiscale methods have been employed to analyze multiscale organization and non-equilibrium dynamics, presenting better results in situations where the classical measures as power spectra and Lyapunov exponents do not present proper results. A review of these methods is presented by Costa et al. (2009).

An alternative for the heart dynamics analysis is via mathematical models. The first mathematical model to describe heart dynamics was proposed by van der Pol and van der Mark (1928) establishing an analogy between heartbeats and electrical circuits described by nonlinear oscillators. Some studies treated different aspects of AF, such as modeling of atrial tissue under atrial fibrillation (Moe *et al.*, 1964) and description of mechanisms that sustain atrial fibrillation (Jalife *et al.*, 1998). Different approaches of ventricular fibrillation are also presented, including reentry mechanisms that cause arrhythmias (Krinsky, 1978); and restitution properties and spiral wave behaviors of cardiac action potential (Fenton *et al.,* 1998, 2002). A review of the most relevant studies about mechanisms of initiation and maintenance of ventricular fibrillation is found in Jalife (2000). Nash & Panfilov (2004) presented an excitable tissue model capable of conducting nonlinear excitation waves, using a constitutive model of the deformed tissue. This model is able to reproduce reentry mechanisms that occur in arrhythmias such as flutter and fibrillation.

Grudzinski & Zebrowski (2004) proposed modifications on the original Van der Pol oscillator (Van der Pol & Van der Mark, 1928) in order to present a more suitable description of the natural pacemaker. Santos et al. (2004) presented a simplified cardiac

system model considering two asymmetrically coupled modified Van der Pol oscillators, representing the behavior of the two cardiac pacemakers, SA and AV nodules. Gois & Savi (2009) proposed a three-coupled oscillator model in order to represent ECG signals. Besides, SA and AV nodules, His-Purkinje complex (HP) is also considered on system modeling. Each oscillator is based on the model due to Grudzinski & Zebrowski (2004) and the system has bidirectional and asymmetric time-delayed couplings to represent the time spent on impulse transmissions. Jawarneh & Staffeldt (2019) developed a study of bifurcations on a modified van der Pol oscillator applying Conley index methods. Cardarilliet al. (2019) proposed a model with four modified Van der Pol oscillators representing the groups: SA and AV nodes, Right and Left bundle branches. This model is based on Fitz-Hugh-Nagumo equations (Ryzhii, 2013) and is motivated as an improvement to simulate branch blocks. Also considering Fitz-Hugh-Nagumo model to describe electrical activity, Pearce & Kim (2021) develop an mechano-electric feedback model by including the organ level dynamics (left ventricular pressure and volume) and contractile dynamics, which allows to study the influence of local mechanical demands over electrical response of the heart.

McSharry *et al.* (2003) presented a model based on a set of three ordinary differential equations to generate synthetic ECG signals. It also considers the respiratory sinus arrhythmia (RSA) where the frequency is calculated from a power spectrum with two Gaussian distributions. Based on the model due to McSharry *et al.* (2003), Evaristo *et al.* (2017) calculated the RSA frequency by using an autoregressive (RA) process, using Poincaré maps to compare results obtained by RA method with experimental data and numerical simulations. Mitchell & Schaeffer (2003) introduced a model for ventricular cardiac membrane dynamics consisting of two temporal functions, representing the membrane potential and current gating variable, both employing a first order ordinary differential equation. Ueno *et al.* (2018) employed Malthusian parameter and recurrence plots in order to investigate correlations between numerical data, generated using model of Gois & Savi (2009), and experimental data (PhysioBank). Silvestri *et al.* (2019) applied neural networks to obtain parameters that satisfy desired ECG signal features employing the model due to Ryzhii & Ryzhii (2014). This procedure allows to generate synthetic ECGs without a deep knowledge of the mathematical model.

The control of cardiac rhythms has been exploited by considering different approaches. Garfinkel *et al*. (1992, 1995) presented the first experiment of chaos control

on biomechanical systems, applying OGY method (Ott *et al.*, 1990) on rabbit cardiac muscle. Ferreira *et al.* (2011) employed time-delayed feedback control for natural pacemaker using a model proposed by Grudzinski & Zebrowski (2004). Afterward, Ferreira *et al.* (2014) employed the same technique for ECG signals built with three-coupled oscillators (Gois & Savi, 2009). Results showed stabilization of unstable periodic orbits embedded on chaotic attractors, avoiding critical situations.

Concerning stochastic modeling, several approaches can be applied for uncertainty quantification. A widely used approach in structural dynamics is the probabilistic approach (Jaynes, 2003). In this regard, the parametric probabilistic approach considers uncertainties in the model parameters, hence a probabilistic model is constructed to each parameter of the system; and the nonparametric probabilistic approach (Soize, 2000) considers uncertainties in the model itself, then a probabilistic model is constructed directly for the generalized matrices of the system. The rationale behind the idea of considering Random Matrix Theory to take into account model uncertainties can be found in Soize (2000), and in Ritto & Fabro (2019). A historical review of the Random Matrix Theory (RTM) can be found in Forester *et al.* (2003).

This work deals with the analysis of cardiac rhythms by considering a nonlinear dynamics perspective. The heart dynamics is described by a mathematical model of the electrical functioning of cardiac system, being represented by ECG signals. The present model is an improvement of the one due to Gois & Savi (2009), by including alternations in coupling terms in order to increase the capability to describe pathological behaviors. Basically, the model has three-coupled nonlinear oscillators with delayed connection. It is represented by delayed differential equations being able to capture the main aspects of heart dynamics, representing normal and pathological rhythms. The use of nonlinear tools, essentially Poincaré maps, Lyapunov exponents and bifurcation diagrams is exploited, showing the potential of these tools and the model itself in comprehension, description and identification of the complex behaviors of the heart. Besides, a global comprehension of the natural pacemaker behavior is provided by bifurcation diagrams for dissipation and external stimulus of the SA oscillator, which allows to identify different kinds of behaviors including chaotic responses. The influence of these different kinds of behaviors on the electrical activity of the heart, represented by ECGs, is investigated establishing a connection with distinct pathologies. Probabilistic approaches are also of concern considering either parametric and nonparametric analysis, contributing to the understanding the physiological details of cardiac system behavior,

which can motivate more efficient clinical strategies. In parametric approach random couplings are individually investigated showing that they can change the ongoing rhythm, inducing different pathologies. Nonparametric probabilistic approach relies on Random Matrix Theory (Mehta,1991) and Gaussian Orthogonal Ensemble (Weaver, 1989; Ritto & Fabro, 2019) to describe uncertainties of the cardiac system. The main idea is to use the proposed mathematical description and introduce random matrices that will create coupling terms, i.e., connections among the oscillators. With the proposed strategy model uncertainties are taken into account, and only one parameter, that controls the uncertainty level, needs to be calibrated. This is advantageous comparing with the strategy of considering individually eighteen uncertain coupling parameters.

The main contributions of this thesis can be resumed in the following topics, and their resultant publications: cardiac system model improvement and the use of nonlinear dynamics tools (Cheffer *et al*., 2021a; Cheffer & Savi, 2021); parametric probabilistic approach by using random couplings (Cheffer & Savi, 2020); and nonparametric approach based in Random Matrix Theory (Cheffer *et al.*, 2021b).

1.1 Work organization

The work is divided in six chapters. In this initial part, an introduction to the subject is made. Also, motivations, intended results and organization are presented. In addition, a brief description of the physiology and functioning of the heart is presented.

The second chapter describes the mathematical models of natural pacemaker and the cardiac system, including ECG generation. Also, two probabilistic modeling, Poincaré maps procedures and details of numerical integration are discussed.

Chapter 3 deals with numerical simulations, which provide some behaviors of the natural pacemaker (SA node), based on bifurcation diagrams; and the cardiac system, highlighting physiological aspects and their effects on the ECG.

Chapter 4 contains the application of Poincaré map procedures in cardiac system responses presented in the previous chapter.

In chapter 5 are presented responses obtained with probabilistic approaches. Results are analyzed by using RR histograms, states spaces and Poincare maps. Finally, chapter 6 presents the conclusions and suggestions for future works.

2 MATHEMATICAL MODELING

This chapter introduces the mathematical model for cardiac dynamics, including natural pacemaker model and cardiac system model. Besides, deterministic equations, the motivations and development of stochastic modeling are also discussed. Afterward, different procedures of construction of Poincaré Maps, numerical method, and Lyapunov exponents estimation are presented.

2.1 Natural Pacemaker Model

The mathematical modeling of the natural pacemaker is the starting point for cardiac modeling. Van der Pol oscillator is often used in the modeling of cardiac functions because its dynamic response presents typical characteristics of biological systems such as: limit cycle, synchronization and chaos (Grudzinski & Zebrowski, 2004; Gois & Savi, 2009). Besides, the Van der Pol equation exhibits an oscillation amplitude that does not depend on the oscillation rate. The model proposed by Grudzinski & Zebrowski (2004) is a modification of the original Van der Pol oscillator replacing the restitution force by a cubic function being expressed as follows:

$$\ddot{x} + \alpha\dot{x}(x - \nu_1)(x - \nu_2) + \frac{x(x+d)(x+e)}{d\ e} = F(t) \tag{1}$$

where α defines the pulse shape, characterizing the time when the heart receives the stimulus; ν_1 and ν_2 determine the signal amplitude, and in order to preserve the self-excitatory nature, $\nu_1\nu_2 < 0$; and $F(t)$ is an external stimulus.

The stability analysis of equilibrium points through the eigenvalues of the Jacobian matrix shows that the system exhibits 3 equilibrium points $(x, \dot{x})$: $(0, 0)$, $(-d, 0)$ and $(-e, 0)$, being respectively characterized by center, saddle and stable node (Grudzinski & Zebrowski, 2004).

2.2 Cardiac System Model

Cardiac system modeling, represented by ECG, can be made from the coupling of three nonlinear oscillators with asymmetrical and bidirectional connections as proposed by Gois & Savi (2009). Figure 2 shows the conceptual model of this approach. Note that the general model presents situations that do not occur in the normal

functioning, but they represent all possible conditions, in some cases associated to pathologies, that can appear in a real heart.

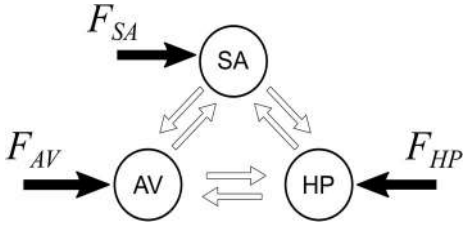

Figure 2 – Conceptual model of the general cardiac functioning represented by sinoatrial node (SA), atrioventricular node (AV) and His-Purkinje complex (HP) with asymmetrical and bidirectional connections. F_{SA}, F_{AV} and F_{HP} are external stimuli.

Therefore, the cardiac system can be modeled by three oscillators (SA, AV and HP) that are coupled by time-delayed terms that represent the transmitting time spent among each one of the oscillators. Each oscillator is described by the model due to Grudzinski & Zebrowski (2004), proposing some modifications in couplings in order to increase the model capability to describe pathologies. Based on that, the synthetic ECG obtained by the model is a result of the behavior of cardiac cells. Therefore, it can be understood as a macroscopic behavior related to the electrical activity of the heart, rather micro or mesoscopic behavior of the heart. Central nervous system stimuli are represented by limit cycle behavior and is considered external stimulus any input different from that exist in normal functioning. Under these assumptions, the cardiac system dynamics is governed by the following equations.

$$
\begin{aligned}
\dot{x}_1 &= x_2 \\
\dot{x}_2 &= F_{SA}(t) - \alpha_{SA} x_2 (x_1 - v_{SA_1})(x_1 - v_{SA_2}) - \frac{x_1 (x_1 + d_{SA})(x_1 + e_{SA})}{d_{SA} e_{SA}} \\
&\quad - k_{AV-SA} x_1 + k^{\tau}_{AV-SA} x_3^{\tau_{AV-SA}} - k_{HP-SA} x_1 + k^{\tau}_{HP-SA} x_5^{\tau_{HP-SA}} \\
\dot{x}_3 &= x_4 \\
\dot{x}_4 &= F_{AV}(t) - \alpha_{AV} x_4 (x_3 - v_{AV_1})(x_3 - v_{AV_2}) - \frac{x_3 (x_3 + d_{AV})(x_3 + e_{AV})}{d_{AV} e_{AV}} \\
&\quad - k_{SA-AV} x_3 + k^{\tau}_{SA-A}\, x_1^{\tau_{SA-AV}} - k_{HP-AV} x_3 + k^{\tau}_{HP-AV} x_5^{\tau_{HP-A}} \\
\dot{x}_5 &= x_6 \\
\dot{x}_6 &= F_{HP}(t) - \alpha_{HP} x_6 (x_5 - v_{HP_1})(x_5 - v_{HP_2}) - \frac{x_5 (x_5 + d_{HP})(x_5 + e_{HP})}{d_{HP} e_{HP}} \\
&\quad - k_{SA-HP} x_5 + k^{\tau}_{SA-HP}\, x_1^{\tau_{SA-HP}} - k_{AV-HP} x_5 + k^{\tau}_{AV-HP}\, x_3^{\tau_{AV-HP}}
\end{aligned}
\qquad (2)
$$

By considering indexes m and n that can represent SA, AV or HP, and $m \neq n$, equation terms are now explained: $F_m(t)$ are external stimuli; k_{m-n} and k^{τ}_{m-n} are coupling coefficients between m and n nodes; and $x_i^{\tau_{m-n}} = x_i(t-\tau_{m-n})$ are delayed terms, where τ_{m-n} is the time delay. Since the couplings have temporal delays, the system is governed by delayed differential equations (DDEs).

The mechanisms of initiation and maintenance of pathological rhythm motivate the assumption of external stimulus in the form $F_m(t) = \rho_m sin(\omega_m t)$. In general, it is mainly associated with reentry mechanisms (Krinsky, 1978), spatiotemporal periodic activity during atrial fibrillation (Skanes et al., 1998) and spiral waves behavior in ventricular fibrillation (Fenton et al., 1998, 2002). On this basis, external stimulus represents spatiotemporal aspects and therefore, is considered as a reduced order representation of spatiotemporal aspects. Note that the external stimulus increases the system dimension based on spatiotemporal information.

The ECG is formed by the signal of each one of the oscillators, being a linear combination of the state variables given by (Gois & Savi, 2009),

$$X = ECG = X_{SA} + X_{AV} + X_{HP} \tag{3}$$

where each oscillator is related to the following signals,

$$\begin{aligned} X_{SA} &= \frac{\beta_0}{3} + \beta_1 x_1 \\ X_{AV} &= \frac{\beta_0}{3} + \beta_2 x_3 \\ X_{HP} &= \frac{\beta_0}{3} + \beta_3 x_5 \end{aligned} \tag{4}$$

where β_0, β_1, β_2 and β_3 are constant coefficients. Therefore,

$$\dot{X} = \frac{d(ECG)}{dt} = \beta_1 x_2 + \beta_2 x_4 + \beta_3 x_6 \tag{5}$$

Since governing equations are presented in dimensionless form, it is interesting to define a dimensional time $\bar{t}$ $[s]$: $\bar{t} = \beta_t\, t$, where $[\beta_t] = s$ can be estimated by the ratio between experimental RR interval, RR_{exp}, and numerical RR interval, RR_{num}, i.e., $\beta_t = \frac{mean(RR_{exp})}{mean(RR_{num})}$.

It is important to highlight model improvements proposed in this work in comparison with (Gois & Savi, 2009). By observing physiological aspects of some pathologies (atrial flutter and fibrillation) arises the necessity to dissociate coupling terms $k(x_i - x_j^\tau)$ into $kx_i - k^\tau\, x_j^\tau$. Thus, are obtained responses qualitatively more adequate (rhythms and related responses presented in sections 3.2.1 to 3.2.5). Another improvement is the definition of β_t, in order to provide quantitative comparisons between experimental and numerical data.

A novel form to write the cardiac system model is proposed to enable the development of the approach based in Random Matrix Theory, which is also an innovative contribution. Therefore, the governing equations of cardiac system can be written in matrix form as follows (Cheffer *et al.*, 2021b):

$$\dot{\boldsymbol{x}} = \boldsymbol{H}(\boldsymbol{x}) + \boldsymbol{F}(t) + \boldsymbol{K}\boldsymbol{x} + \boldsymbol{K}^{\boldsymbol{\tau}}\boldsymbol{x}^{\boldsymbol{\tau}} \tag{6}$$

where $\boldsymbol{x}$ is the state space vector; $\boldsymbol{x^\tau}$ is the delayed state space vector; $\boldsymbol{H}(\boldsymbol{x})$ is the system vector field, which gathers the nonlinear oscillator terms; $\boldsymbol{F}(t)$ represents external stimuli; $\boldsymbol{K}$ is the coupling matrix; and $\boldsymbol{K^\tau}$ is the delayed coupling matrix. The definition of each one of these terms depends upon the choice of the format of state space vectors $\boldsymbol{x}$ and $\boldsymbol{x^\tau}$. One possibility is shown below:

$$\boldsymbol{x} = \begin{bmatrix} x_1 & x_3 & x_5 & x_2 & x_4 & x_6 \end{bmatrix}^{\boldsymbol{T}} \;;$$

$$\boldsymbol{x^\tau} = \begin{bmatrix} x_5^{\tau_{HP-SA}} & x_1^{\tau_{SA-AV}} & x_3^{\tau_{AV-HP}} & x_3^{\tau_{AV-SA}} & x_5^{\tau_{HP-AV}} & x_1^{\tau_{SA-HP}} \end{bmatrix}^{\boldsymbol{T}} \;;$$

$$\boldsymbol{H}(\boldsymbol{x}) = \begin{bmatrix} x_2 \\ x_4 \\ x_6 \\ -\alpha_{SA} x_2 (x_1 - \nu_{SA1})(x_1 - \nu_{SA}) - \dfrac{x_1(x_1 + d_{SA})(x_1 + e_{SA})}{d_{SA} + e_{SA}} \\ -\alpha_{AV} x_4 (x_3 - \nu_{AV})(x_3 - \nu_{AV2}) - \dfrac{x_3(x_3 + d_{AV})(x_3 + e_{AV})}{d_{AV} + e_{AV}} \\ -\alpha_{HP} x_6 (x_5 - \nu_{HP1})(x_5 - \nu_{HP}) - \dfrac{x_5(x_5 + d_{HP})(x_5 + e_{HP})}{d_{HP} + e_{HP}} \end{bmatrix}; \; \boldsymbol{F}(t) = \begin{bmatrix} 0 \\ 0 \\ 0 \\ F_{SA}(t) \\ F_{AV}(t) \\ F_{HP}(t) \end{bmatrix} \;;$$

$$\boldsymbol{K} = \begin{bmatrix} 0 & 0 & 0 & 0 & 0 & 0 \\ 0 & 0 & 0 & 0 & 0 & 0 \\ 0 & 0 & 0 & 0 & 0 & 0 \\ -(k_{AV-SA} + k_{HP-S}) & 0 & 0 & 0 & 0 & 0 \\ 0 & -(k_{SA-A} + k_{HP-AV}) & 0 & 0 & 0 & 0 \\ 0 & 0 & -(k_{SA-HP} + k_{AV-HP}) & 0 & 0 & 0 \end{bmatrix} \;;$$

$$\boldsymbol{K^{\tau}} = \begin{bmatrix} 0 & 0 & 0 & 0 & 0 & 0 \\ 0 & 0 & 0 & 0 & 0 & 0 \\ 0 & 0 & 0 & 0 & 0 & 0 \\ k^{\tau}_{HP-SA} & 0 & 0 & k^{\tau}_{AV-SA} & 0 & 0 \\ 0 & k^{\tau}_{SA-AV} & 0 & 0 & k^{\tau}_{HP-} & 0 \\ 0 & 0 & k^{\tau}_{AV-HP} & 0 & 0 & k^{\tau}_{SA-} \end{bmatrix}.$$

2.3 **Stochastic Models**

Coupling terms can be associated with nondeterministic aspects of the heart dynamics. In this regard, random aspects are incorporated in the mathematical model to perform a broader description of the cardiac dynamics. Therefore, probabilistic approaches are of concern considering either parametric and nonparametric analysis.

Concerning parametric modeling, coupling parameters can be described by random variables that follow probability models, such as uniform, exponential and gamma. A representative probability model for natural phenomena is the normal (or Gaussian) distribution. Therefore, coupling parameters are modeled as uncorrelated stationary Gaussian stochastic process $\{k_t, t > 0\}$, i.e., for each t the random variable k_t follows a normal distribution independent of $k_s,\ s \neq t$. Based on that, coupling terms can be written as follows,

$$\{k_t, t > 0\}\ ,\qquad k \sim N(\bar{k}\ , \sigma_k^2) \tag{7}$$

where $\bar{k}$ is the mean, nominal value, and σ_k is the standard deviation of the normal distribution. This approach is exploited in Section 5.1.

The idea of stochastic modeling of coupling terms can be extended by considering a nonparametric approach, that allows to describing uncertainties in the model itself and therefore, the probabilistic model is constructed directly for the generalized matrices of the system. This strategy is based in Random Matrix Theory and Gaussian Orthogonal Ensemble, which is treated in Section 5.2.

The considered nonparametric probabilistic model is based on Gaussian Orthogonal Ensemble, being employed by Ritto & Fabro (2019) to treat structural dynamics. The symmetry is preserved by the following random germ matrix:

$$\boldsymbol{G_s} = (\boldsymbol{G} + \boldsymbol{G^T})/2 \tag{8}$$

where $\boldsymbol{G}$ is a random matrix with dimension $m \times m$, composed of independent and identically distributed Normal random variables, with zero mean and standard deviation

σ_M, algebraically $G_{ij} \sim N(0, \sigma_M^2)$. Therefore, only one parameter, σ_M, controls the level of uncertainty of the stochastic system.

The deterministic symmetric system matrix $\boldsymbol{X_{det}}$ is perturbed by the symmetric random matrix germ $\boldsymbol{G_s}$ yielding the symmetric random matrix $\boldsymbol{X_S}$:

$$\boldsymbol{X_S} = \boldsymbol{X_{det}} + \boldsymbol{G_s} \tag{9}$$

Note that $\boldsymbol{X_S}$ is symmetric by construction, and its mean value is $\boldsymbol{X_{det}}$.

2.4 Poincaré Map

Poincaré map is a stroboscopic representation of the dynamical system response. It reduces the time continuous dynamics to a discrete set of states, a map, allowing a better understanding of the global system dynamics. There are different ways to build a Poincaré map and two approaches are employed in this work: secant section and reference period.

2.4.1 Secant section map

Secant section map uses a geometrical inspiration to build Poincaré map. Figure 3 shows a schematic picture of the use of a secant plane to build a Poincaré map on state space. Basically, map points are related to the vector field that transversally crosses a specific section in the positive direction of ξ, defining a state space subspace.

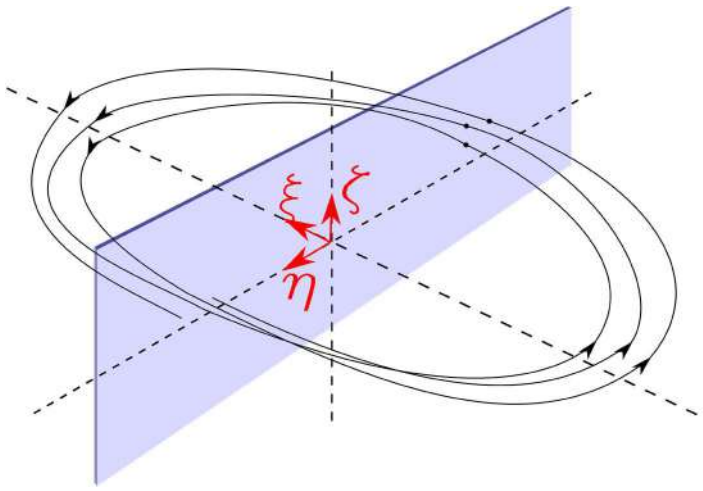

Figure 3 – Schematic picture of the Poincaré map construction using a secant section.

2.4.2 Reference period map

Poincaré map can be built by considering a reference period that defines the stroboscopic sample time. This procedure establishes the section position spaced by a period T through time, observing system dynamics states through the section, as presented in schematic picture of Figure 4.

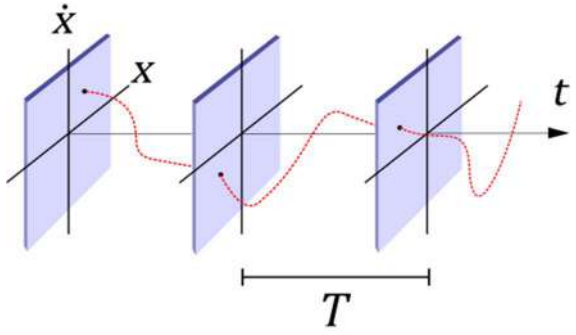

Figure 4 – Schematic picture of Poincaré map built using a reference period that defines the stroboscopic sample time.

2.5 Numerical Procedures

The fourth order Runge-Kutta method is used to integrate governing equations for pacemaker (eq. 1) and cardiac system (eq. 2) (Mensour & Longtin, 1998). In order to treat the DDEs system (eq. 2), it is necessary to approximate their solutions for time instants before τ_j. A Taylor series expansion is proposed (Cunningham, 1954; Gois & Savi, 2009).

$$x_i^{\tau} = x_i - \tau\left(\frac{x_{i+1} - x_i}{h}\right) \tag{10}$$

A convergence analysis reveals that time steps smaller than 10^{-3} presents error of the order of 10^{-6}, considered satisfactory.

Lyapunov exponents are important to be estimated in order to identify chaotic response of cardiac systems. The classical algorithm due to Wolf et al. (1985) is employed to estimate Lyapunov exponents for pacemaker model (eq. 1). The time-delayed states dependence, present in cardiac system model (eq. 2), requires an appropriate approach for calculating the Lyapunov exponents. The same procedure considered by Ferreira et al. (2011) is adopted in this work.

3 SIMULATIONS OF HEART RHYTHMS

This section presents results of pacemaker (eq. 1) and cardiac system (eq. 2), obtained by numerical integration. Initially, pacemaker dynamics is exploited by means of bifurcation diagrams, constructed for dissipation and external stimuli parameters. Thus, several pacemaker behaviors are identified.

In sequel, cardiac system is treated. Some heart rhythms, including normal and pathological behaviors, are described in terms of physiological and electrical aspects. Moreover, numerical responses (synthetic ECGs) are compared with experimental data. At the end of the chapter, the selected pacemaker responses are used to drive the cardiac system, which enables obtaining novel ECGs characteristics with clinical relevance.

3.1 Pacemaker simulations

Natural pacemaker behavior is now in focus considering the oscillator of the SA node, governed by a nonlinear differential equation. A global comprehension of the pacemaker behavior is obtained by considering bifurcation diagrams, that are built by using Poincare maps based on secant section. A section orthogonal to $\{x_1, x_2\}$ in $x_2 = 0$ is adopted and transversal intersections in negative x_2 direction are collected, as schematically showed in Figure 5. Initial conditions (Cheffer *et al.,* 2021a) are given by: $\{x_1, x_2\} = \{-0.1, -0.025\}$. Parameters for natural pacemaker normal functioning is presented in Table 1 that assumes that there is not an external stimulus $F(t) = 0$ (Ferreira *et al.*, 2011).

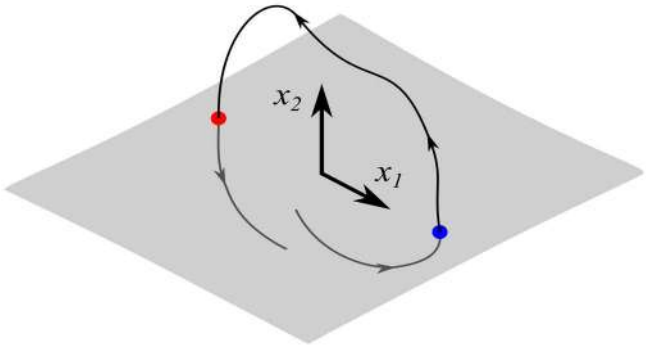

Figure 5 – Poincare Map employed to build bifurcation diagrams. Red and blue points are related to negative and positive x_2 directions, respectively.

Table 1- Natural pacemaker parameters associated with normal functioning (Cheffer *et al.*, 2021a)

α	ν_1	ν_2	d	e
3	1	-1.9	1.9	0.55

Natural pacemaker behavior is treated by evaluating the influence of two different parameters: dissipation and external stimuli. The analysis is based on bifurcation diagrams where different kinds of behaviors are identified by numbers that are employed from now on as representative of each kind of behavior. The slow quasi-static variation of parameters considers the last state of previous simulation as initial conditions.

3.1.1 **Influence of dissipation**

The influence of dissipation coefficient (α) is now of concern. Figure 6 presents the analysis of system response due to parameter variation. A bifurcation diagram is built by considering α in interval [0.5 ,9] with steps of 0.1 and simulations with $t \in [0\ ,1000]$. Different responses identified in the bifurcation diagrams are highlighted by considering phase spaces and time history. Note that bifurcation diagrams indicate regular responses that can be either periodic or quasi-periodic. Lyapunov exponent analysis points those responses are quasi-periodic since an extra null exponent is identified, in addition with time dimension. Besides, it is observed that as α increases, oscillator frequency decreases. It should be pointed out that the typical normal functioning is associated with response 2 ($\alpha = 3$).

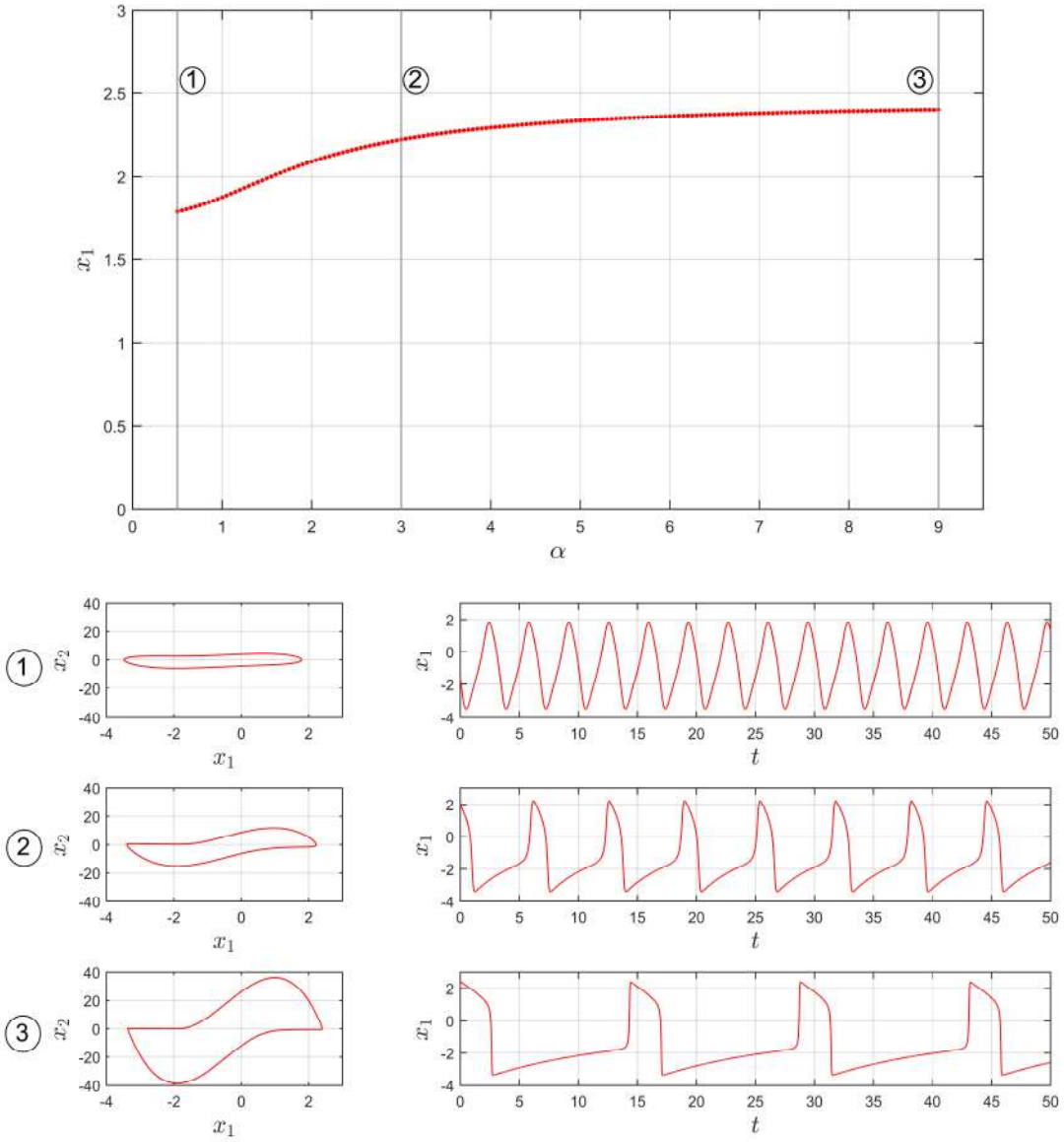

Figure 6 – Influence of dissipation α on natural pacemaker behavior. (Top) Bifurcation diagram; (Bottom) state spaces and time series referring to numbered responses marked in diagram.

3.1.2 **Influence of external stimulus**

This section evaluates the influence of external stimulus by considering a harmonic external stimulus, $F(t) = \rho\ sin(\omega\ t)$. On this basis, the investigation is based on two parameters: amplitude (ρ) and frequency (ω). The other parameters (including α) are related to normal functioning of the pacemaker presented in Table 1. In general, external stimulus induces pathological behaviors as atrial and ventricular fibrillation (Cheffer *et al.*, 2021a).

External stimulus amplitude analysis considers $\rho \in [0\ ,10]$ with steps of 0.025, simulations with $t \in [0\ ,5000]$, and a constant frequency is adopted, $\omega = 2.1$ (Cheffer *et al.*, 2021a). Figure 7 presents a bifurcation diagram, identifying four responses associated with chaotic-like behaviors. Each response has one positive exponent, which assure the existence of chaos. The following values are obtained for the maximum exponents: 0.06 (Response 4); 0.10 (Response 5); 0.14 (Response 6); 0.13 (Response 7).

External stimulus frequency is treated considering $\omega \in [0\ ,10]$ with steps of 0.025 and simulations with $t \in [0\ ,5000]$. Amplitude value is constant $\rho = 5.45$ (referring to response 4 in Fig.7 - first chaotic region) and the other parameters are related to normal functioning of the pacemaker (Table 1). Figure 8 presents bifurcation diagram showing different kinds of behaviors including chaotic-like responses and periodic windows. Selected responses are highlighted showing chaotic-like responses with positive Lyapunov exponents, with the following maximum values: 0.08 (Response8); 0.19 (Response 9); 0.32 (Response 10); 0.38 (Response 11); 0.38 (Response 12); 0.38 (Response 13).

It should be pointed out that parameter variations result in different kinds of responses that are related to electrical activity of the heart. Natural pacemaker is the driving signal that defines the electrical activity of the heart, represented by the ECG. The main objective to be treated in the section 3.2.6 is to establish a relation between each one of the natural pacemaker behaviors and the global electrical heart activity.

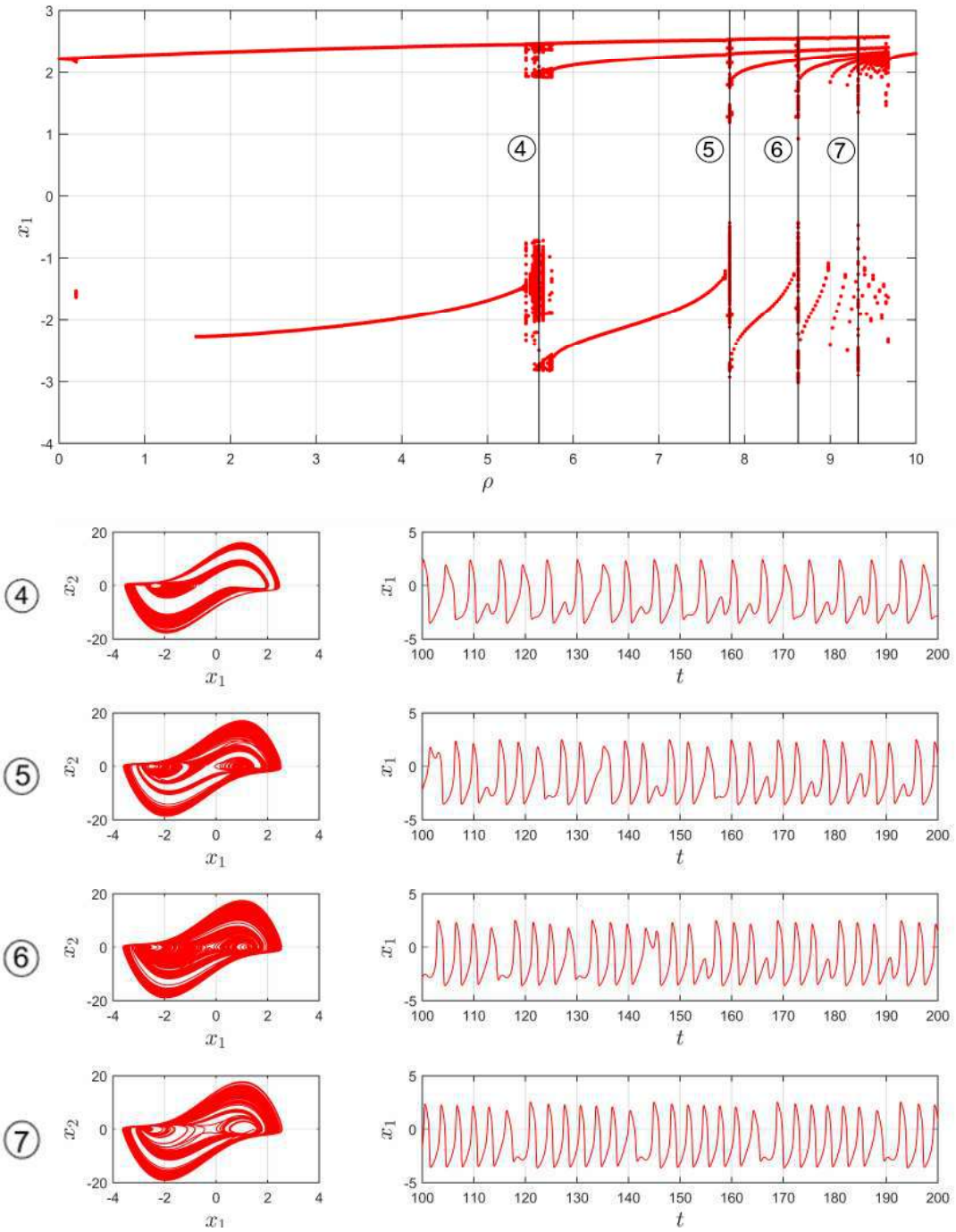

Figure 7 – Influence of external stimulus amplitude ρ on natural pacemaker behavior. (Top) Bifurcation diagram; (Bottom) state spaces and time series referring to numbered responses marked in diagram.

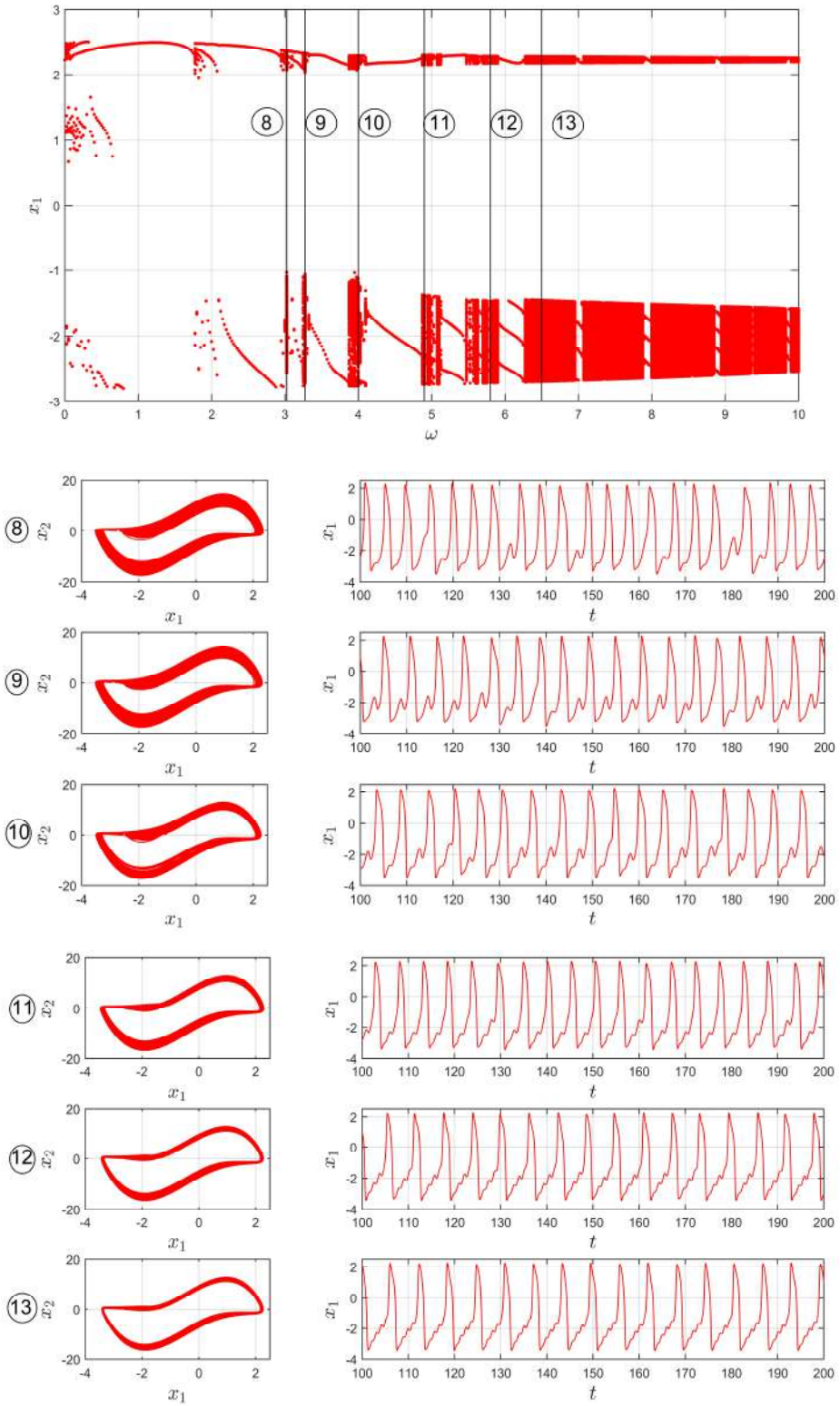

Figure 8 – Influence of external stimulus frequency ω on natural pacemaker behavior. (Top) Bifurcation diagram; (Bottom) state spaces and time series reffering to numbered responses marked in diagram.

3.2 Cardiac system simulations

Numerical simulations of the cardiac system model are performed with the objective of presenting different system behaviors. The idea is to compare normal and pathological responses represented by ECGs. Experimental ECG data available on *Physionet* (www.physionet.org) and Canabrava (2014) are used as a reference. In all simulations the following parameters are used: $\beta_0 = 1\,mV$, $\beta_1 = 0.06\,mV$, $\beta_2 = 0.1\,mV$, $\beta_3 = 0.3\,mV$; and the following initial conditions are applied (Ferreira *et al.*, 2014):

$$x_0 = \left[-0.1 \quad 0.025 \quad -0.6 \quad 0.1 \quad -3.3 \quad \frac{10}{15}\right]^T \tag{11}$$

Six cases are investigated in order to evaluate the model capability to represent heart dynamics: normal rhythm, atrial flutter, atrial fibrillation, ventricular flutter and two different ventricular fibrillation cases, with and without external stimulus. Table 1 summarizes parameter values employed for simulations of different cardiac rhythms. Each case is treated in the sequence, highlighting the conceptual model of each one of them, elucidating the parameters presented in Table 2.

Table 2– Cardiac system parameters.

	Normal rhythm	Atrial flutter	Atrial fibrillation	Ventricular flutter	Ventricular fibrillation with stimulus	Ventricular fibrillation without stimulus
SA oscillator						
α_{SA}	3	3	3	3	3	3
ν_{SA_1}	1	1.65	1	1	1	1
ν_{SA_2}	-1.9	-4.2	-1.9	-1.9	-1.9	-1.9
d_{SA}	1.9	1.9	1.9	1.9	1.9	1.9
e_{SA}	0.55	0.55	0.55	0.55	0.55	0.55
AV oscillator						
α_{AV}	3	7	7	3	3	3
ν_{AV_1}	0.5	0.5	0.5	0.5	0.5	0.5
ν_{AV_2}	-0.5	-0.5	-0.5	-0.5	-0.5	-0.5
d_{AV}	4	4	4	4	4	4
e_{AV}	0.67	0.67	0.67	0.67	0.67	0.67
HP oscillator						
α_{HP}	7	7	7	7	0.5	0.5
ν_{HP_1}	1.65	1.65	1.65	1.65	1.65	1.65
ν_{HP_2}	-2	-2	-2	-2	-2	-2
d_{HP}	7	7	7	7	7	7
e_{HP}	0.67	0.67	0.67	0.67	0.67	0.67
External stimuli						
ρ_{SA}	0	0	8	0	0	0
ρ_{HP}	0	0	0	0	30	0
ω_{SA}	0	0	2.1	0	0	0
ω_{HP}	0	0	0	0	0.8	0
Couplings						
k_{SA-AV}	3	0.66	0.66	3	3	3
k_{AV-HP}	55	14	14	45	30	14
k_{SA-AV}^{τ}	3	0.02	0.09	3	3	0.4
k_{AV-HP}^{τ}	55	60	38	20	30	38
Time delays						
τ_{SA-AV}	0.8	0.66	0.8	0.8	0.8	0.8
τ_{AV-HP}	0.1	0.1	0.1	0.1	0.1	0.1
Ratio experimental/numerical RR interval						
β_t	0.1048	0.0809	0.0230	0.1111	0.1048	0.5283

3.2.1 **Normal rhythm**

Normal heart rhythm has unidirectional couplings in such a way that the electrical impulse is conducted from SA node to AV node and then, from AV node to HP complex. External stimulus does not exist in this case. The conceptual model of this behavior is schematically represented in Figure 9.

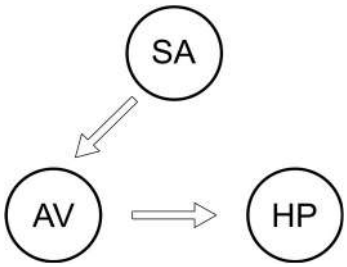

Figure 9 – Conceptual model of the normal heart functioning.

Figure 10-a shows experimental data of a normal ECG (www.physionet.org). Figure 10-b presents simulated normal ECG and each oscillator response that compose ECG response. Figure 8-c presents state space represented by subspace $\{X, \dot{X}\}$. Note that simulations capture the main features of the experimental ECG, presenting P, QRS and T waves, being in close agreement with experimental data.

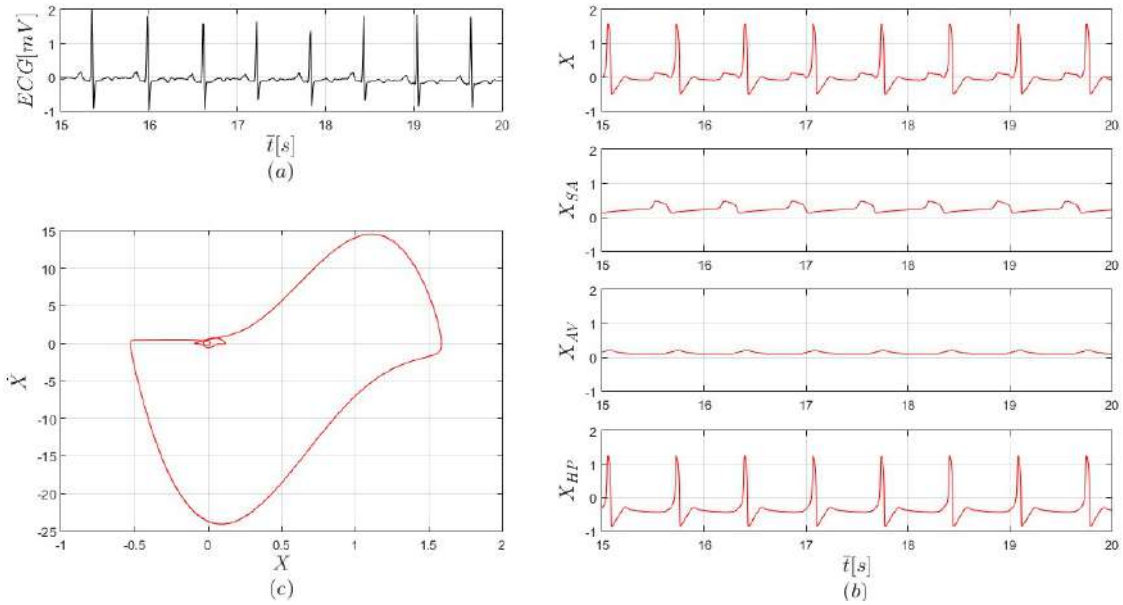

Figure 10 - Normal rhythm functioning by different perspectives: (a) experimental signal (physionet.com); (b) simulated time series response of ECG signal (X) and each oscillator (X_{SA}, X_{AV} and X_{HP}); (c) state space represented by subspace $\{X, \dot{X}\}$.

3.2.2 **Atrial flutter**

Atrial flutter is a rhythmic disorder classified as supraventricular tachycardia, characterized by very high atrial rate, usually 300bpm, ranging from 240 to 430bpm

(Brugada *et al.*, 1991). According to the electrophysiological mechanism, flutter is classified into two types: type I (or typical) and type II (or atypical). Type I is characterized by a macro-circuit of reentry in the right atrium with counterclockwise (most common) or clockwise rotation, presenting an ECG with P-waves with "sawtooth" form, called *f* waves (Canabrava, 2014). Atrial flutter of type II is also caused by a reentry macro-circuit, but does not present a defined pattern of rotation direction, being more complex (Obel & Camm, 1997).

Atrial flutter of type I is now of concern. Atrial flutter heart rate response depends on the refractory period of the AV node. Under normal conditions, AV node filters the atrial stimuli which means that if the AV nodule is half the atrial rate, the AV conduction is 2:1. Conceptual model is similar to the one employed to the normal ECG (Figure 9), making parameter changes in order to increase self-excitation frequency of the SA oscillator. In addition, coupling term value between SA and AV oscillators is reduced representing the filtering behavior of the SA signal frequency (see Table 2). Figure 11 presents different perspective of the atrial flutter including experimental data with 4:1 conduction (Figure 11-a), numerical simulation time series for the ECG and each node signal (Figure 11-b) and state space (Figure 11-c). It is noticeable the good qualitative agreement between numerical and experimental results.

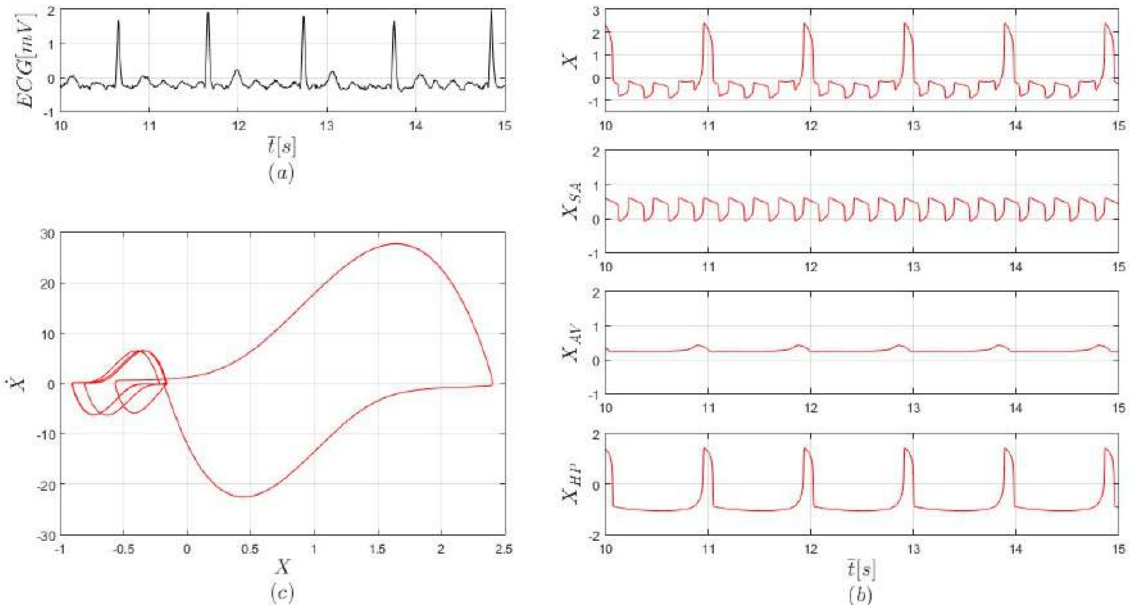

Figure 11 – Atrial flutter by different perspectives: (a) experimental data with 4:1 conduction (physionet.com); (b) simulated time series response of ECG signal (X) and each oscillator (X_{SA}, X_{AV} *and* X_{HP}); (c) state space plot of subspace $\{X, \dot{X}\}$.

3.2.3 **Atrial fibrillation**

Atrial fibrillation is a pathological heart rhythm characterized to the existence of several atrial reentry circuits. These multiple circuits are formed at different times and locations in the atrial myocardium, leading to chaotic atrial contraction, with a frequency of 400 to 600bpm (Fuster *et al*., 2006). This causes a non-effective atrial contraction, resulting in the formation of atrial thrombi that may break off and cause a cerebrovascular accident (CVA).

The AV node prevents these high-frequency stimuli to reach ventricles, promoting a filter that reduces frequencies to be from 90 to 170bpm, avoiding ventricular fibrillation. Atrial fibrillation is characterized by an irregular RR interval. In terms of mathematical model, the multiple ectopic foci may be represented by an SA node external stimulus. According to Skanes *et al.* (1998), "Reentry in anatomically or functionally determined circuits forms the basis of spatiotemporal periodic activity during AF (Atrial Fibrillation)". The conceptual model of this situation is shown in Figure 12. In addition, proper couplings need to be considered as presented in Table 2.

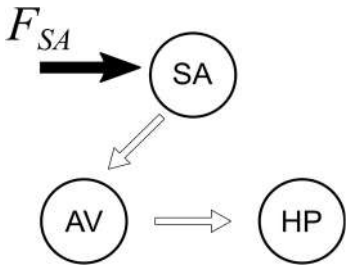

Figure 12 – Conceptual model of atrial fibrillation considering an external stimulus at the SA node.

Figure 13 presents results related to the atrial fibrillation. Figure 13-a shows experimental data where it is possible to observe the irregular RR interval. ECG numerical simulation is presented in Figure 13-b together with each oscillator response. Figure 13-c presents state space showing a dense region around the orbit of normal state space. It is noticeable that the model captures the general behavior of the experimental atrial fibrillation, presenting a RR interval irregularity and the actuation of the AV node as a pacemaker.

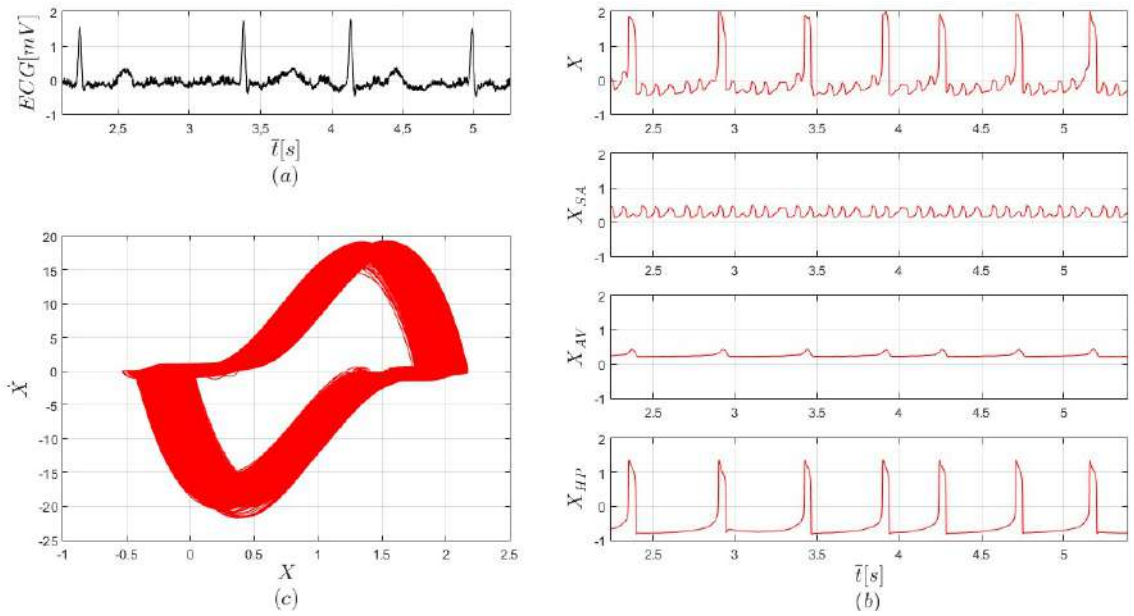

Figure 13 – Atrial fibrillation by different perspectives: (a) experimental signal (physionet.com); (b) simulated time series response of ECG signal (X) and each oscillator (X_{SA}, X_{AV} *and* X_{HP}); (c) state space plot of subspace $\{X, \dot{X}\}$.

3.2.4 **Ventricular flutter**

Ventricular flutter is a tachycardia caused by a single ectopic focus or peripheral reentry mechanisms. Usually, it evolves to ventricular fibrillation, the most dangerous pathological heart rhythm. High frequency ventricular contraction (300bpm) causes changes in muscle tissue stiffness in different cell groups, reflecting differences on the stimuli conduction velocity. Thus, multiple ventricular outbreaks are activated, establishing the fibrillatory process (Klein *et al.*, 1979).

Flutter are usually caused by chronic processes (hypertensive, atherosclerotic, rheumatic), but can be induced by acute myocardial infarction that end up seriously heart compromising. Typically, ventricular flutter ECG is characterized to present the QRS complex, the S-T segment and the T wave incorporated into a single bell large-wave form, differing from the atrial flutter *f* waves.

Ventricular flutter conceptual model is the same of the one employed to describe atrial flutter (Figure 9). Nevertheless, in order to obtain the effect of a ventricular ectopic focus, HP complex oscillator parameters are changed, keeping the other oscillator parameters equal to the normal case. Figure 14 presents ventricular flutter results. Figure 14-a shows an experimental response. Once again, numerical results presented in Figure

14-b capture the general experimental behavior, presenting an ECG with similar characteristics. Numerical state space is presented in Figure 14-c where it is possible to observe an enlargement of orbits around the greater loop of normal response.

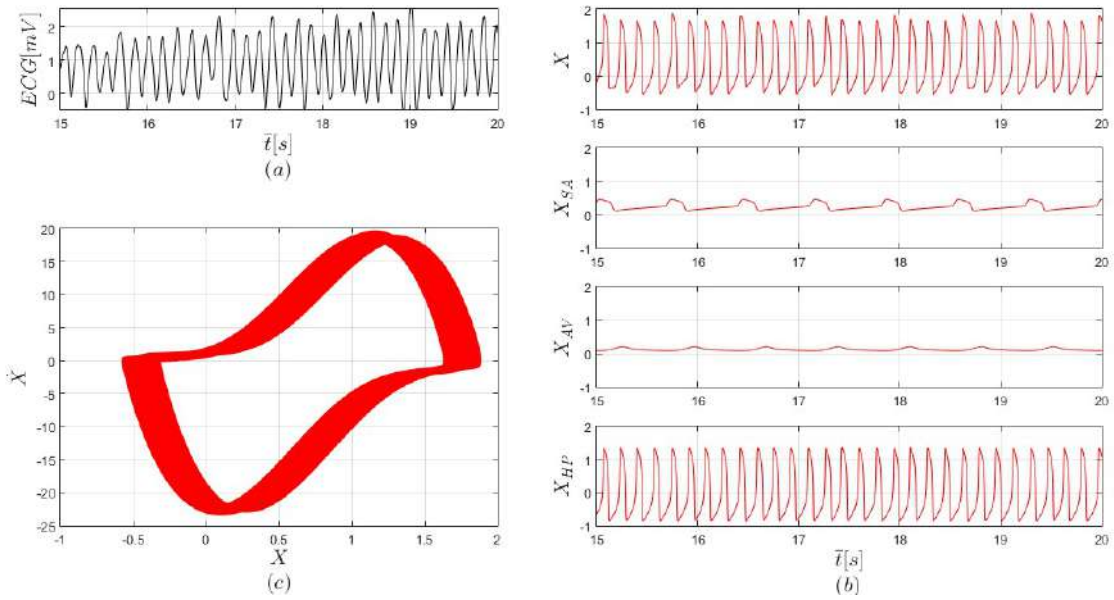

Figure 14 – Ventricular flutter by different perspectives: (a) experimental signal (physionet.com); (b) simulated time series response of ECG signal (X) and each oscillator (X_{SA}, X_{AV} and X_{HP}); (c) state space plot of subspace $\{X, \dot{X}\}$.

3.2.5 **Ventricular fibrillation**

Ventricular fibrillation is a disordered myocardial contraction due to the chaotic activity of several ectopic foci located in the ventricles. This behavior results in total heart pumping inefficiency and, from the hemodynamic point of view, corresponds to cardiac arrest (Klein *et al.*, 1979). The causes of ventricular fibrillation are similar to the ones of ventricular flutter: Purkinje ventricular fibers produce irregular electrical distribution that characterizes irregular tracing in which P waves, QRS complex and T waves are not recognized. There are several variations of ventricular fibrillation ECGs and some possibilities are shown in Figure 15.

Figure 15 – Different ventricular fibrillation experimental ECGs (Canabrava, 2014) characterized by irregular electrical distribution with irregular tracing in which P waves, QRS complex and T waves are not recognized.

There are different possibilities for the mathematical description of the ventricular fibrillation. Here, two alternatives are treated: with and without external stimulus. The first one uses a conceptual model presented in Figure 16, similar to the one employed to represent atrial fibrillation, but applying the external stimulus on the HP oscillator in order to represent multiple ectopic foci stimulation.

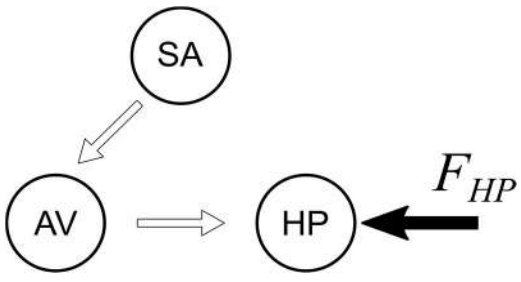

Figure 16 – Ventricular fibrillation conceptual model with external stimulus.

Figure 17-a shows experimental data. Figure 17-b shows ECG and individual oscillator time series with external stimulus. Note that simulated results represent the

irregular behavior of the ventricular fibrillation, being in agreement with the experimental ECGs. State space is presented in Figure 17-c, where a filled space indicating a chaotic-like response.

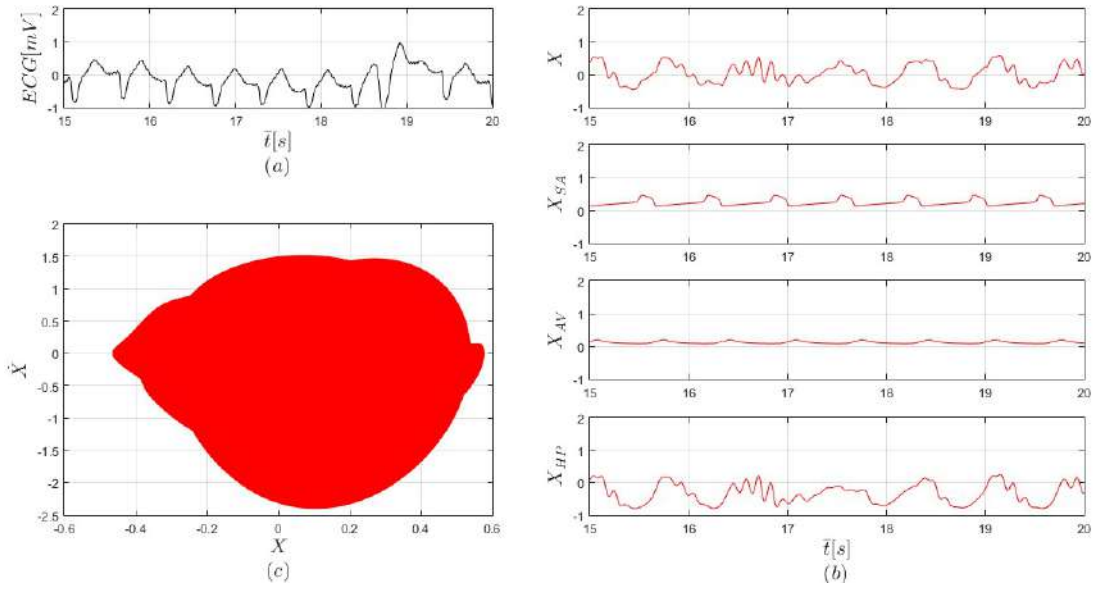

Figure 17 – Ventricular fibrillation with external stimulus: (a) experimental signal (physionet.com); (b) simulated time series response with external stimulus of ECG signal (X) and each oscillator (X_{SA}, X_{AV} and X_{HP}); (c) state space plot of subspace $\{X, \dot{X}\}$.

Another possibility to represent ventricular fibrillation is considering a conceptual model similar to the normal one, without external stimulus. The effect of multiple ectopic foci is now represented by different coupling parameters (see Table 2). Figure 18-a shows experimental data while Figure 18-b presents simulations related to ECG and each oscillator time evolution. Once again, a filled chaotic-like state space is shown in Figure 18-c.

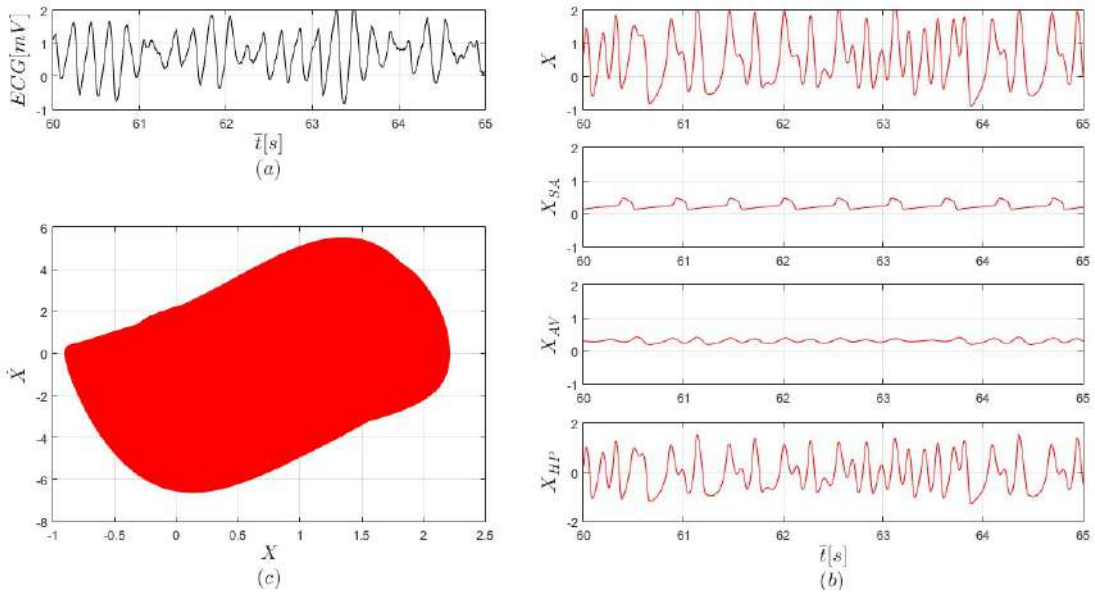

Figure 18 – Ventricular fibrillation without external stimulus: (a) experimental signal (physionet.com); (b) simulated time series response without external stimulus of ECG signal (X) and each oscillator (X_{SA}, X_{AV} and X_{HP}); (c) state space plot of subspace $\{X, \dot{X}\}$.

3.2.6 **Influence of different pacemaker responses**

This section develops an analysis of the influence of different pacemaker behaviors on the response of cardiac system, considering the behaviors discussed in section 3.1. In this regard, quasi-periodic and chaotic behaviors of the natural pacemaker are employed in order to evaluate the resulting cardiac system behavior represented by the ECG. Each pacemaker response is associated with a number identified in the bifurcation diagrams.

Initially, situations related to the variation of the dissipation parameter α, discussed based on the bifurcation diagram of Figure 6, are of concern. On this basis, ECG shown in Figure 19 are induced by quasi-periodic responses of the natural pacemaker. Response 1 (small dissipation) exhibits higher frequency and QRS complexes with double R peaks. State space is a closed curve with 4 large loops. Response 2 presents normal rhythm showing well defined main waves and its state space is a closed curve, with two loops: a small one (around $\{0,0\}$) and a large one (related to QRS complex). Response 3, with high dissipation, has a small frequency compared with the other cases,

and double R peaks, which is a characteristic of incomplete branch blocks. The state space is formed by a closed curve with one small and two large loops.

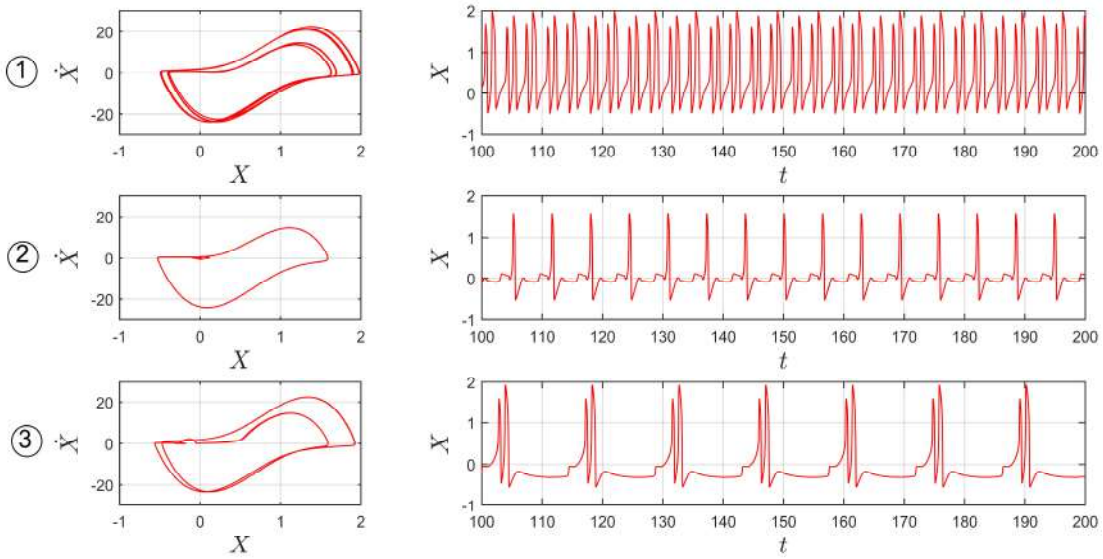

Figure 19 – Influence of dissipation α in ECGs. Each line shows simulated ECG (state space - left column, time series - right column) driven by numbered SA responses displayed in Fig.4.

Pacemaker responses associated with different stimulus amplitude ρ (Responses 4 to 7) are now investigated, as selected in bifurcation diagram shown in Figure 7. ECGs induced by these pacemaker signals, shown in Figure 20, allow the identification of some clinical characteristics. It is noticeable non-periodic rhythms, with irregular occurrence of R peaks, which is a characteristic of atrial tachycardia. In addition, double R peaks are identified, being associated with branch blocks. Alternations of the P and T waves are observed as well. P wave deviations are related to junctional tachycardia (Brugada *et al.*, 1991). Historically, the development of proper methods for identification of alternation of T waves is of great interest, since T wave alternations are useful as clinical indicator of cardiac sudden death (Barbosa *et al.*, 2004). State spaces are characterized by filled regions around large loops, indicating a high density of orbits than previous cases, pointing to a more complex response that, however, it is not easy to be observed through time series.

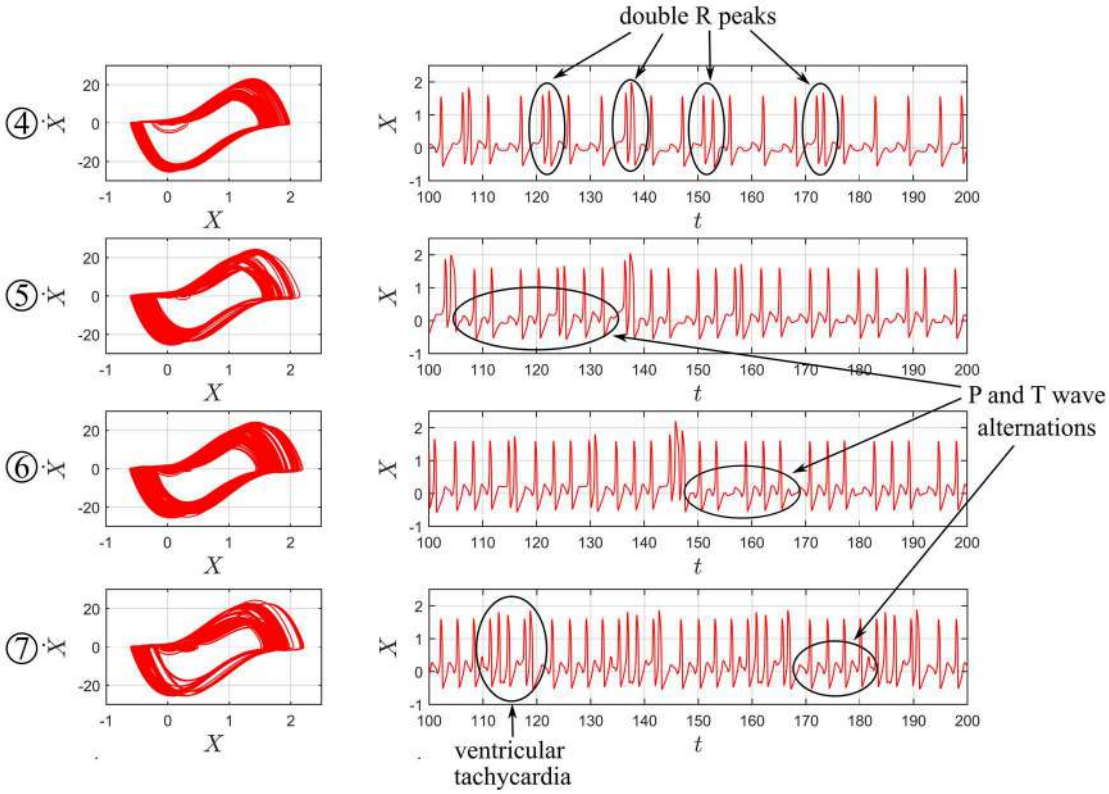

Figure 20 – Influence of stimulus amplitude ρ in ECGs. Each line shows simulated ECG (state space - left column, time serie - right column) driven by numbered SA responses displayed in Fig.5.

Figure 21 presents ECGs induced by responses associated with different stimulus frequency values ω, Responses 8 to 13 selected in bifurcation diagram showed in Figure 8. Simulated ECGs exhibit non-periodic rhythms, including alternation of single and double R peaks. It should be pointed out that these cases present deviations from normal rhythm being more pronounced in small oscillations (P and T waves). State spaces present filled regions around larger loop, with small density of orbits than the previous cases.

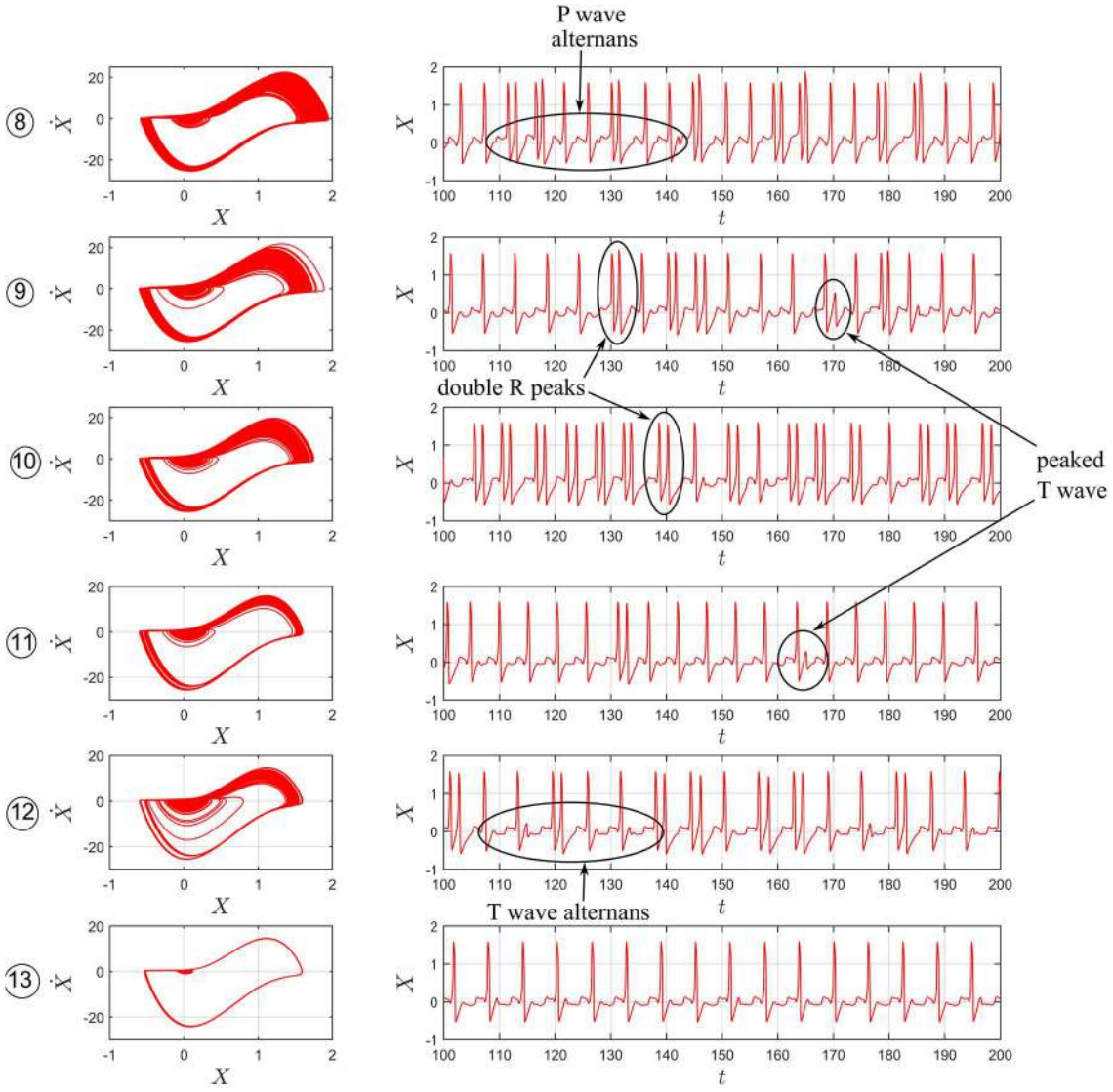

Figure 21 – Influence of dissipation ω in ECGs. Each line shows simulated ECG (state space - left column, time series - right column) driven by numbered SA responses displayed in Fig.6.

4 THE USE OF POINCARÉ MAPS

Poincare Map is employed to analyze cardiac systems. The rhythms reproduced in the previous chapter are of concern: normal, atrial flutter, atrial fibrillation, ventricular flutter the two types of ventricular fibrillation.

In order to obtain the quantitative measure of the dynamics of reproduced rhythms, Lyapunov exponents are evaluated for DDEs and it is concluded that normal and flutter (atrial and ventricular) are quasiperiodic responses while fibrillation (atrial and ventricular) is a chaotic response.

4.1 Secant section map

Heart dynamics analysis considers a subspace $\{x_1, X, \dot{X}\}$ where it is positioned a secant section according to the following equation, allowing the observation of states that crosses the section in the positive direction of x_1.

$$x_1 + \frac{6}{4}X - 3\dot{X} + 3 = 0 \tag{12}$$

Figure 22 presents system trajectory in blue, the Poincaré section, represented by the gray plane, and the projections of system trajectory in black and of Poincaré map in red. Different cardiac rhythms discussed in the previous section are evaluated: normal rhythm; atrial flutter; atrial fibrillation; ventricular flutter; ventricular fibrillation with and without external stimulus. It is noticeable that Poincaré maps furnish a system dynamics perspective different from which is usually employed in clinical purposes (time series). Thus, this strategy provides to health professionals additional information that may help to take decisions.

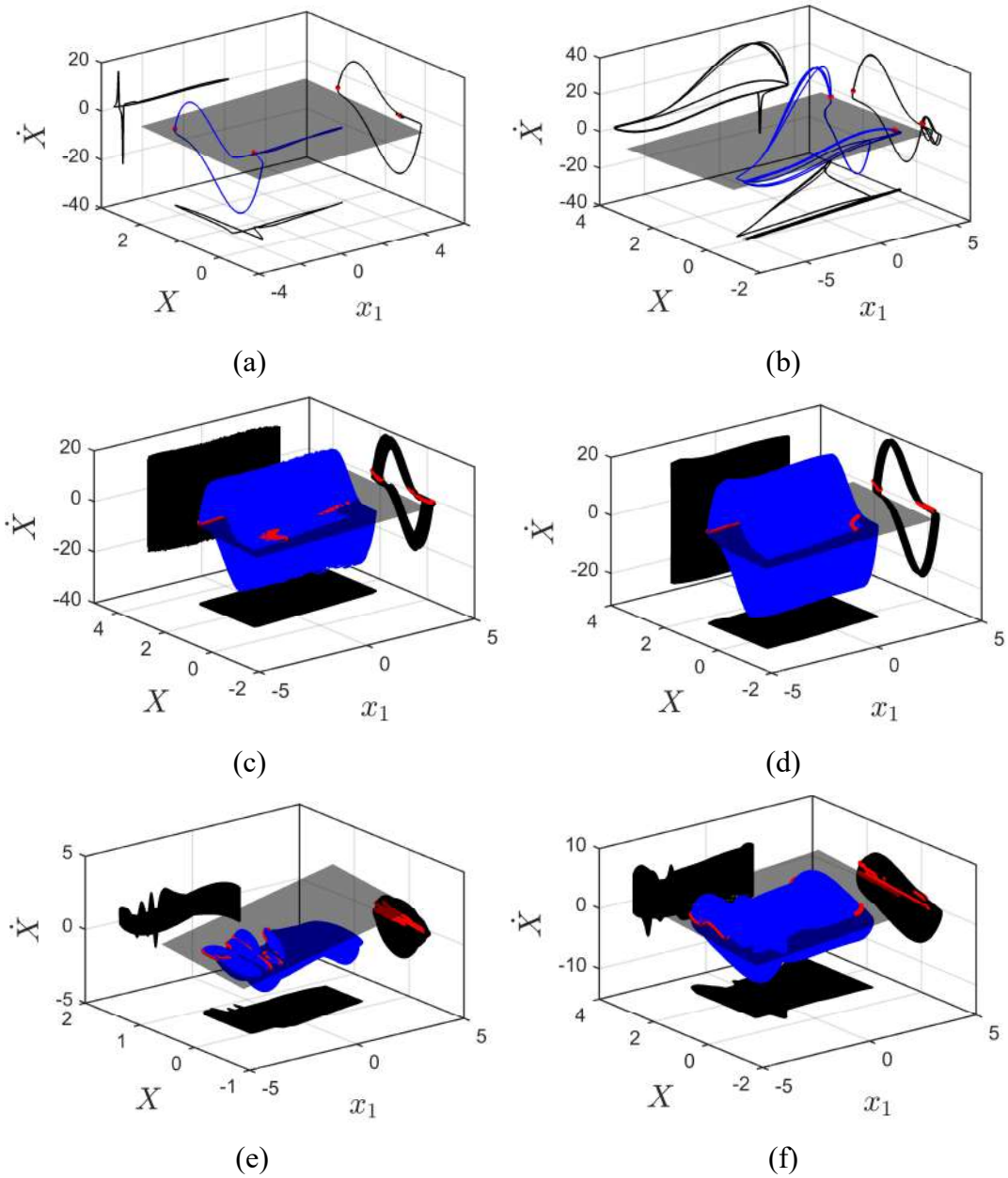

Figure 22 – Poincaré sections built with secant section approach. (a) Normal rhythm; (b) atrial flutter; (c) atrial fibrillation; (d) ventricular flutter; (e) ventricular fibrillation with external stimulus; (f) ventricular fibrillation without external stimulus.

Figure 23 presents an overlap of all the Poincaré maps in $A - B$ plane, allowing a comparative analysis among different rhythms. In general, it is possible to identify the main differences from the normal rhythm, considered as the system signature reference. Normal rhythm is characterized by a map containing two points (black). Atrial flutter has three clusters of points (purple). Ventricular flutter map covers one straight line and one

closed curve (yellow). Ventricular fibrillation without external stimulus shows a map (blue) with a discontinuous structure. This same kind of behavior is observed in the ventricular fibrillation with external stimulus (red). Atrial fibrillation map (green) also shows a discontinuous structure, with higher irregularity. This analysis suggests that critical pathological behaviors are distinguishable using Poincaré maps.

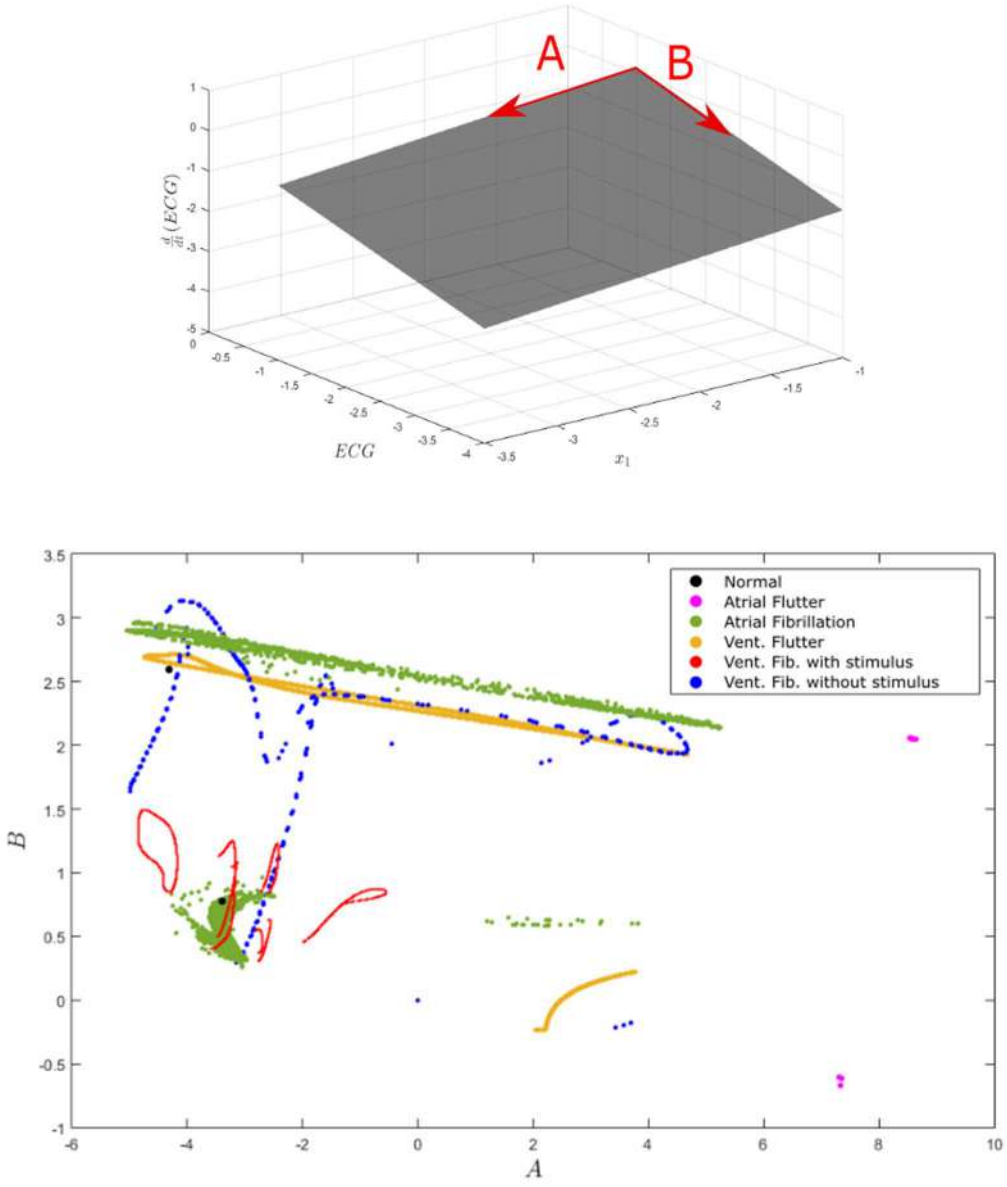

Figure 23 – Projections of Poincaré maps in $A - B$ plane built with secant section for different heart rhythms.

4.2 **Reference period map**

A straightforward approach to define reference period is when the system is subjected to a harmonic excitation, and the excitation frequency defines the reference period. Otherwise, it is necessary to define a proper reference period, a self-excitation period. The self-excitation period of the heart rhythm can be analyzed from the RR interval measurement. In this regard, a histogram of the RR interval is built, establishing the mean value, μ, that defines the reference period for the Poincaré map construction.

In the sequel, this procedure is applied to evaluate system dynamics considering results discussed in the preceding chapter. Note that atrial fibrillation and ventricular fibrillation with external stimulus are built using external excitation period; the other rhythms use the self-excitation period. Figure 24 presents RR interval histogram for the cases without external stimulus: normal rhythm, atrial flutter, ventricular flutter and ventricular fibrillation without external stimulus. Based on this analysis, it is possible to establish a mean value of each case that is employed to define the self-excitation period. Table 3 presents mean values of each one of the cases. By considering the ventricular fibrillation without external stimulus, it should be pointed out that there are two peaks 1.68 and 3.35 that can suggest another reference period.

Figure 25 presents Poincaré maps for all the cases, built with the appropriate procedure. It is again important to observe that Poincaré map is an interesting approach to identify the kind of response, since the rhythms can be more easily distinguished. It should be pointed out that ventricular fibrillation without external stimulus has other possibilities due to a two-peak RR interval histogram. Figure 26 presents the three possibilities, showing that they are similar.

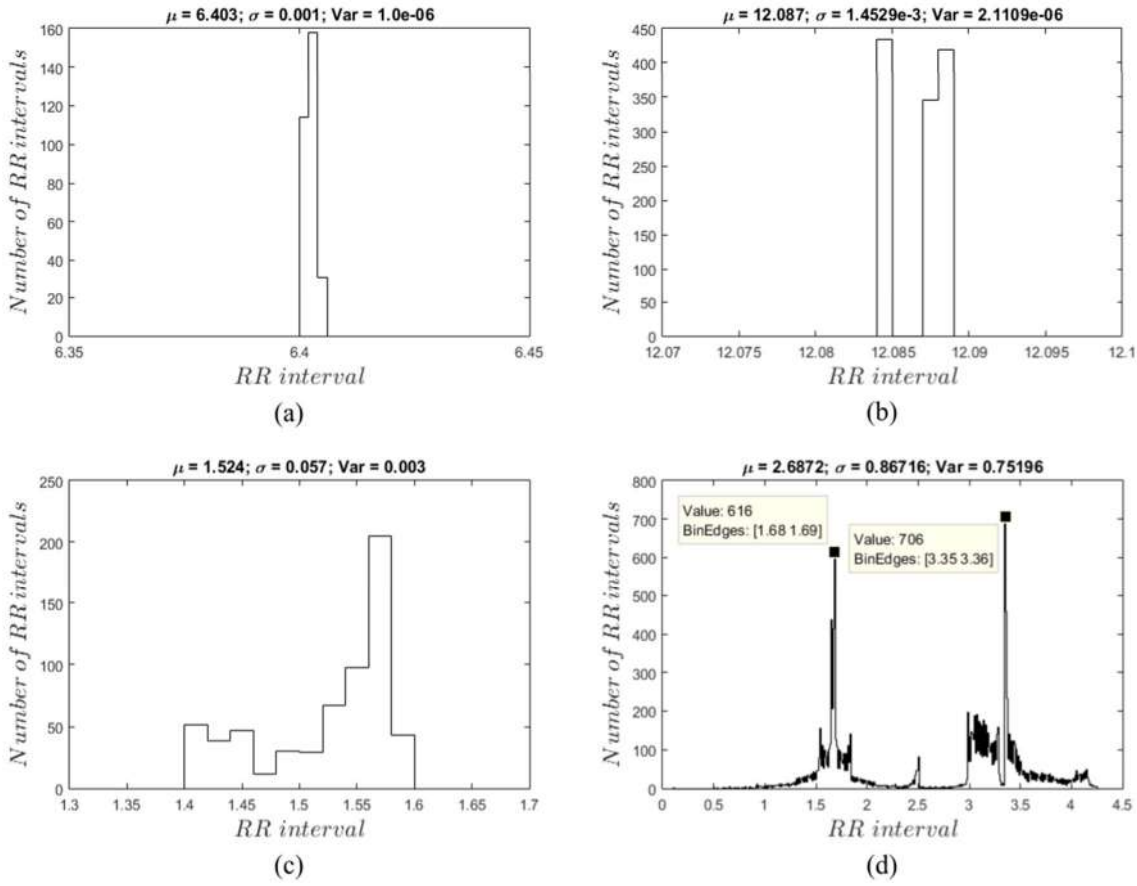

Figure 24 – RR interval histogram for different cardiac rhythms. (a) Normal rhythm; (b) atrial flutter; (c) ventricular flutter; (d) ventricular fibrillation without external stimulus.

Table 3 - Mean values employed as self-excitation period that defines Poincaré map period.

Heart rhythm	**Mean value** (μ)
Normal rhythm	6.403
Atrial flutter	12.067
Ventricular flutter	6.403
Ventricular fibrillation without external stimulus	2.67

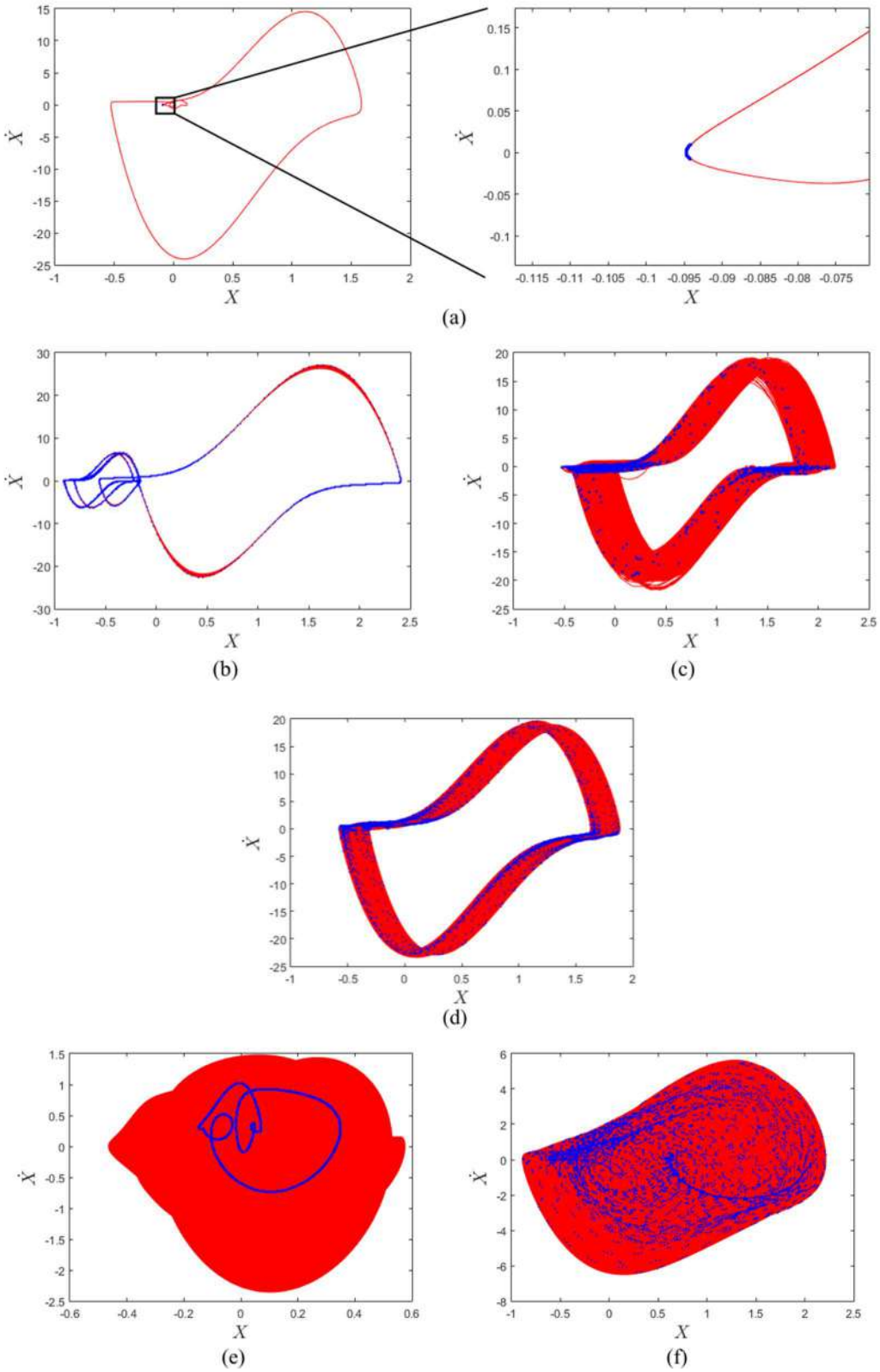

Figure 25 - Poincaré sections (blue) built with reference period. (a) Normal rhythm; (b) atrial flutter; (c) atrial fibrillation; (d) ventricular flutter; (e) ventricular fibrillation with external stimulus; (f) ventricular fibrillation without external stimulus.

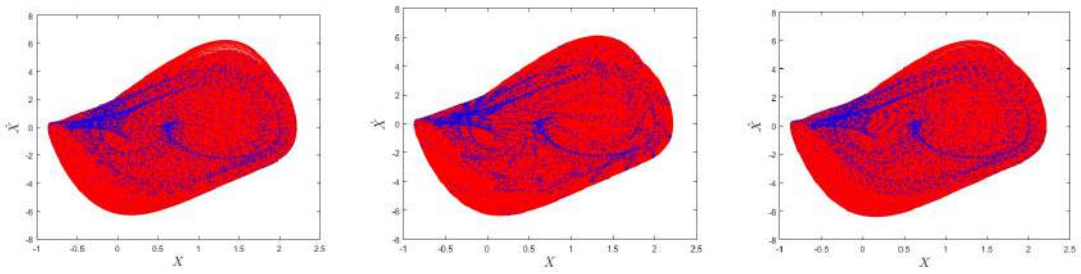

(a) (b) (c)

Figure 26 - Ventricular fibrillation without external stimulus ECG state space (red) and Poincare maps (blue) built with the following reference period: (a) $T = 1.68$; (b) $T = 2.67$ and (c) $T = 3.35$.

Figure 27 presents a comparative analysis of all rhythms using Poincaré maps built with reference period. Once again, it is possible to identify variations of pathological responses from the normal rhythm. Normal rhythm is not characterized by a point, but as a small neighbor (black). Atrial flutter (yellow) and ventricular flutter (purple) maps are closed curves with different amplitudes, representing a quasi-periodic behavior. Atrial fibrillation shows a chaotic-like map with two distinguishable clouds of points (green). Ventricular fibrillation with external stimulus has a closed curve map, with smaller amplitude compared with the previous cases (red). Ventricular fibrillation without external stimulus shows a chaotic-like attractor map (blue). Results allow one to obtain similar conclusions with the ones with the other Poincaré map construction, but point that different alternatives can be imagined to build Poincaré maps.

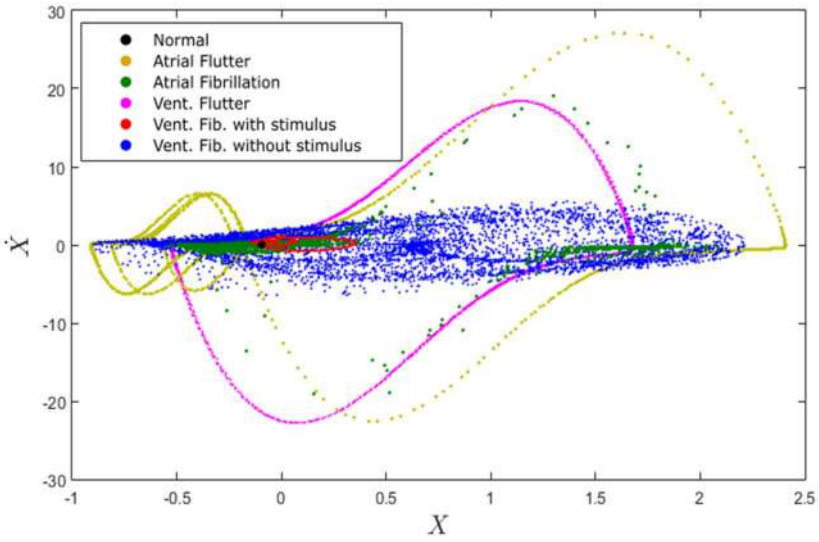

Figure 27 - Comparison of Poincaré maps built with reference period for different rhythms.

5 RANDOMNESS EFFECTS

Pathological responses are simulated by changing model parameters, exhibiting stationary behavior. The idea that heart rhythms have a stationary nature motivates some reflections about pathologies. The emerging of pathologies needs to be related to some parameter change, which makes sense especially considering external stimulus. Nevertheless, it is possible to imagine some different evolution due to random reasons. The next sections introduce the idea of random connections that can explain the evolution of pathologies from a normal rhythm. In this regard, two stochastic approaches are investigated: parametric, considering couplings described by random variables; and non-parametric, by means of random matrix theory.

Parametric approach, where the coupling parameters are individually exploited and vary with time according to a normal distribution is investigated as presented in Section 5.1. Non-parametric approach, where the random aspects are used to describe uncertainties of the model is investigated as discussed in section 5.2. This approach allows to simultaneously vary parameters and control the global level of randomness. Monte Carlo procedure is applied, in which, for each level of randomness, a set of simulations are performed with a set of coupling parameters that follow normal distributions. But in each simulation, the parameters do not vary along time.

5.1 Random parameters

Mathematically, this approach represents a stochastic process, which by definition is a sequence of random variables indexed to the time or events (Cataldo, 2012). Since mean and standard deviation are considered constant along time, the process can be classified as stationary of second order.

In next subsections are treated four couplings and are presented results for different processes (different standard deviations). Although is presented only one observation of each process, the duration of observations is sufficient (investigated by inspection) for the system to exhibit all dynamic characteristics that can be generated in each process.

It is important to highlight the difference between mean and standard deviation of the coupling distribution ($\bar{k}$ and σ_k) and the mean and standard deviation on RR interval histograms (μ and σ), discussed in the previous chapter.

5.1.1 **Random SA-AV coupling**

Consider the SA-AV coupling represented by the parameter $k_{SA-AV} \sim N(\bar{k}_{SA-AV}, \sigma_k^2)$. Normal heart function has a nominal value $\bar{k}_{SA-AV} = 3$. Figure 28 identifies the couplings, highlighting the random coupling.

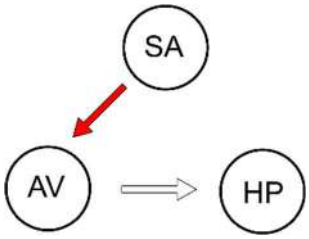

Figure 28 - Conceptual model with SA-AV random coupling.

Results for different values of standard deviation, σ_k, are presented in Figure 29 showing ECGs, phase spaces (red), Poincaré maps (blue) and RR histograms. Left column presents ECG time series and it is noticeable that the increase of σ_k induces incomplete and complete branch blocks (bb) (Canabrava, 2014) changing the ECG characteristic. Incomplete bb is characterized by QRS complex with double R peaks and complete bb causes absence of QRS complex. Pathological characteristics induced by the random coupling are highlighted and compared with experimental data. Phase planes and Poincaré maps (middle column) show that the increase of σ_k causes the spreading of orbits around the normal orbit and also the increase of Poincaré map space portion. RR interval histograms are shown in right column. When $\sigma_k = 0.5$, the RR is close to the deterministic case. When $\sigma_k = 1.5$, peaks appear below the reference RR, which may be related to incomplete bb, where the QRS complex has double R peaks. For values greater than $\sigma_k = 2.5$, response reaches a complete bb (absence of QRS complex), which is characterized by the appearance of peaks to the right of the histogram, corresponding to RR values greater than μ.

Figures 30 show comparisons of the RR histograms and Poincaré maps for the treated cases. The trend of decreasing the mean μ of the RR intervals with the increase of σ_k shows a correlation between the variability of the parameter k_{SA-A} and the Branch Block. Poincare Maps starts as a line (black) for normal case and, as σ_k increases, evolves to a cloud (red) around this line. For $\sigma_k = 1.5$, when incomplete bb appears, Poincare section changes its shape presenting also a curved cloud (green and blue) above the initial

cloud. When $\sigma_k = 3.5$, complete bb occurs and is possible to observe a spreading of the initial cloud (purple).

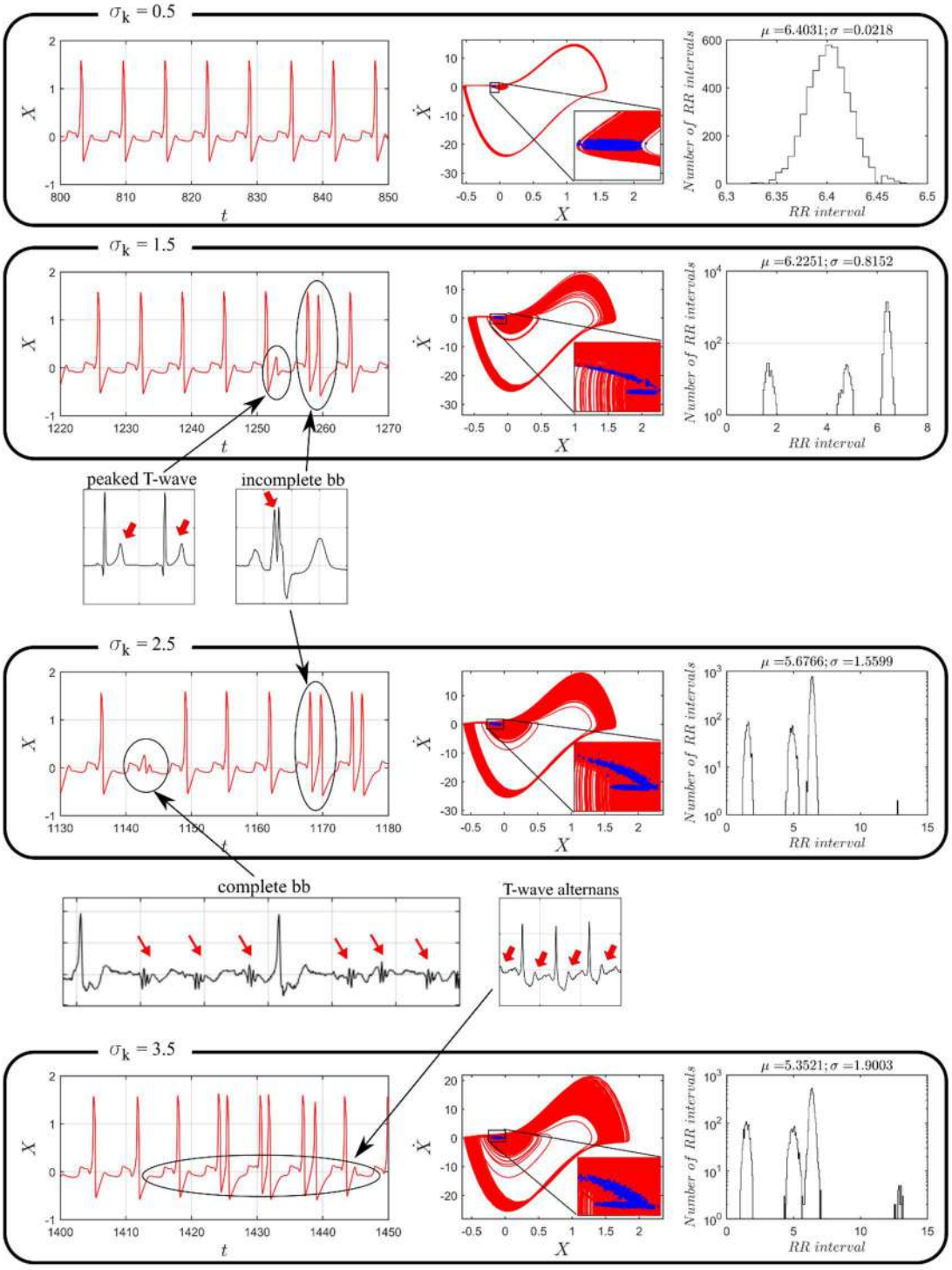

Figure 29 – Random SA-AV coupling results for different σ_k: (left column) synthetic ECGs; (middle column) phase plane (red) and Poincaré map (blue); and (right column) RR histogram. Also, identified pathologies are highlighted and compared with experimental data.

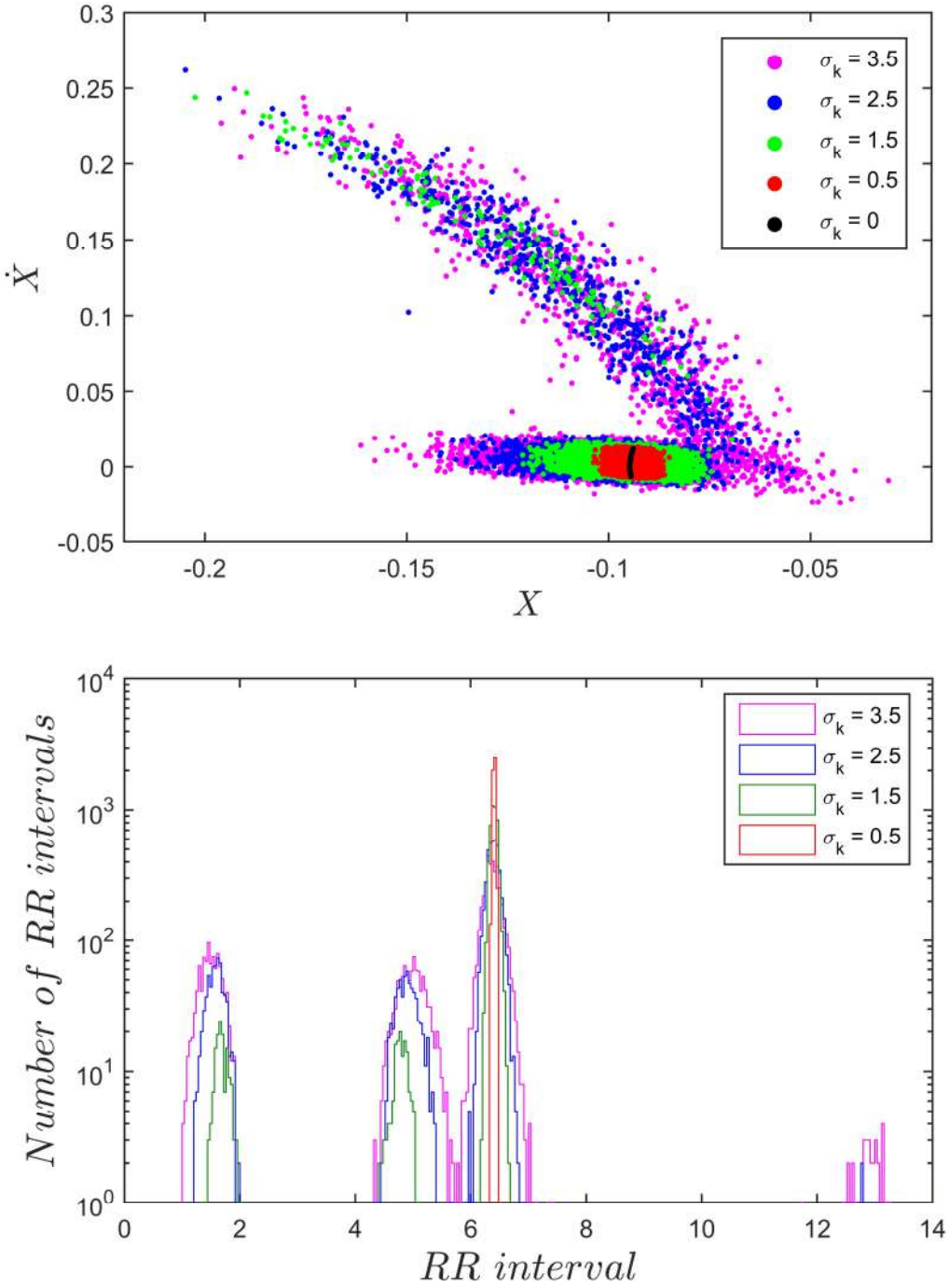

Figure 30 – SA-AV random coupling: (top) Poincaré maps for different standard deviations; (bottom) comparison of RR histograms for different standard deviations.

5.1.2 **Random AV-SA coupling**

Random variations of the coupling AV-SA are now in focus considering the conceptual model presented in Figure 34. This coupling is represented by the parameter $k_{AV-SA} \sim N(\bar{k}_{AV-} \quad, \sigma_k^2)$, where the normal ECG has a nominal value $\bar{k}_{AV-SA} = 0$.

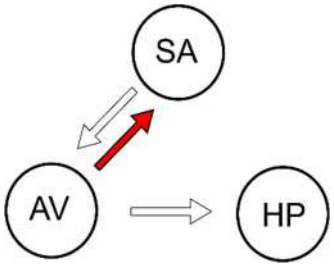

Figure 31 – Conceptual model of the AV-SA random coupling.

Results of different values of σ_k are presented in Figure 32. ECGs are show in left column. Note that the increase of σ_k is related to an increase of RR irregularity. This behavior is physiologically related to atrial fibrillation where irregular contractions in atria, caused by multiple electrical foci, are reflected in irregularities of the RR interval. Experimental data illustrate these changes. ECG state spaces and Poincaré maps are exhibited in middle column showing that for $\sigma_k < 0.5$, which responses in time series are apparently normal, there is significant change in state spaces and Poincare sections. For greater values: $\sigma_k = 2.0$ and $\sigma_k = 6.0$, incomplete and complete bb are related to analogous behaviors of the previous sections, but covering a larger area. Also, for $\sigma_k = 2.0$ it is possible to observe the appearance of bradycardia (reduction of cardiac frequency). The occurrence of atrial fibrillation, for $\sigma_k = 14.0$, is related to denser state spaces and Poincaré sections. RR interval histograms are shown in right column. Note that for $\sigma_k > 2.0$, RR values are distributed over a larger range than the previous case, which is reflected on the considerable increase of RR standard deviation. This spread of histogram values with Poincaré map patterns is an indication that the response presents chaotic characteristics.

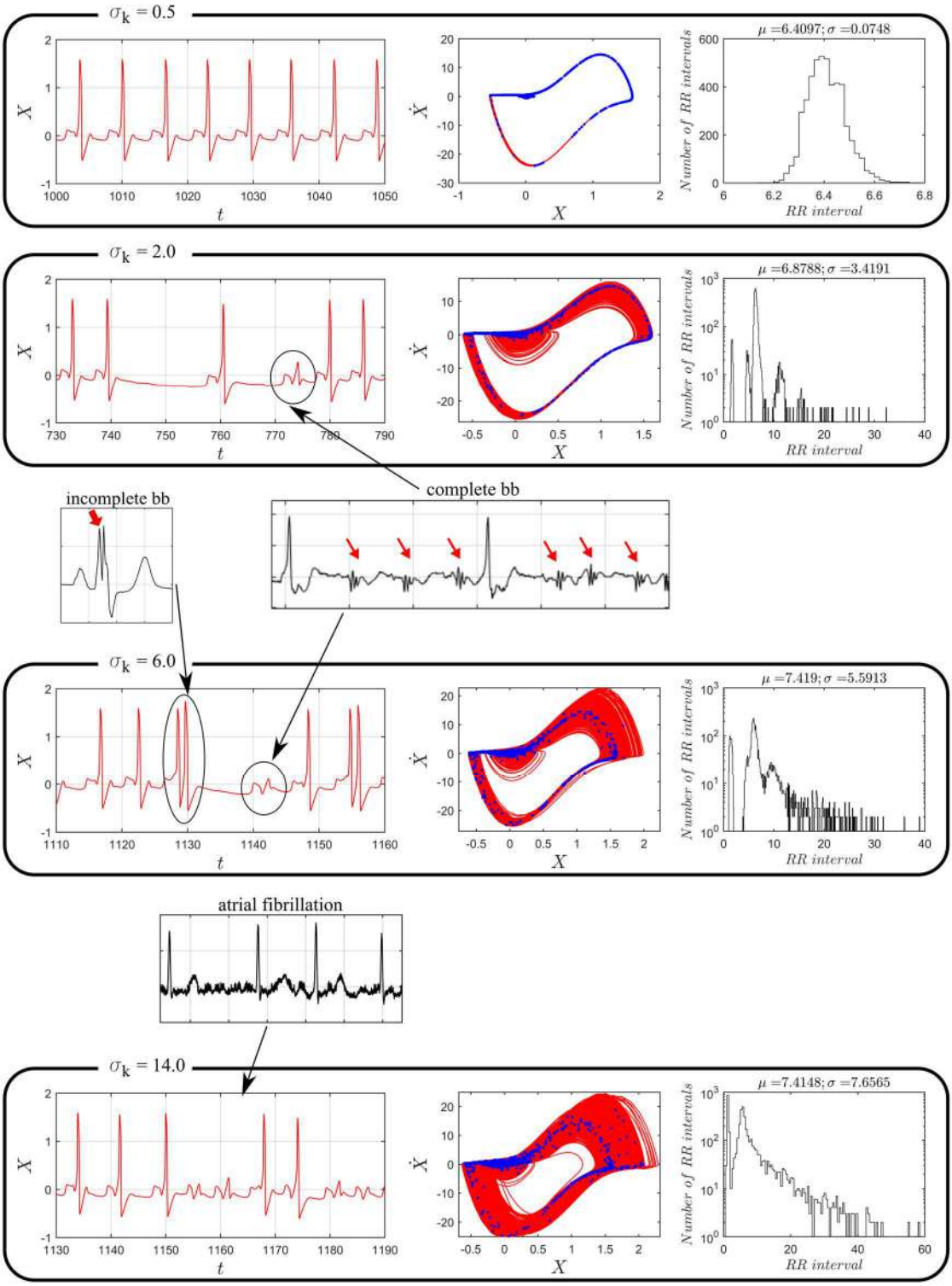

Figure 32 - AV-SA random coupling results for different σ_k: (left column) synthetic ECGs; (middle column) phase plane (red) and Poincaré map (blue); and (right column) RR histogram. Also, identified pathologies are highlighted and compared with experimental data.

Figure 33 provides comparisons of the RR histograms and the Poincaré maps. In this case, it is reasonable to think of a possible relation between the variability k_{AV-SA} and atrial fibrillation. In addition, it is observed that Poincaré maps occupy a region greater than the ones related to normal rhythm, which can be used as a diagnostic tool. In this case, while σ_k increases the evolution of histograms and Poincaré sections exhibit characteristics explained earlier for incomplete and complete bb and also characteristics that can be related to atrial fibrillation (larger range in histograms and area of the Poincaré sections).

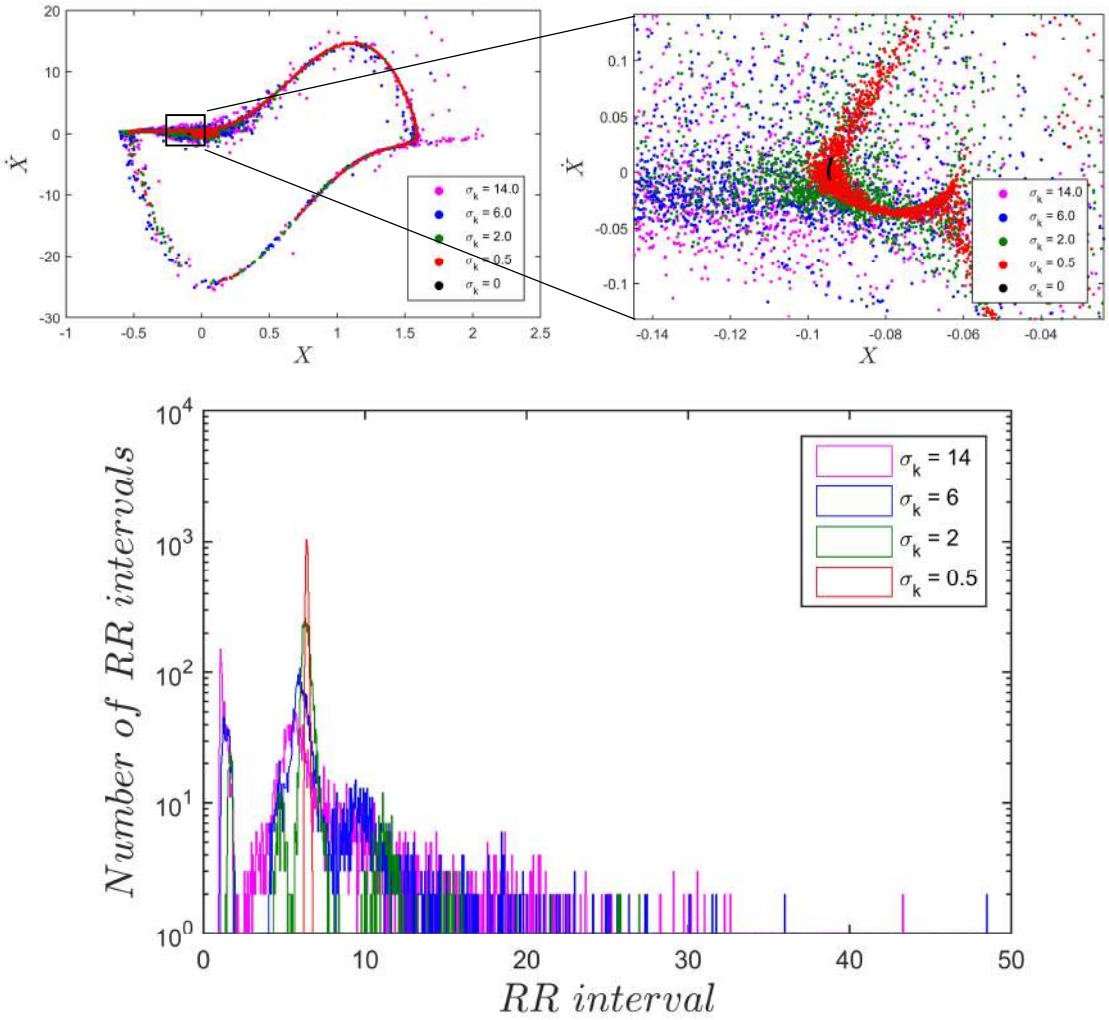

Figure 33 – AV-SA random coupling: (top) Poincaré maps for different standard deviations; (bottom) comparison of RR histograms for different standard deviations.

5.1.3 **Random AV-HP coupling**

Random AV-HP coupling is now of concern considering coupling parameter as $k_{AV-HP} \sim N(\bar{k}_{AV-H}, \sigma_k^2)$ with nominal value $\bar{k}_{AV-} = 55$. Figure 40 presents the conceptual model.

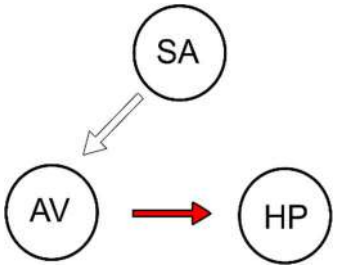

Figure 34 - Conceptual model for AV-HP coupling.

Figure 35 shows results considering different standard deviations, σ_k. In left column are ECG time series. For $\sigma_k < 55.0$, ECG does not have significant differences when compared to the normal one. Nevertheless, the increase of standard deviations tends to alter the ECG in a dramatic way. Initially appears peaked T-wave and incomplete bb, and in sequence, small QRS complexes and T-wave alternans. For $\sigma_k = 440$, occurs a behavior thar indicates a ventricular tachycardia (Dubin, 1996), where sequential R-peaks appear or QRS complex becomes greater due to irregular functioning of ventricles. Once again, experimental data confirm the changes helping their visualization. Middle column shows ECG state spaces and Poincaré maps. Even for imperceptible changes in time series (for $\sigma_k \leq 55.0$), it is possible to see significant changes in state space. Once again, one can observe characteristic changes of state space and Poincaré sections due to incomplete bb (for $\sigma_k = 110$ and $\sigma_k = 220$). It should be highlighted that the enlargement around the bigger loop of state space can be related to ventricular tachycardia ($\sigma_k = 440$), indicating a trend. RR histograms are presented in right column, where it is possible to observe a trend of decreasing the mean μ with the increase of σ_k. The occurrence of peaks smaller than the reference mean ($\mu = 6.403$) represent that R waves are becoming closer, which means that heart frequency is increasing, a behavior related to a ventricular tachycardia (Dubin, 1996).

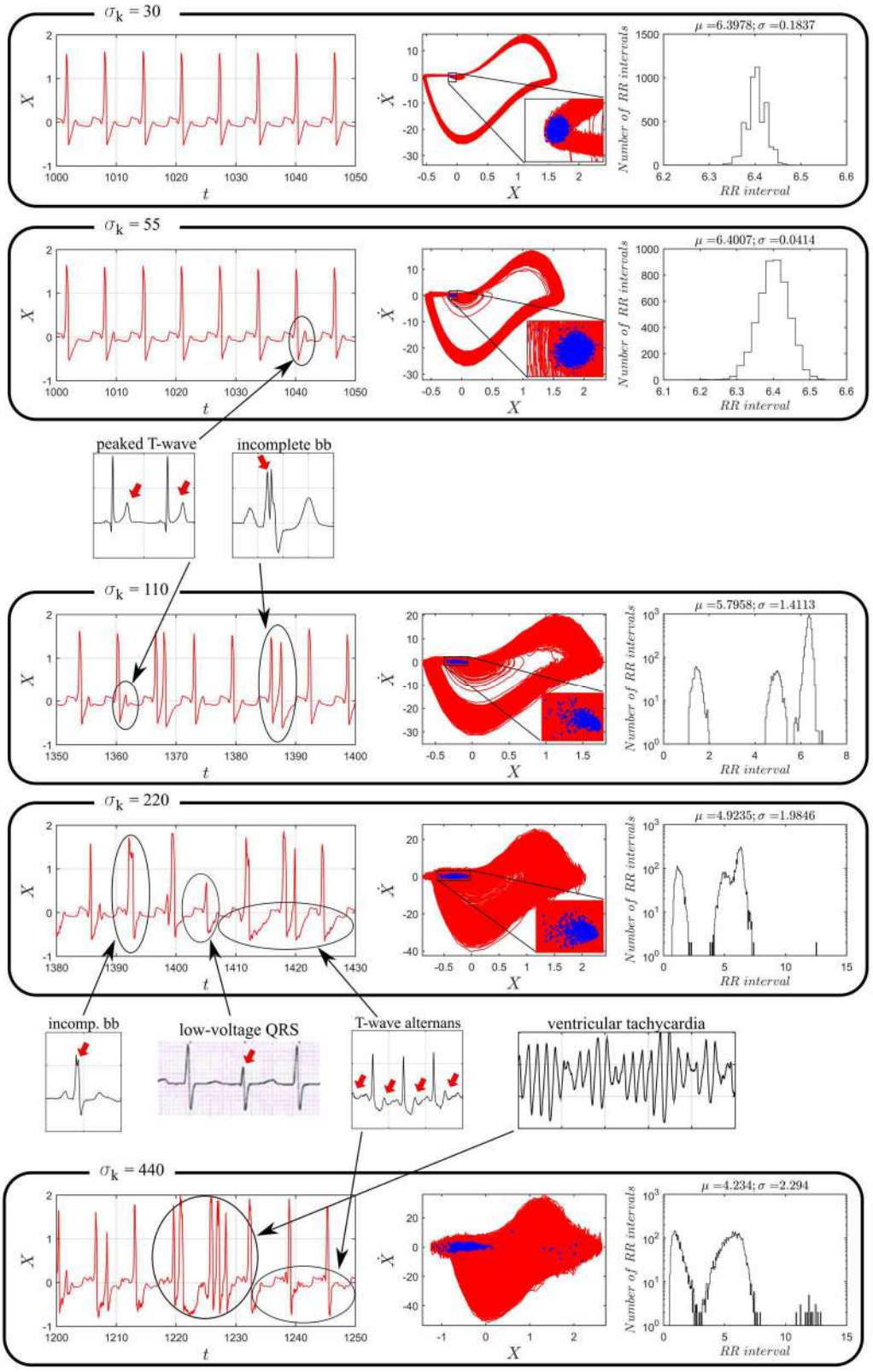

Figure 35 – AV-HP random coupling results for different σ_k: (left column) synthetic ECGs; (middle column) phase plane (red) and Poincaré map (blue); and (right column) RR histogram. Also, identified pathologies are highlighted and compared with experimental data.

Poincaré maps comparison is presented in Figure 36 (top). Once again, the increase of σ_k causes the Poincaré map spreading to a different pattern from previous cases. Incomplete bb response causes expansion of a cloud around normal Poincaré section, while ventricular tachycardia trends to stretch section to the left. This can be used to identify and classify different responses. A comparison of RR histograms is presented in Figure 36 (bottom). Note that peaks appear on left side of histogram reflecting the RR interval reduction caused by closer and closer R peaks.

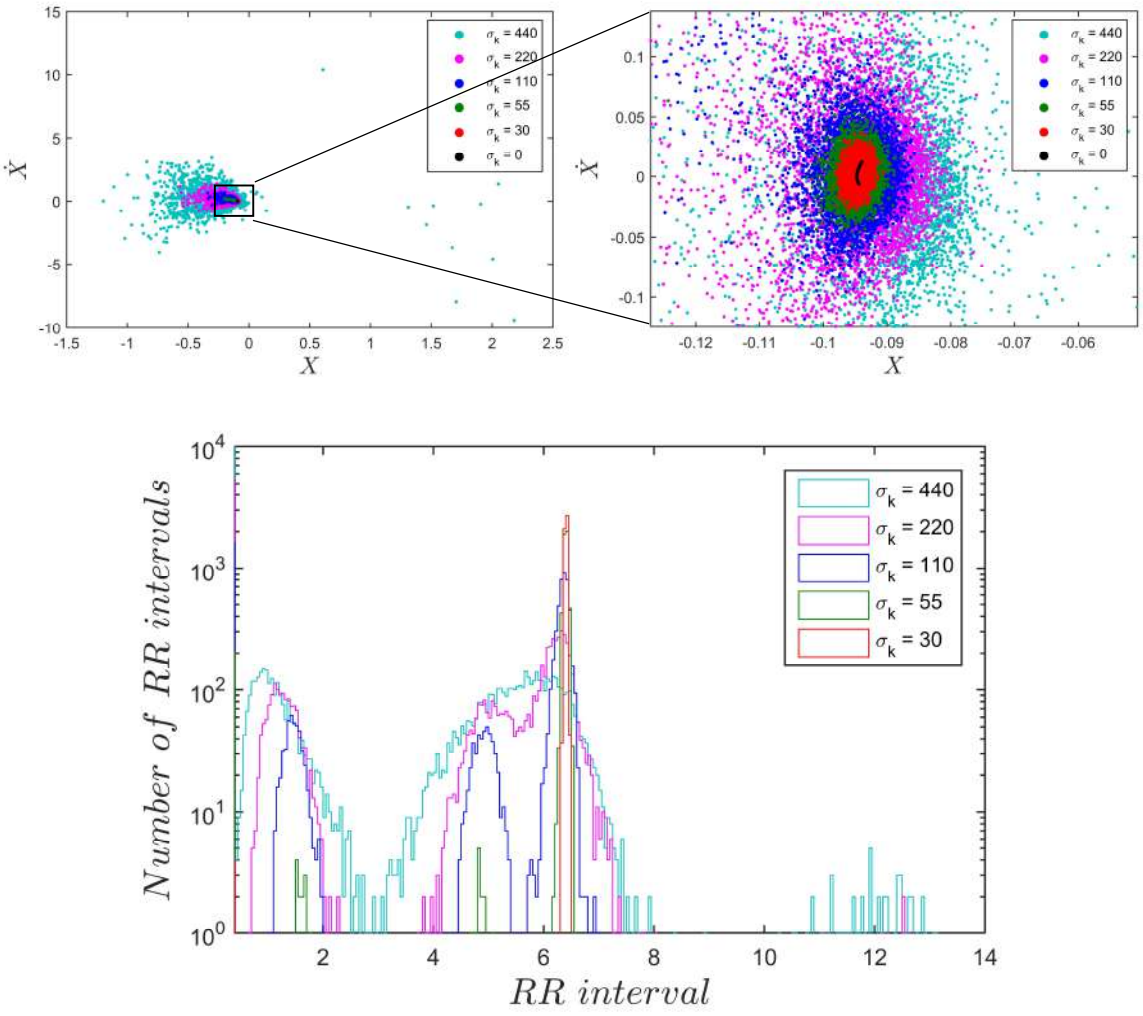

Figure 36 – AV-HP random coupling: (top) Poincaré maps for different standard deviations; (bottom) comparison of RR histograms for different standard deviations.

5.1.4 **Random HP-AV coupling**

Random HP-AV coupling is now in focus considering $k_{HP-AV} \sim N(\bar{k}_{HP-AV}, \sigma_k^2)$ where nominal value is $\bar{k}_{HP-AV} = 0$. Conceptual model is presented in Figure 46 represents.

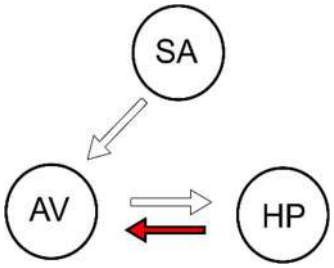

Figure 37 - Conceptual model for HP-AV random coupling.

ECGs are presented in Figure 38 (left column) showing that the increase of σ_k tends to induce the occurrence of R waves sequences, characteristic of ventricular flutter. For values greater than $\sigma_k = 20.0$, typical changes of complete bb appear (absence of R waves). All these variations are with experimental data. Figure 38 (middle column) shows state spaces and Poincaré maps that give a different visualization of the involved rhythms. Accompanied by changes caused by incomplete bb ($\sigma_k < 20.0$), already explained, the enlargement of greater loop ($\sigma_k = 30.0$) can be related to ventricular flutter. Figure 38 (right column) shows RR interval histograms. In this case, a decrease in the mean μ is observed as σ_k increases (sequential R waves). When $\sigma_k = 30$, there is an increase of the mean value, related to the absence of R waves.

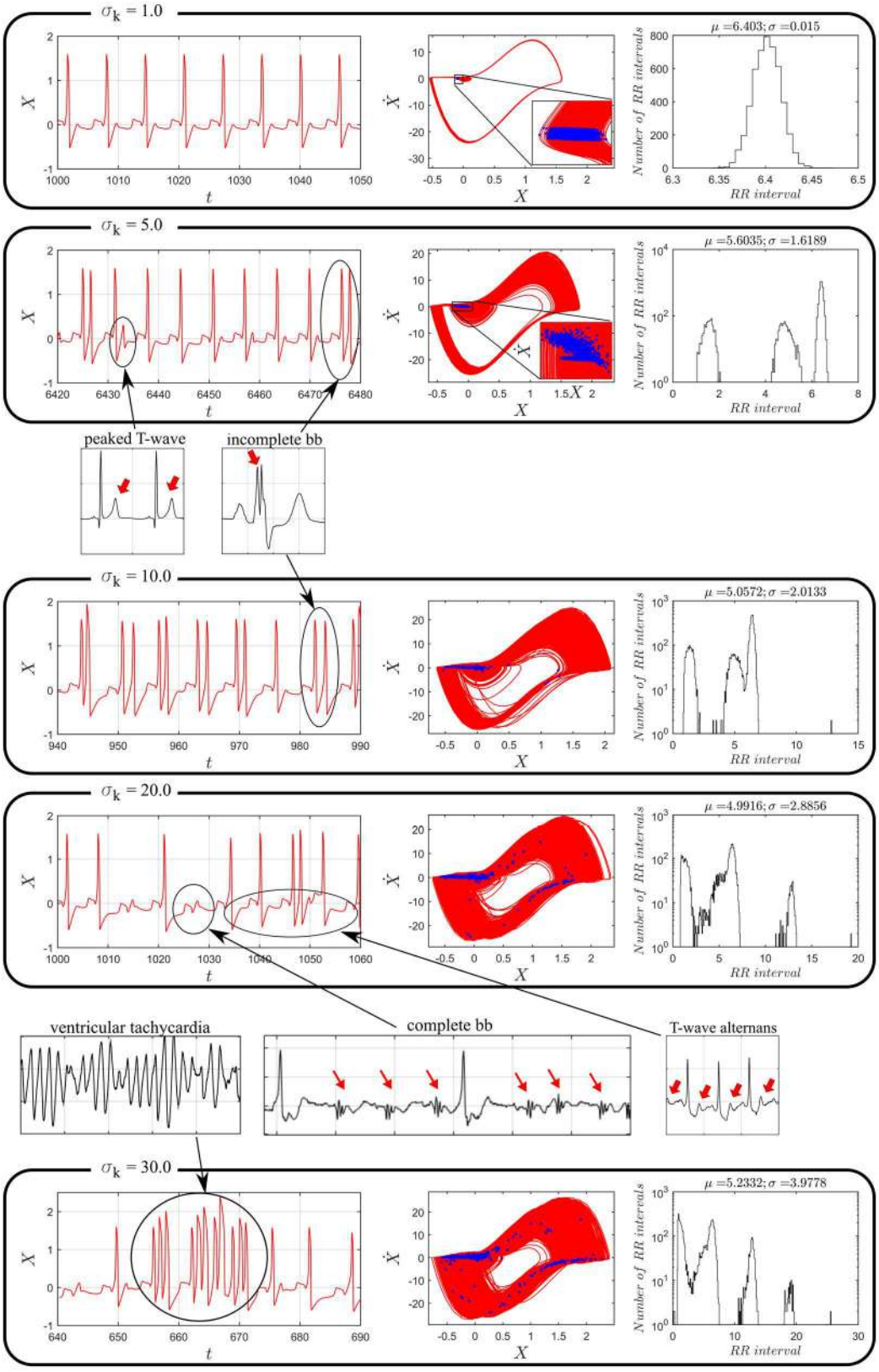

Figure 38 – HP-AV random coupling results for different σ_k: (left column) synthetic ECGs; (middle column) phase plane (red) and Poincaré map (blue); and (right column) RR histogram. Also, identified pathologies are highlighted and compared with experimental data.

A comparative analysis Poincaré maps (Figure 39 - top) of and RR histograms (Figure 39 - bottom) shows different shapes of RR peaks and different shapes of Poincaré maps from the other studied cases. Once again, it helps to identify responses and pathologies. As σ_k increases, Poincaré section evolves to a stretched cloud to the left, which can be associated with incomplete bb. This cloud around greater loop is related to ventricular flutter behavior indicating a trend to this pathology occurrence.

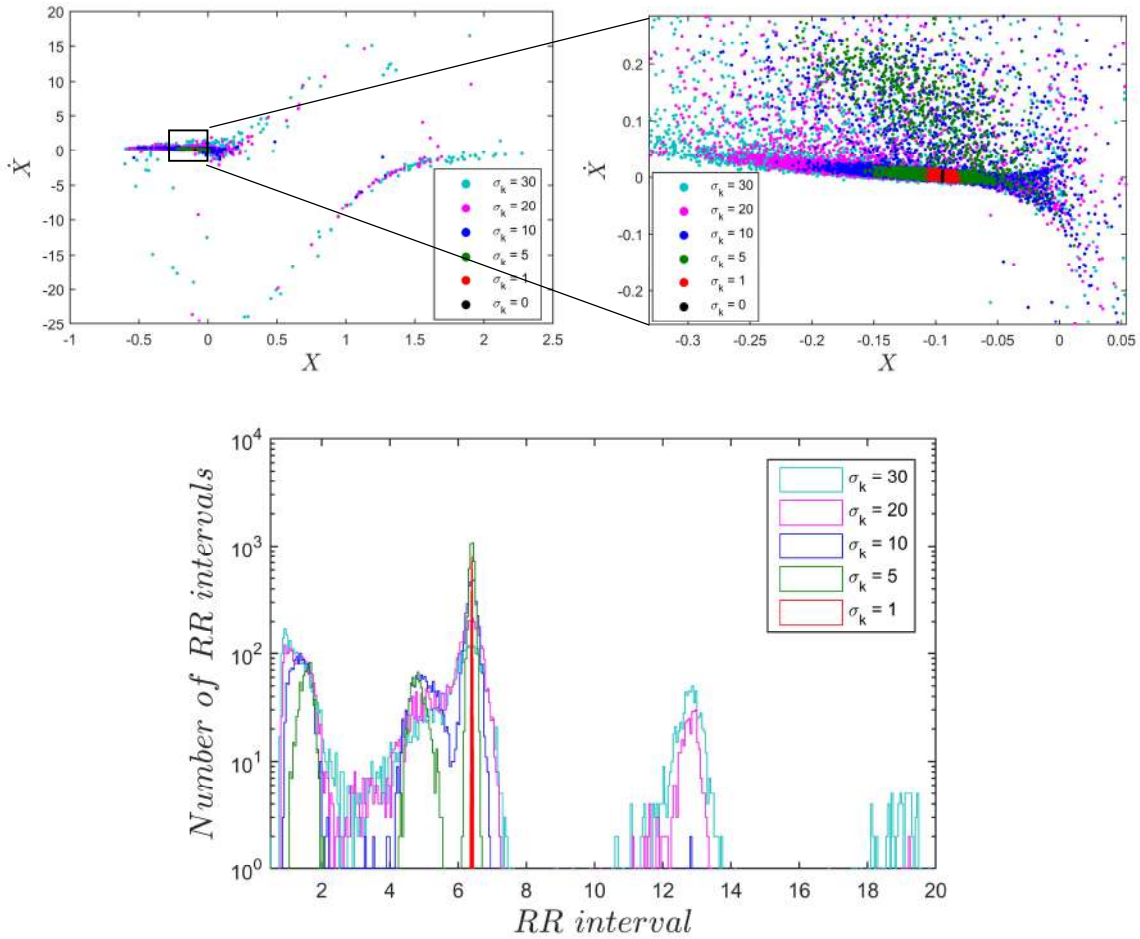

Figure 39 – HP-AV random coupling: (top) Poincaré maps for different standard deviations; (bottom) comparison of RR histograms for different standard deviations.

5.2 Random Matrix Theory

This section deals with the use of nonparametric probabilistic approach that relies on Random Matrix Theory (Mehta, 1991) and Gaussian Orthogonal Ensemble (Weaver, 1989; Ritto & Fabro, 2019) to describe uncertainties of the cardiac system. The main idea is to use the mathematical description proposed by Cheffer *et al.* (2021a) establishing the coupling terms by random matrices. Under this assumption, the connection can be analyzed by a simplified uncertainty modeling based on matrix blocks, avoiding the analysis of eighteen coupling parameters. Different kinds of connection are evaluated establishing situations where pathological behaviors evolve from normal rhythm and random connections.

The matrix representation (eq. 9) is necessary to apply the random matrix strategy. In addition, the delayed coupling term, $\boldsymbol{K^{\tau}}$, can be split into matrix blocks as follows:

$$\boldsymbol{K^{\tau}} = \begin{bmatrix} \mathbf{0} & \mathbf{0} \\ \boldsymbol{K_{BD}} & \boldsymbol{K_{BI}} \end{bmatrix} \tag{13}$$

where $\boldsymbol{K_{BD}}$ and $\boldsymbol{K_{BI}}$ represent diagonal matrix blocks that can be interpreted, respectively, as direct and inverse directions of signal transmission between oscillators.

By applying the described stochastic modeling to the system matrices $\boldsymbol{K_{BD}}$ and $\boldsymbol{K_{BI}}$, uncertainties are introduced not only in the main diagonal, but also in the extra diagonal terms, which introduces coupling (model uncertainties). Hence, it is possible to jointly analyze effects of eighteen uncertain elements, of these matrices, on the system response by varying one parameter: the standard deviation σ_M.

Stochastic modeling (eq. 8) is applied on $\boldsymbol{K_{BD}}$ and $\boldsymbol{K_{BI}}$ in order to investigate effects of their uncertainties, which are measured by the standard deviation σ_M, on heart model response for three cases: $\boldsymbol{K}_{BD}$ is stochastic; $\boldsymbol{K}_{BI}$ is stochastic; and both $\boldsymbol{K}_{BD}$ and $\boldsymbol{K}_{BI}$ are stochastic. This analysis is motivated by a physiology interpretation that points that some pathologies are driven by stimulus propagation in a certain direction. In previous section, it is possible to observe that random coupling can induce different kinds of pathologies that evolve from normal rhythm. Therefore, since $\boldsymbol{K}_{BD}$ and $\boldsymbol{K}_{BI}$ represent different directions of propagation, it is reasonable to consider each matrix as random and both combined in order to represent different kinds of pathologies.

As a first approach, only diagonal terms of $\boldsymbol{G_S}$ are summed to $\boldsymbol{K_{BD}}$ and $\boldsymbol{K_{BI}}$. In this case, there is no additional coupling considered in the analysis. In order to analyze results, time series, and phase plane $\{X, \dot{X}\}$ are presented. Monte Carlo simulations are employed: 100 simulations for each case and gray-shaded regions that defines the bounds of all responses are constructed. RR histograms are also constructed with Monte Carlo procedure, where 100 histograms are superimposed and each one has its mean μ_i. The mean μ, standard deviation, σ, and coefficient of variation ($CV = \frac{\sigma}{\mu}$) of this set of 100 μ_i are calculated from simulations. Convergence analysis shows that 100 simulations are sufficient to obtain converged behaviors of state spaces and RR histograms (including respective mean and standard deviation).

5.2.1 $\boldsymbol{K_{BD}}$ Stochastic

Uncertainty analysis starts by considering that only K_{BD} is modeled as stochastic. Figure 40 presents results of this analysis showing ECG, state spaces and RR histograms from Monte Carlo procedure. Note that for small values of σ_M, only normal rhythm is appearing. Time series seem desynchronized but state space shows that they are in the same orbit. RR histograms show, for each response, single peaks close to deterministic normal case. The calculated RR statistics are $\mu = 6.4110$, $\sigma = 0.1548$ and $CV = 0.0241$.

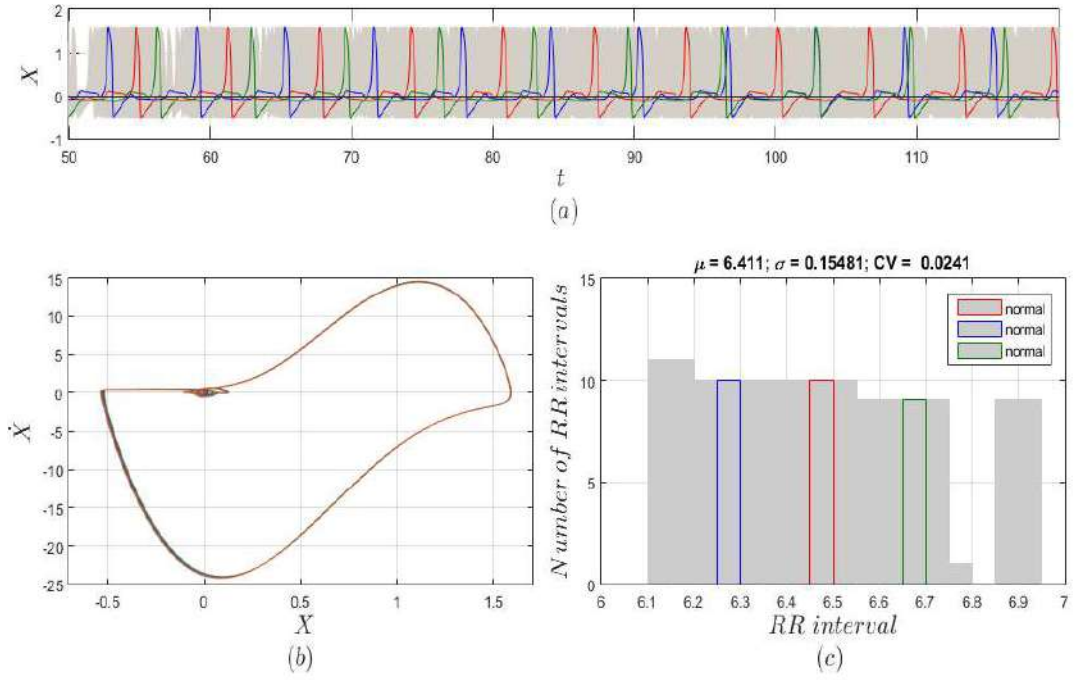

Figure 40 – Stochastic analysis of $\boldsymbol{K_{BD}}$ with $\sigma_M = 0.01$: (a)ECG Monte Carlo response samples; (b) respective states spaces and (c) RR histograms.

By increasing the standard deviation for $\sigma_M = 0.1$, normal, incomplete branch block (bb) rhythms and a mix of them are identified in Figure 41. The normal response (blue) presents an orbit similar to previous case, but the RR mean is reduced, as can be seen on RR histogram. Two responses for incomplete bb are presented. One is only incomplete bb (red) characterized by double R wave and two peaks on histogram. The other (green) is composed of incomplete bb (double R wave) and T-waves with variable amplitude, generating a histogram with three peaks. Responses different from normal are highlighted in Figures 41-d (incomplete bb) and 41-e (incomplete bb and variable T-wave), being compared with respective typical experimental data. In this case RR statistics are $\mu = 4.7634$, $\sigma = 1.6536$ and $CV = 0.3471$.

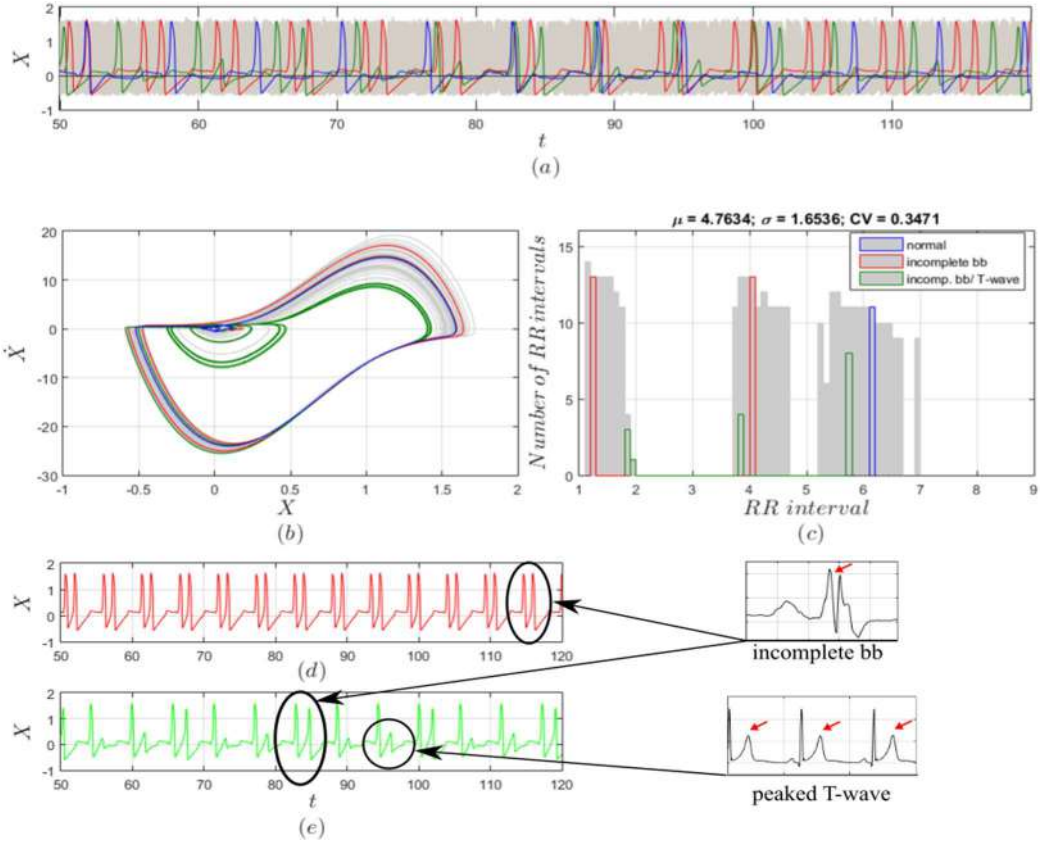

Figure 41 – Stochastic analysis of $\boldsymbol{K_{BD}}$ with $\sigma_M = 0.1$: (a)ECG Monte Carlo response samples; (b) respective states spaces and (c) RR histograms; (d) Incomplete bb and (e) incomplete bb with variable T-wave.

On Figure 42 are presented responses to $\sigma_M = 1.0$. It is possible to identify six rhythms: normal (black), incomplete bb (red), complete bb (blue), ventricular flutter (purple), a variation of normal with small QRS (yellow) and one type (we called in this work type 1) of ventricular fibrillation (green). Besides rhythms previously described, the three new identified responses are highlighted and compared with experimental data.

Complete bb (Figure 42-d) is characterized by the absence of R-waves, presenting small region loops on state space and a zero-horizontal line on histogram. Ventricular flutter (Figure 42-e) presents states space with orbits around larger loop of normal case and one peak on RR histogram, indicating presence of one frequency in response. The response with small QRS (Figure 42-f) exhibits on states space a closed curve with three loops: a smaller representing P and T waves, a larger referring to normal QRS and an intermediary generated by abnormal QRS. RR histogram presents a peak to the left of reference period, representing the interval between two normal QRS. Ventricular fibrillation (Figure 42-g) exhibits a denser states space around larger loop and a distribution of peaks in the interval [1,1.7] in histogram. For this case RR statistics are $\mu = 2.8148$, $\sigma = 1.5964$ and $CV = 0.5671$.

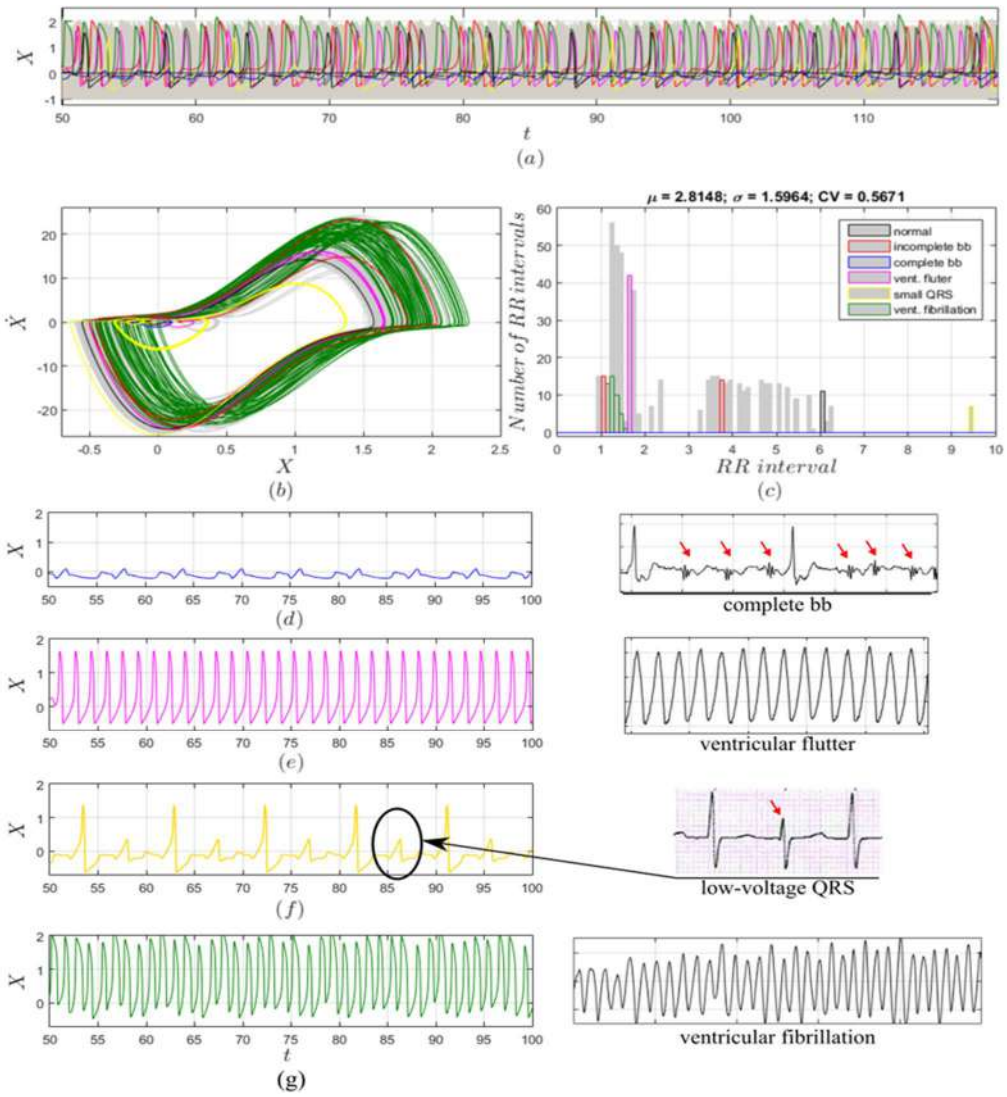

Figure 42 – Stochastic analysis of $\boldsymbol{K_{BD}}$ with $\sigma_M = 1.0$: (a)ECG Monte Carlo response samples; (b) respective states spaces and (c) RR histograms; (d) Complete bb; (e) ventricular flutter; (f) low-voltage QRS and (g) ventricular fibrillation type 1.

Figure 43 considers even a bigger standard deviation, $\sigma_M = 3.0$. Some variations of the previous responses can be identified: incomplete bb (blue), complete bb (red), ventricular flutter (black) and ventricular fibrillation (green). In addition, two new rhythms are observed: composition of ventricular flutter and fibrillation (purple, Figure 43-d) and a variation of normal with inverse T-wave (yellow, Figure 43-e). Inverse T-wave exhibits state space close to normal case but with the bigger loop a little bit smaller and one peak on RR histogram. The calculated RR statistics are $\mu = 2.3473$, $\sigma = 1.1055$ and $CV = 0.4710$.

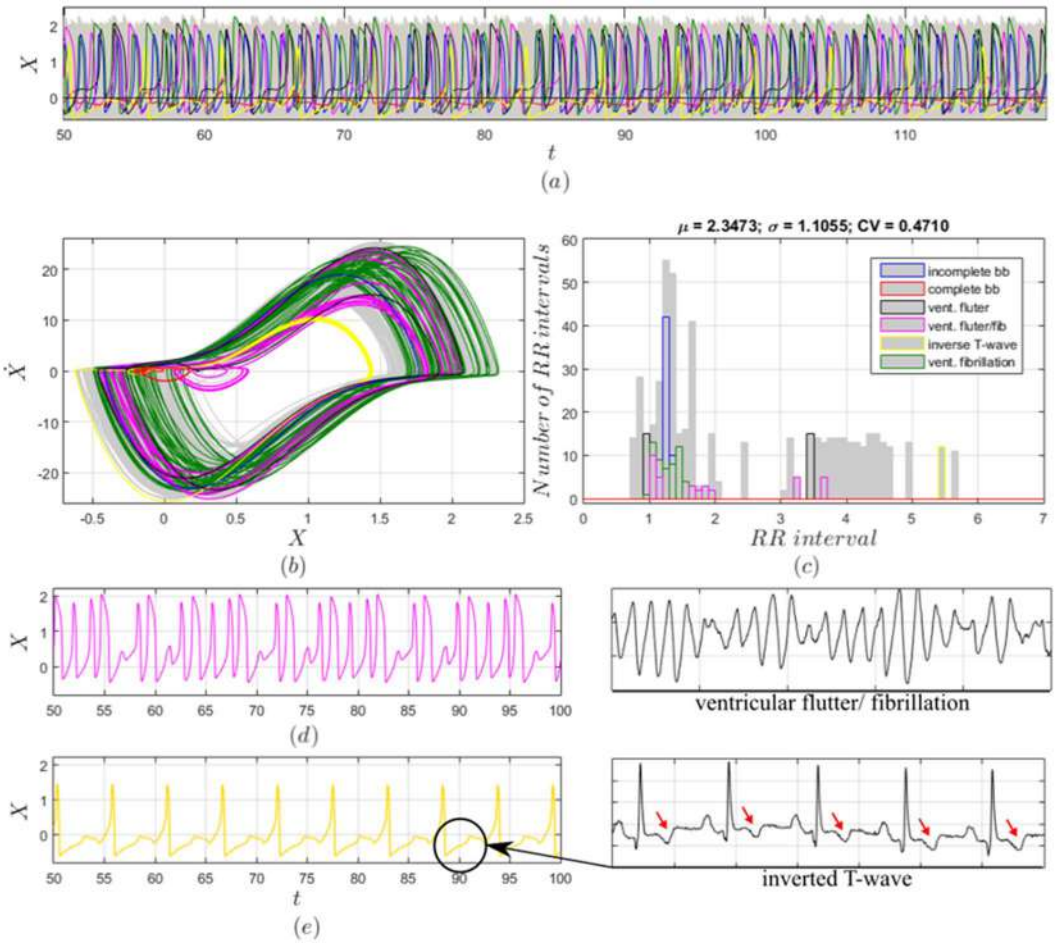

Figure 43 – Stochastic analysis of $\boldsymbol{K_{BD}}$ with $\sigma_M = 3.0$: (a)ECG Monte Carlo response samples; (b) respective states spaces and (c) RR histograms; (d) Ventricular flutter and fibrillation combination and (e) inverted T-wave.

5.2.2 $\boldsymbol{K_{BI}}$ Stochastic

A new coupling characteristic is now of concern treating the case where K_{BI} is stochastic. Analogous to the previous case, small values of σ_M tends to be associated with

normal rhythm, with a desynchronized time series and the same orbit on state space. Figure 44 shows the system response for $\sigma_M = 0.01$ together with RR histograms that show single peaks, but with mean μ greater than previous cases with statistics $\mu = 6.4590$, $\sigma = 0.1581$ and $CV = 0.0245$.

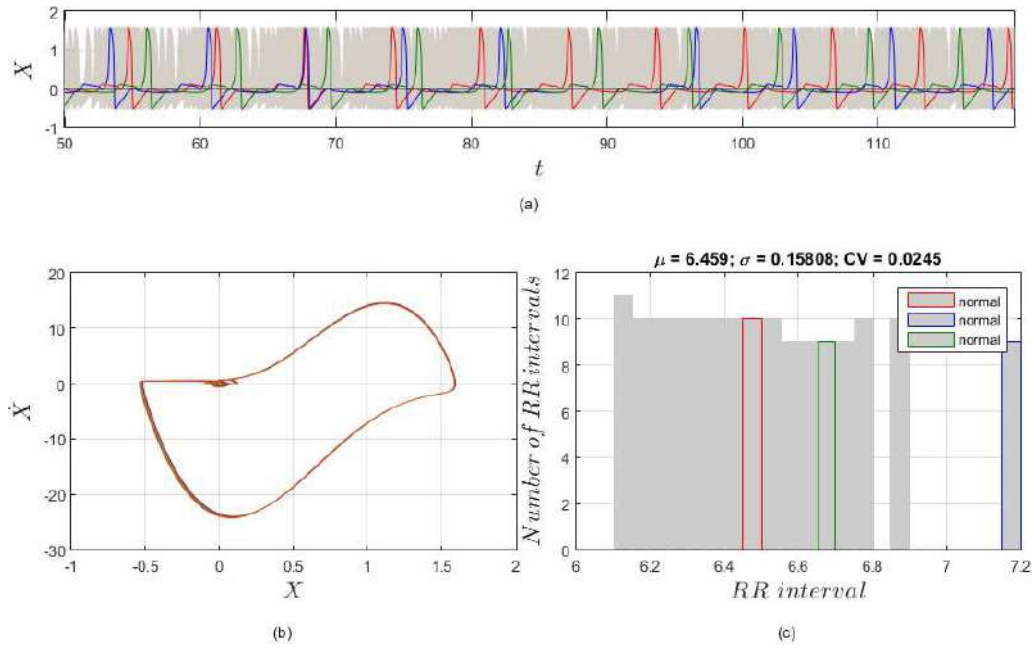

Figure 44 – Stochastic analysis of $\boldsymbol{K_{BI}}$ with $\sigma_M = 0.01$: (a)ECG Monte Carlo response samples; (b) respective states spaces and (c) RR histograms.

By increasing the standard deviation to $\sigma_M = 0.1$, normal (green), a variation of normal (blue) and incomplete bb (red) are identified (Figure 45). The variation of normal rhythm presents a T-wave with greater amplitude and can be seen on spaces states as the wider loop around $(0, 0)$. The calculated RR statistics are $\mu = 4.9733$, $\sigma = 1.5817$ and $CV = 0.3180$.

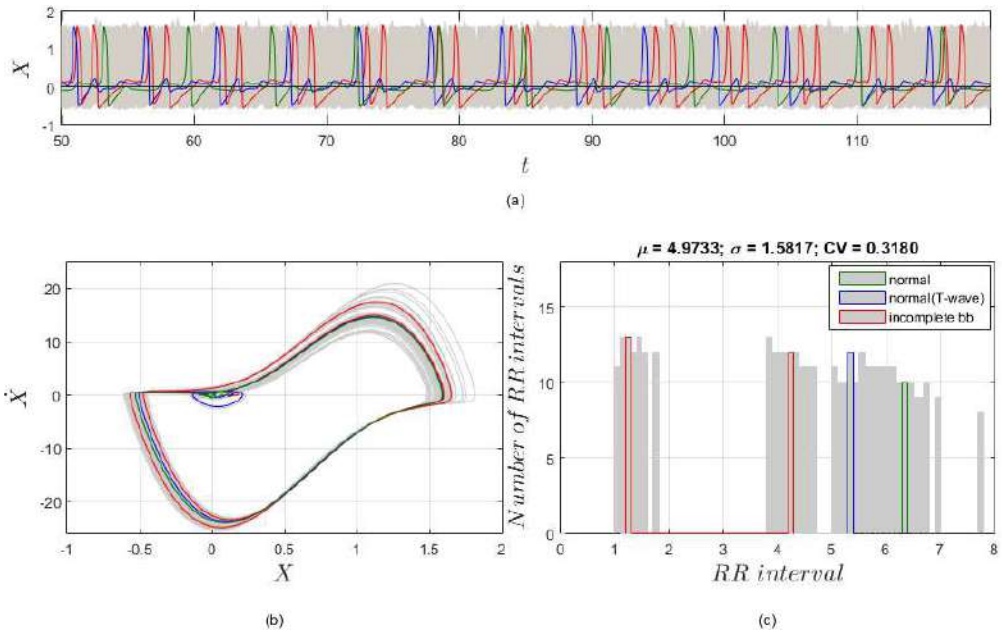

Figure 45 – Stochastic analysis of $\boldsymbol{K_{BI}}$ with $\sigma_M = 0.1$: (a)ECG Monte Carlo response samples; (b) respective states spaces and (c) RR histograms.

Figure 46 presents responses for $\sigma_M = 1.0$ where it is possible to identify five rhythms: normal (black), incomplete bb (green), complete bb (red), ventricular flutter (blue) and ventricular fibrillation type 1 (purple). For this case RR statistics are $\mu = 2.6187$, $\sigma = 0.8275$ and $CV = 0.3542$.

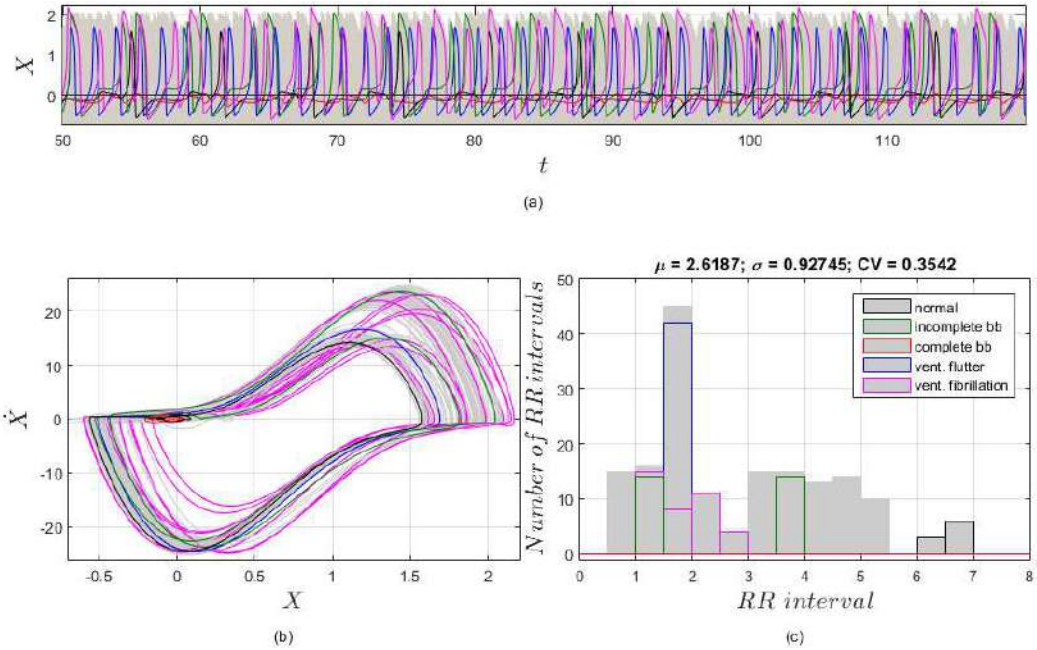

Figure 46 – Stochastic analysis of $\boldsymbol{K_{BI}}$ with $\sigma_M = 1.0$: (a)ECG Monte Carlo visualization and identified responses; (b) respective states spaces and (c) RR histograms.

Figure 47 shows the case with $\sigma_M = 3.0$, presenting four kinds of response: incomplete bb (blue), complete bb (red), ventricular flutter (purple) and a different type of ventricular fibrillation (green, Figure 47-d), called here type 2. Now it exhibits different orbits also around smaller loop on spaces states and several peaks spread over a larger interval in RR histogram Histogram statistics in this case are $\mu = 2.0587$, $\sigma = 0.4929$ and $CV = 0.2394$.

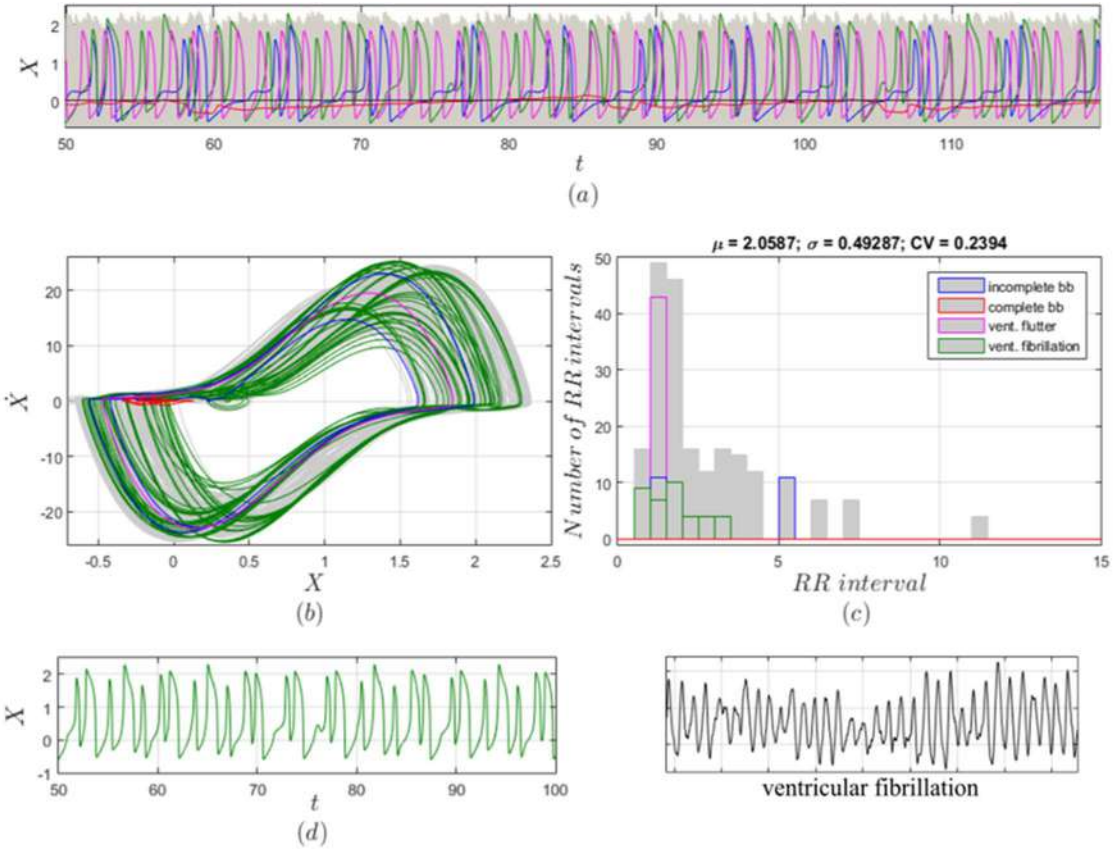

Figure 47 – Stochastic analysis of $\boldsymbol{K_{BI}}$ with $\sigma_M = 3.0$: (a)ECG Monte Carlo Carlo response samples; (b) respective state spaces and (c) RR histograms; (d) Ventricular fibrillation type 2.

5.2.3 $\boldsymbol{K_{BD}}$ and $\boldsymbol{K_{BI}}$ Stochastic

A general random situation is now concerned considering that both $\boldsymbol{K}_{BD}$ and $\boldsymbol{K}_{BI}$ has stochastic characteristics. Initially, a small value of standard deviation is treated, $\sigma_M = 0.01$. inducing pathological responses, different from the previous cases. Figure 48 shows three identified rhythms: normal (blue), a variation of normal with greater T-wave (green) and incomplete bb (red), whose characteristics have been already explained. The calculated RR statistics are $\mu = 6.3536$, $\sigma = 0.5406$ and $CV = 0.0851$.

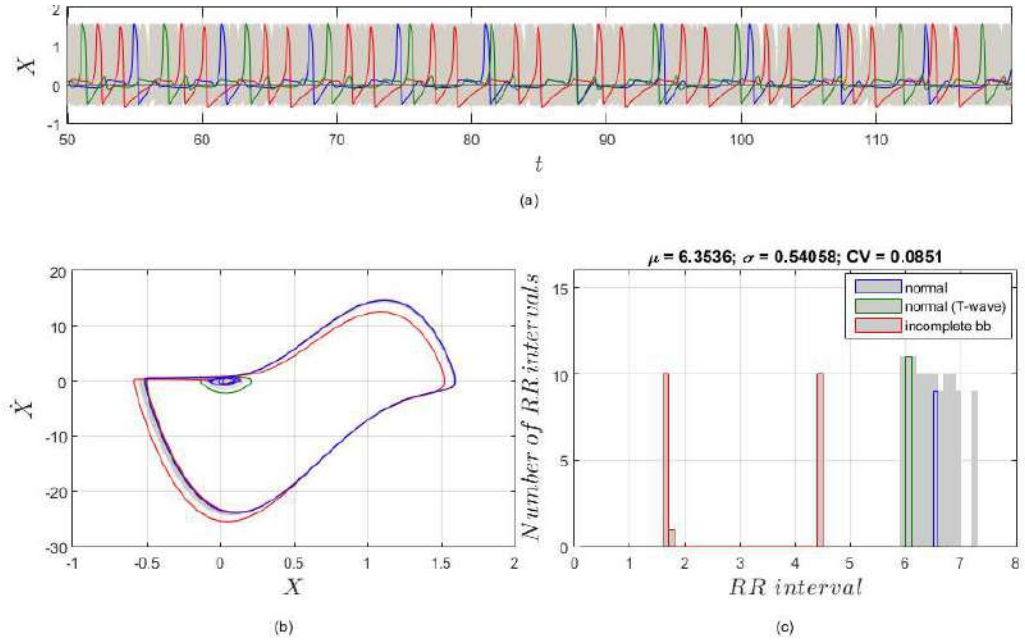

Figure 48 – Stochastic analysis of $\boldsymbol{K_{BD}}$ and $\boldsymbol{K_{BI}}$ with $\sigma_M = 0.01$: (a)ECG Monte Carlo response samples; (b) respective states spaces and (c) RR histograms.

By increasing the standard deviation to $\sigma_M = 0.1$, normal (black) with slightly higher RR mean, two incomplete bb (blue and green) and complete bb (red) are identified (Figure 49). Both incomplete bb responses have double R-waves, but with different frequencies. These results can be confirmed by different peaks location on histograms. The calculated RR statistics are $\mu = 3.6296$, $\sigma = 1.4812$ and $CV = 0.4081$.

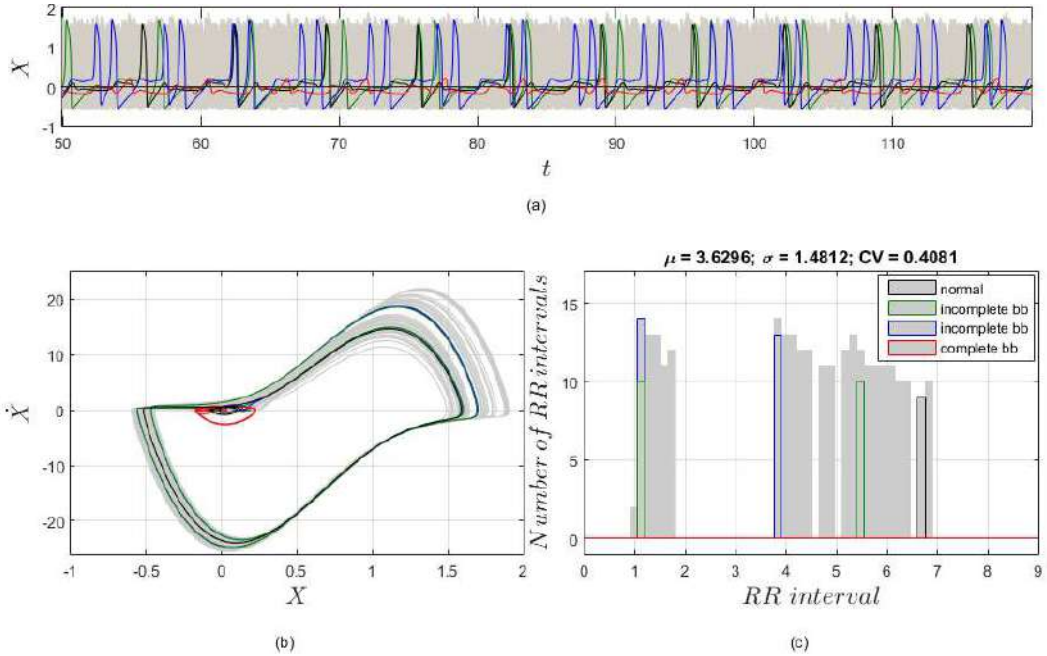

Figure 49 – Stochastic analysis of $\boldsymbol{K_{BD}}$ and $\boldsymbol{K_{BI}}$ with $\sigma_M = 0.1$: (a)ECG Monte Carlo response samples; (b) respective states spaces and (c) RR histograms.

Figure 50 presents responses for $\sigma_M = 1.0$, showing five kinds of rhythms: normal with a lower RR mean (black), incomplete bb (blue), complete bb (red), ventricular flutter (purple) and ventricular fibrillation type 2 (green), which exhibit same response characteristics previously described. Histogram statistics are $\mu = 2.2685$, $\sigma = 0.9756$ and $CV = 0.4301$.

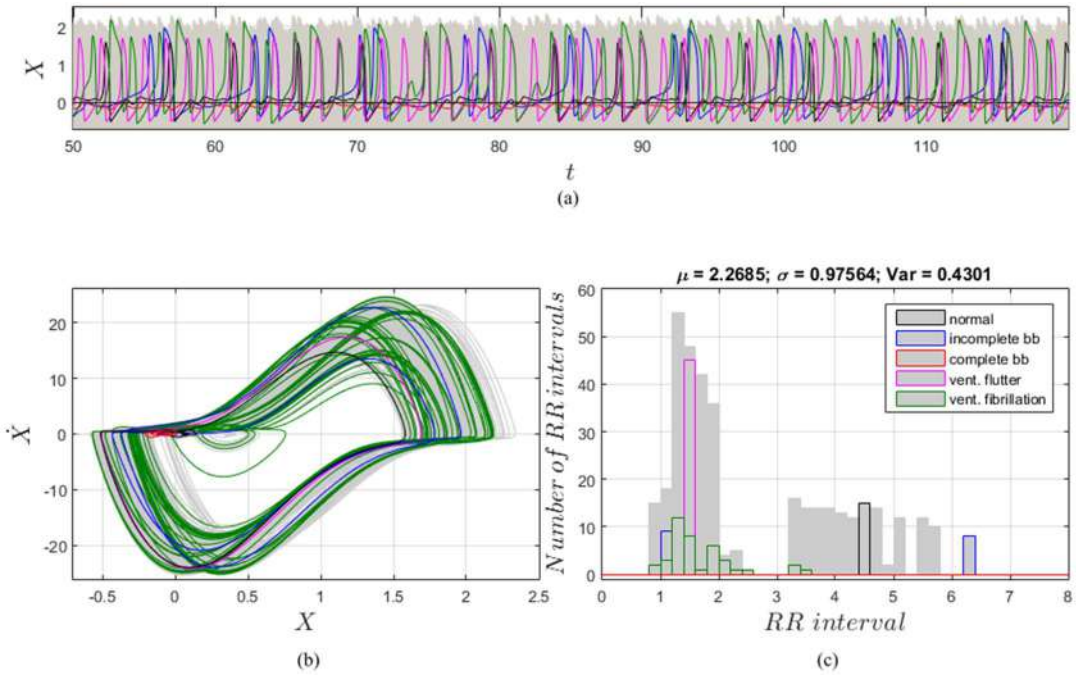

Figure 50 – Stochastic analysis of $\boldsymbol{K_{BD}}$ and $\boldsymbol{K_{BI}}$ with $\sigma_M = 1.0$: (a)ECG Monte Carlo response samples; (b) respective states spaces and (c) RR histograms.

Figure 51 considers a bigger standard deviation, $\sigma_M = 3.0$, showing incomplete bb (purple), complete bb (red), ventricular flutter (yellow), ventricular fibrillation type 2 (green) and a composition of incomplete bb and bradycardia (blue). The ventricular flutter now identified presents a closed curve with four loops on state space. Bradycardia designates a decrease in heart rate, which can be related to long RR interval observed on histogram. In this case RR statistics are $\mu = 2.7472$, $\sigma = 2.3288$ and $CV = 0.8477$.

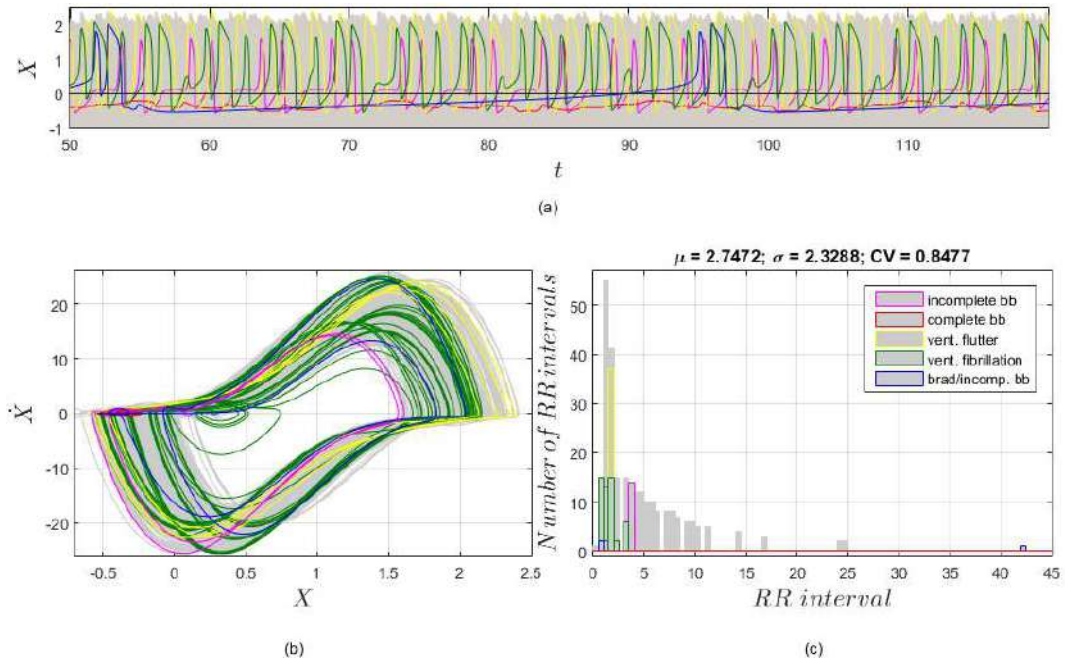

Figure 51 – Stochastic analysis of $\boldsymbol{K_{BD}}$ and $\boldsymbol{K_{BI}}$ with $\sigma_M = 3.0$: (a)ECG Monte Carlo response samples; (b) respective states spaces and (c) RR histograms.

6 CONCLUSIONS

Cardiac rhythms are analyzed from a mathematical model composed by three-coupled oscillators with time-delayed couplings. The proposed improvement (dissociation of coupling terms) enhances the model capability to capture the main aspects of cardiac dynamical response, reproducing ECGs for various situations of heart functioning, normal and pathological rhythms, including atrial flutter, atrial fibrillation, ventricular flutter and two types of ventricular fibrillation (with and without external stimulus). Poincaré map construction is discussed pointing that it is an interesting diagnostic tool to characterize pathological rhythms. Two different approaches are proposed considering secant plane and reference period, both providing similar conclusions.

In addition, a global comprehension of the SA behavior is provided by an analysis of bifurcation diagrams, in which distinct kinds of pacemaker responses are evaluated and classified as quasi-periodic and chaotic. The effect of these rhythms in the electrical activity of the cardiac system, represented by ECGs, is then investigated. The variety of generated ECG behaviors reveals some relevant cardiac arrhythmic responses as branch blocks and junctional tachycardia that may lead to dangerous rhythms as atrial and ventricular fibrillations. Also, T wave alternations are identified, which is useful since it is usually employed as clinical indicator of cardiac sudden death.

The investigation of the effects of randomness on the system response, which represent the main contribution of the thesis, is performed by considering random couplings . Basically, pathological behaviors can evolve from normal rhythms due to random couplings. This investigation allows one to conclude that cardiac system model has great potential to assist the rich heart dynamics comprehension, being useful for disease diagnosis. Nonlinear dynamics analysis as state space and Poincaré maps have proved to be useful for diagnosis because they highlight response variations that are imperceptible on time series. Regarding state space characteristics, it is noticeable that normal rhythm presents a closed curve with two loops and pathological rhythms tend to an open trajectory with denser orbits around the normal one. Poincaré map presents normal response characterized by a line. On the other hand, pathological responses exhibit clouds of points around the normal one. Poincaré section evolves to different areas and shapes that can be used to identify and predict different pathologies.

A nonparametric probabilistic approach is employed, based on the Random Matrix Theory, which has the advantages of introducing coupling (model uncertainties) among the oscillators, and having only one parameter to control the level of uncertainty; the standard deviation σ_M. In order to analyze results, time series, states spaces and RR histograms constructed by Monte Carlo method. By increasing σ_M, some pathologies are identified, as incomplete and complete branch block (bb), bradycardia, atrial fibrillation, inverse T-wave, larger T-wave, small QRS, ventricular flutter and ventricular fibrillation.

The analysis leads to the following conclusions: Poincaré map shows to be a satisfactory tool to characterize dynamical characteristics, where both methods exhibit potential to be implemented in real-time ECG monitoring devices or arrhythmia discrimination algorithms; Due to the great range of behaviors that the model can reproduce, it can also be used in algorithms for device therapy and rhythm identification purposes; The proposed stochastic model is consistent, being able to generate cardiac pathological dynamical responses that evolve from normal rhythm. In this regard, it should be highlighted that dynamical perspective is able to provide a deeper comprehension of pathological rhythms, which can be useful for identification, monitoring and controlling of cardiac rhythms

Regardless, future research could continue to explore coupling modeling, improving the description of spatiotemporal and biological aspects. For example, one can investigate nonlinear couplings such as Duffing-type; HKB model (Haken *et al.,* 1985), which represent phase transitions observed in biomechanics; Hui *et al.* (2021) recently present an study of effects of time delay in coupled oscillators, involving both theoretical and experimental approaches. Moreover, stochastic modeling can be extended in context of Random Matrix Theory. One possibility is investigating the effect of terms out of diagonal of coupling matrices.

Some possibilities for using the presented model for clinical purposes can be found in Cheffer & Savi (2021) In this context, development of algorithms and machine learning techniques for device therapy and rhythm identification can be cited as promising future works. Furthermore, chaos control of cardiac rhythms, as performed by Ferreira *et al.* (2011, 2014), represent a relevant application that still exhibits several issues to be exploited.

7 REFERENCES

ABARBANEL, H. D. I., BROWN, R., KADTKE, J. B., “Prediction in chaotic nonlinear systems: Methods for time series with broadband Fourier spectra”. *Phys. Rev. A*, v. 41, pp. 1782–1807, 1990.

ALVAREZ-RAMIREZ, J., RODRIGUEZ, E., AND ECHEVERRÍA, J. C., “Delays in the human heartbeat dynamics”. *Chaos*, v. 19, 028502, 2009.

ARONIS, K.N., BERGER, R.D., CALKINS, H., CHRISPIN, J., MARINE, J.E., SPRAGG, D.D., TAO, S., TANDRI, H. AND ASHIKAGA, H., “Is human atrial fibrillation stochastic or deterministic? – Insights from missing ordinal patterns and causal entropy-complexity plane analysis”, *Chaos: An Interdisciplinary Journal of Nonlinear Science*, v. 28, n. 6, 063130, 2018.

BARAHONA, M. AND POON, C. S., “Detection of nonlinear dynamics in short, noisy data”. Nature (London), v. 381, pp. 215–217, 1996.

BOZÓKI, Z., “Chaos theory and power spectrum analysis in computerized cardiotocography”, *European Journal of Obstetrics & Gynecology and Reproductive Biology,* v. 71, n. 2, pp. 163-168, 1997.

BRUGADA, P., BRUGADA, J., MONT, L., “A new approach to the differential diagnosis of a regular tachycardia with a wide QRS complex”, *Circulation*, v. 83, n. 5, pp. 1649-1659, 1991.

CANABRAVA, S., “*Eletrocardiografia*”, Med eLearning Cursos Interativos, Belo Horizonte, 2014.

CARDARILLI, G.C., DI NUNZIO, L., FAZZOLARI, R., RE, M. AND SILVESTRI, F., “Improvement of the cardiac oscillator-based model for the simulation of bundle branch blocks”. *Applied Sciences*, v. 9, n. 18, 3653, 2019.

CATALDO, E., “Introdução aos processos estocásticos (Notas em Matemática Aplicada)”, Sociedade Brasileira de Matemática Aplicada e Computacional, São Carlos, Brazil, 2012.

CHEFFER, A., RITTO, T. G., SAVI, M. A., “Uncertainty analysis of heart dynamics using Random Matrix Theory”. *International Journal of Non-Linear Mechanics*, v. 129, 103653, 2021b.

CHEFFER, A., SAVI, M. A., “Random effects inducing heart pathological dynamics: An approach based on mathematical models”. *Biosystems*, 104177, 2020.

CHEFFER, A., SAVI, M. A., PEREIRA, T. L., DE PAULA, A. S., “Heart rhythm analysis using a nonlinear dynamics perspective”. *Applied Mathematical Modelling*, v. 96, pp. 152-176, 2021a.

CHEFFER, A., SAVI, M. A., “Analysis of Cardiovascular Rhythms Using Mathematical Models”. *J Cardio Cardiovasc Med*, v. 5, 100022, 2021.

CHEN, P. S., GARFINKEL, A., WEISS, J. N., KARAGUEUZIAN, H. S., “Computerized mapping of fibrillation in normal ventricular myocardium”. *Chaos*, v. 8, n. 1, pp. 127-136, 1998.

COSTA, M. D., PENG, C.-K., AND GOLDBERGER, A. L., “Multiscale analysis of heart rate dynamics: Entropy and time irreversibility measures”. *Cardiovasc. Eng*., v. 8, pp. 88–93, 2009.

CUNNINGHAM, W. J., “A nonlinear differential-difference equation of growth”, *Proceedings of the National Academy of Sciences*, v. 40, n. 8, pp. 708-713, 1954.

DENG, M., WANG, C., TANG, M. AND ZHENG, T., “Extracting cardiac dynamics within ECG signal for human identification and cardiovascular diseases classification”. *Neural Networks*, vol. 100, pp.70-83, 2018.

DOS SANTOS, A. M., LOPES, S. R., VIANA, R. R. L., “Rhythm synchronization and chaotic modulation of coupled Van der Pol oscillators in a model for the heartbeat”, *Physica A: Statistical Mechanics and its Applications*, v. 338, n. 3, pp. 335-355, 2004.

DUBIN, D., “*Interpretação rápida do ECG*”, Editora de Publicações Biomédicas – EPUB, Rio de Janeiro, 1996.

EVARISTO, R. M., BATISTA, A. M., VIANA, L. R., IAROSZ, K. C., SZEZECH JR, J. D., GODOY, M. F., “Mathematical model with autoregressive process for electrocardiogram signals”, *Communications on Nonlinear Science and Numerical Simulations*, v. 57, pp. 415-421, 2017.

FARMER, J. D. AND SIDOROWICH, J. J., “Predicting chaotic time series”. *Phys. Rev. Lett*., v. 59, pp. 845–848, 1987.

FENTON, F. H., CHERRY, E. M., HASTINGS, H. M., EVANS, S. J., “Multiple mechanisms of spiral wave breakup in a model of cardiac electrical activity”. *Chaos*, v. 12, n. 3, p. 852-892, 2002.

FENTON, F., KARMA, A., “Vortex dynamics in three-dimensional continuous myocardium with fiber rotation: Filament instability and fibrillation”. *Chaos*, v. 8, pp. 20-47, 1998.

FERREIRA, B. B., DE PAULA, A. S., SAVI, M. A., “Chaos control applied to heart rhythm dynamics”, *Chaos, Solitons & Fractals*, v. 44, n. 8, pp. 587-599, 2011.

FERREIRA, B. B., SAVI, M. A., DE PAULA, A. S., “Chaos Control Applied to Cardiac Rhythms Represented by ECG Signals”, *Physica Scripta*, v. 89, 105203, 2014.

FORRESTER, P.J., SNAITH, N.C., VERBAARSCHOT, J.J.M., “Developments in random matrix theory”. *Journal of Physics A: Mathematical and General,* v. 36, n. 12, 2003.

FUSTER, V., RYDEN, L. E., CANNOM, D. S., “Guidelines for the management of patients with atrial fibrillation”, *Journal of American College of Cardiology*, pp. 48-149, 2006.

GARFINKEL, A., SPANO, M., DITTO, W., WEISS, J., “Controlling cardiac chaos”. *Science,* v. 257, p. 1230-1235, 1992.

GARFINKEL, A., WEISS, J., M., DITTO, SPANO, M., “Chaos control of cardiac arrhythmias”. *Trends in Cardiovascular Medicine*, v. 5, p. 76-80, 1995.

GLASS, L., “Introduction to controversial topics in nonlinear science: Is the normal heart rate chaotic?”, *Chaos: An Interdisciplinary Journal of Nonlinear Science*, v. 19, n. 2, 028501, 2009.

GLASS, L., MACKEY, M. C., “*From Clocks to Chaos: The Rhythms of Life*”. Princeton University Press, Princeton, 1988.

GOIS, S. R. S. M., SAVI, M. A., “An analysis of heart rhythm dynamics using a three-coupled oscillator model”, *Chaos, Solitons & Fractals*, v. 41, n. 5, pp. 2553-2565, 2009.

GOLDBERGER, A. L., RIGNEY, D. R., WEST, B. J., “Chaos and fractals in human physiology”. Sci. Am., v. 262 n. 2, pp. 42–49, 1990.

GOLDBERGER, A.L., GOLDBERGER, E., “*Clinical Electrocardiography*”, Mosby, 1977.

GOMES, M. E. D., SOUZA, A. V. P., GUIMARAES, H. N., AND AGUIRRE, L. A., “Investigation of determinism in heart rate variability”. *Chaos*, v. 10, pp. 398–410, 2000.

GOVINDAN, R. B., NARAYANAN, K., AND GOPINATHAN, M. S., “On the evidence of deterministic chaos in ECG: Surrogate and predictability analysis”. *Chaos*, v. 8, pp. 495–502, 1998.

GRUDZINSKI, K., ZEBROWSKI, J. J., “Modeling Cardiac Pacemakers with Relaxation Oscillators”, *Physica A*, v. 336, pp. 153-162, 2004.

HAKEN, H., KELSO, J. S., BUNZ, H., “A theoretical model of phase transitions in human hand movements”. *Biological cybernetics*, v. 51, n. 5, pp. 347-356, 1985.

HERBSCHLEB, J. N., HEETHAAR, R. M., TWEEL, I., MEIJLER, F. L., “Frequency analysis of the ECG before and during ventricular fibrillation”. *Computers in Cardiology*, pp. 365-368, 1980.

HU, B., WEI, S., WEI, D., ZHAO, L., ZHU, G., LIU, C., “Multiple time scales analysis for identifying congestive heart failure based on heart rate variability”, *IEEE Access*, v. 7, p. 17862-17871, 2019.

HUI, N., BISWAS, D., BANERJEE, T., KURTHS, J., “Effects of propagation delay in coupled oscillators under direct–indirect coupling: Theory and experiment”. *Chaos*, v. 31, n. 7, 073115, 2021.

ICONARU, E. I., CIUCUREL, M. M., GEORGESCU, L., TUDOR, M., CIUCUREL, C., “The Applicability of the Poincaré Plot in the Analysis of Variability of Reaction Time during Serial Testing”. *International Journal of Environmental Research and Public Health*, v. 18, n. 7, 3706, 2021.

JALIFE, J., “Ventricular fibrillation: mechanisms of initiation and maintenance”. *Annual review of physiology*, v. 62, n. 1, p. 25-50, 2000.

JALIFE, J., BERENFELD, O., SKANES, A., MANDAPATI, R., “Mechanisms of atrial fibrillation: mother rotors or multiple daughter wavelets, or both?”. *Journal of cardiovascular electrophysiology*, v. 9, n. 8 Suppl, p. S2, 1998.

JAWARNEH, I., STAFFELDT, R., “Conley index methods detecting bifurcations in a modified van der Pol oscillator appearing in heart action models”, *arXiv*, v. 1901, 11180, 2019.

JAYNES E.T., “Probability Theory: The Logic of Science.”, Cambridge University Press, 2003.

KAPLAN, D. T., “Simultaneous QRS detection and feature extraction using simple matched filter basis functions”, *Proceedings IEEE*, pp. 503-506, 1990.

KLEIN, G. J., BASHORE, T. M., SELLERS, T. D., PRITCHETT, E. L., SMITH, W. M., GALLAGHER, J. J., “Ventricular fibrillation in the Wolff-

Parkinson-White syndrome", *New England Journal of Medicine*, v. 301, n. 20, pp. 1080-1085, 1979.

KRINSKY, V. I., "Mathematical models of cardiac arrhythmias (spiral waves)". *Pharmacology & Therapeutics. Part B: General and Systematic Pharmacology*, v. 3, n. 4, p. 539-555, 1978

LEFEBVRE, J. H., GOODINGS, D. A., KAMATH, M. V., AND FALLEN, E. L., "Predictability of normal heart rhythms and deterministic chaos". *Chaos*, v. 3, pp. 267–276, 1993.

MALIK, M., CAMM, A. J., "*Heart Rate Variability*", Armonk, NY, Futura, 1995.

McSHARRY, P. E., CLIFFORD, G. D., TARASSENKO, L., SMITH, L. A.," A dynamical model for generating synthetic electrocardiogram signals", *IEEE Transactions on Biomedical Engineering*, v. 50, n. 3, pp. 289-294, 2003.

MEHTA, M. L., "Random matrices, revised and enlarged". 2º ed - *Academic Press*, New York, USA, 1991.

MENSOUR, B., LONGTIN, A., "Power spectra and dynamical invariants for delay-differential and difference equations", *Physica D: Nonlinear Phenomena*, v. 113, n. 1, pp. 1-25, 1998.

MITCHELL, C. C.; SCHAEFFER, D. G., "A two-current model for the dynamics of cardiac membrane", *Bulletin of Mathematical Biology*, v. 65, n. 5, pp. 767-793, 2003.

MOE, G. K., RHEINBOLDT, W. C., ABILDSKOV, J. A., "A computer model of atrial fibrillation". *American heart journal*, v. 67, n. 2, p. 200-220, 1964.

MOODY, G. B., MARK, R. G., ZOCCOLA, A., MANTERO, S., "Derivation of respiratory signals from multi-lead ECGs", *Computers in Cardiology*, v. 12, n. 1985, pp. 113-116, 1985.

NASH, M. P.; PANFILOV, A. V., "Electromechanical model of excitable tissue to study reentrant cardiac arrhythmias", *Progress in Biophysics and Molecular Biology*, v. 85, n. 2, pp. 501-522, 2004.

OBEL, O. A., CAMM, A. J., "Supraventricular tachycardia", *European Heart Journal*, v. 18, pp. 2-11, 1997.

OTT, E., GREBOGI, C., YORKE, J. A., "Controlling chaos". *Physical Review Letters*, v. 64, p. 1196, 1990.

PAN, J., TOMPKINS, W. J., “A real-time QRS detection algorithm”, *IEEE Transactions on Biomedical Engineering*, v. 3, pp. 220–236, 1985.

PEARCE, N., KIM, E. J., “Modelling the cardiac response to a mechanical stimulation using a low-order model of the heart”. *Mathematical Biosciences and Engineering*, v. 18, n. 4, p. 4871-4893, 2021.

PENG, C. K., HAVLIN, S., STANLEY, H. E., AND GOLDBERGER, A. L., “Quantification of scaling exponents and crossover phenomena in nonstationary heartbeat time series”. *Chaos*, v. 5, pp. 82–87, 1995.

POOL, R., “Is it healthy to be chaotic?” *Science*, v. 243, pp. 604–607, 1989.

POON, C. S. AND BARAHONA, M., “Titration of chaos with added noise”. *Proc. Natl. Acad. Sci. U.S.A*., v. 98, pp. 7107–7112, 2001.

RAPP, P. E., “Chaos in the neurosciences: Cautionary tales from the frontier”. *Biologist (London)*, v. 40, pp. 89–94, 1993.

RITTO, T. G., FABRO, A. T., “Investigation of random matrix applications on structural dynamics using a tensor decomposition”. *Journal of the Brazilian Society of Mechanical Sciences and Engineering*, v. 41, n. 8, pp. 352, 2019.

RYZHII, E., RYZHII, M., “Modeling of heartbeat dynamics with a system of coupled nonlinear oscillators”, *Communications in Computer and Information Science*, v. 404, pp. 67-75, 2014.

SAVI, M. A., “Chaos and order in biomedical rhythms”, *Journal of the Brazilian Society of Mechanical Sciences and Engineering*, v. 27, n. 2, pp. 157-169, 2005.

SHIRAISHI, Y., KATSUMATA, Y., SADAHIRO, T., AZUMA, K., AKITA, K., ISOBE, S., YASHIMA, F., MIYAMOTO, K., NISHIYAMA, T., TAMURA, Y., KIMURA, T., NISHIYAMA, N., AIZAWA, Y., FUKUDA, K., TAKATSUKI, S., “Real-time analysis of the heart rate variability during incremental exercise for the detection of the ventilatory threshold.”, *Journal of the American Heart Association*, v. 7, n. 1, e006612, 2018.

SILVESTRI, F., ACCIARITO, S., KHANAL, G. M., “Relationship between mathematical parameters of modified van der Pol oscillator model and ECG morphological features”, *International Journal on Advanced Science, Engineering and Information Technology*, v. 9, n. 2, p. 601-608, 2019.

SKANES, A.C., MANDAPATI, R., BERENFELD, O., DAVIDENKO, J.M. AND JALIFE, J., “Spatiotemporal periodicity during atrial fibrillation in the isolated sheep heart”, *Circulation*, v. 98, n. 12, pp.1236-1248, 1998.

SKINNER, J. E., GOLDBERGER, A. L., MAYER-KRESS, G., AND IDEKER, R. E., “Chaos in the heart: Implications for clinical cardiology”. *Nat. Biotechnol*. v. 8, pp. 1018–1024, 1990.

SOIZE, C., “A nonparametric model of random uncertainties for reduced matrix models in structural dynamics”. *Probabilistic engineering mechanics*, v. 15, n. 3, pp.277-294, 2000.

SON, J., DU, D., DU, Y., “Stochastic modeling and dynamic analysis of the cardiovascular system with rotary left ventricular assist devices”, *Mathematical Problems in Engineering*, 2019.

SPROTT, J.C., “A Simple Chaotic Delay Differential Equation”, *Physics Letters A*, v. 366, pp. 397-402, 2007.

SUGIHARA, G. AND MAY, R., “Nonlinear forecasting as a way of distinguishing chaos from measurement error in forecasting”. *Nature (London)*, v. 344, pp. 734–741, 1990.

TOBÓN, D. P., JAYARAMAN, S., FALK, T. H., “Spectro-temporal electrocardiogram analysis for noise-robust heart rate and heart rate variability measurement.”, *IEEE journal of translational engineering in health and medicine*, v. 5, pp. 1-11, 2017.

UENO, H., TOTOKI, Y., MATSUO, T., “ECG characterization of sinus bradycardia and ventricular flutter using malthusian parameter and recurrence plot”, *ICIC express letters. Part B, Applications: an international journal of research and surveys*, v. 9, n. 1, pp. 23-30, 2018.

VAN DER POL, B., VAN DER MARK, J., “The Heartbeat Considered as a Relaxation Oscillator and an Electrical Model of the Heart”, *Philosophical Magazine*, v. 6, pp. 763-775, 1928.

WANG, Y., WEI, S., ZHANG, S., ZHANG, Y., ZHAO, L., LIU, C., & MURRAY, A., “Comparison of time-domain, frequency-domain and non-linear analysis for distinguishing congestive heart failure patients from normal sinus rhythm subjects.”, *Biomedical Signal Processing and Control*, v. 42, pp. 30-36, 2018.

WEAVER, R. L., “Spectral statistics in elastodynamics”. *The Journal of the Acoustical Society of America*, v. 85, n. 3, pp. 1005–1013, 1989.

WOLF, A., SWIFT, J.B., SWINNEY, H.L., VASTANO, J.A., “Determining Lyapunov exponents from a time series”, *Physica D: Nonlinear Phenomena*, v. 16, n. 3, pp. 285-317, 1985.

WU, G. Q., ARZENO, N. M., SHEN, L. L., TANG, D. K., ZHENG, D. A., ZHAO, N. Q., ECKBERG, D. L., AND POON, C. S., “Chaotic signatures of heart rate variability and its power spectrum in health, aging and heart failure”. *PLoS ONE*, v. 4, e423, 2009.

YATES, F. E., BENTON, L.A., “Variance structure in the human cardiovascular system – periodicity, chaos, or old-fashioned noise?”, *Mathematical and computer modelling*, v. 19, n. 6-8, pp. 161-170, 1994.